NASA/CR—2008-215140

Initial Noise Assessment of an Embedded-Wing-Propulsion Concept Vehicle

James R. Stone and Eugene A. Krejsa
Diversitech, Inc., Westlake, Ohio

April 2008

NASA STI Program . . . in Profile

Since its founding, NASA has been dedicated to the advancement of aeronautics and space science. The NASA Scientific and Technical Information (STI) program plays a key part in helping NASA maintain this important role.

The NASA STI Program operates under the auspices of the Agency Chief Information Officer. It collects, organizes, provides for archiving, and disseminates NASA's STI. The NASA STI program provides access to the NASA Aeronautics and Space Database and its public interface, the NASA Technical Reports Server, thus providing one of the largest collections of aeronautical and space science STI in the world. Results are published in both non-NASA channels and by NASA in the NASA STI Report Series, which includes the following report types:

- TECHNICAL PUBLICATION. Reports of completed research or a major significant phase of research that present the results of NASA programs and include extensive data or theoretical analysis. Includes compilations of significant scientific and technical data and information deemed to be of continuing reference value. NASA counterpart of peer-reviewed formal professional papers but has less stringent limitations on manuscript length and extent of graphic presentations.

- TECHNICAL MEMORANDUM. Scientific and technical findings that are preliminary or of specialized interest, e.g., quick release reports, working papers, and bibliographies that contain minimal annotation. Does not contain extensive analysis.

- CONTRACTOR REPORT. Scientific and technical findings by NASA-sponsored contractors and grantees.

- CONFERENCE PUBLICATION. Collected papers from scientific and technical conferences, symposia, seminars, or other meetings sponsored or cosponsored by NASA.

- SPECIAL PUBLICATION. Scientific, technical, or historical information from NASA programs, projects, and missions, often concerned with subjects having substantial public interest.

- TECHNICAL TRANSLATION. English-language translations of foreign scientific and technical material pertinent to NASA's mission.

Specialized services also include creating custom thesauri, building customized databases, organizing and publishing research results.

For more information about the NASA STI program, see the following:

- Access the NASA STI program home page at *http://www.sti.nasa.gov*

- E-mail your question via the Internet to *help@sti.nasa.gov*

- Fax your question to the NASA STI Help Desk at 301–621–0134

- Telephone the NASA STI Help Desk at 301–621–0390

- Write to:
  NASA Center for AeroSpace Information (CASI)
  7115 Standard Drive
  Hanover, MD 21076–1320

NASA/CR—2008-215140

Initial Noise Assessment of an Embedded-Wing-Propulsion Concept Vehicle

James R. Stone and Eugene A. Krejsa
Diversitech, Inc., Westlake, Ohio

Prepared under Contract NNC–05VD49P

National Aeronautics and
Space Administration

Glenn Research Center
Cleveland, Ohio 44135

April 2008

This work was sponsored by the Fundamental Aeronautics Program at the NASA Glenn Research Center.

Level of Review: This material has been technically reviewed by NASA technical management.

Available from

NASA Center for Aerospace Information
7115 Standard Drive
Hanover, MD 21076–1320

National Technical Information Service
5285 Port Royal Road
Springfield, VA 22161

Available electronically at http://gltrs.grc.nasa.gov

Contents

Initial Noise Assessment of an Embedded-Wing-Propulsion Concept Vehicle

James R. Stone and Eugene A. Krejsa
Diversitech, Inc.
29317 Briar Lane
Westlake, Ohio 44145

Abstract

This report describes work performed by consultants to Diversitech for the NASA Glenn Research Center (GRC). Vehicle acoustic requirements are considered for a Cruise-Efficient Short Take-Off and Landing (CESTOL) vehicle concept using an Embedded-Wing-Propulsion (EWP) system based on a review of the literature. Successful development of such vehicles would enable more efficient use of existing airports in accommodating the anticipated growth in air traffic while at the same time reducing the noise impact on the community around the airport.

NASA and the aerospace industry made a considerable investment in Short Take-Off and Landing (STOL) technology development in the 1960s and 1970s. A number of concepts were studied, considerable hardware was developed and a number of experimental research aircraft were built and tested, with two becoming prototypes. Flight research was conducted on the Augmentor Wing (AW). NASA's research and development culminated in the Quiet STOL Research Aircraft (QSRA), an Over-The-Wing (OTW)/Externally-Blown-Flap (EBF) craft, and the Quiet, Clean Short-haul (earlier STOL) Experimental Engine Program (QCSEE) that conducted a ground demonstration of a very high bypass ratio variable pitch geared fan. The extensive research culminated in 2 prototypes leading into a production program. The YC-14 Upper-Surface-Blowing (USB) and YC-15 EBF prototypes validated the technologies leading to the C17 with EBF as a military program. Civil applications have been offered but to date have not materialized.

A noise prediction capability for CESTOL-EWP aircraft is developed, based largely on NASA's FOOTPR code and other published methods, with new relations for high aspect ratio slot nozzles and wing shielding. The predictive model is applied to a preliminary concept developed by Boeing for NASA GRC. Significant noise reduction for such an aircraft relative to the current state-of-the-art is predicted, and technology issues are identified which should be addressed to assure that the potential of this design concept is fully achieved with minimum technical risk.

Introduction

NASA's efforts on Short Take-Off and Landing (STOL) were initiated in the early 1970s to provide service to heavily congested areas, leading to the requirement for very quiet and pollution free aircraft (ref. 1). That NASA effort was initiated largely in response to the joint Department of Transportation (DOT)-NASA Civil Aviation Research and Development (CARD) study (refs. 2 and 3). The CARD Study identified noise abatement and traffic congestion relief as the two highest priority needs in assessing national benefits related to aviation research and development. The continued growth in air traffic and the growth of commercial and residential developments near airports make these needs just as valid today as they were over 30 years ago. No firm noise specifications existed at that time for STOL systems, but a much-used figure of merit was 95 PNdB on a 500-ft sideline (ref. 1). NASA's research and developments on STOL technology aimed at this goal.

A concept currently being developed in England, called the "Jetpod," aimed at entering service by 2010 (ref. 4) evolved from the early STOL concepts. The design features two low-noise turbofans mounted on top of the cabin. Some of the bypass flow would be exhausted downward through the wings to provide lifting thrust. The plane is intended to carry seven passengers at 350 mph and take off in 410 ft. While this is a rather extreme example of STOL, it does indicate real commercial interest in such concepts. Some recent small-scale research has been conducted on distributed propulsion aerodynamics and acoustics (refs. 5 and 6). Although not specific to the concept of current interest, these results may be of interest.

The concept currently under consideration is described by Kim and Saunders (ref. 7) as a part of NASA's Revolutionary Aeropropulsion Concepts (RAC) project. Reference 7 reports on system and computational fluid dynamics studies of Embedded Wing Propulsion (EWP) to assess the feasibility of such a propulsion system to large transports such as Blended-Wing-Body (BWB) aircraft. A number of potential benefits were identified, including noise reduction. Early analysis of an 800 passenger BWB was conducted. In comparing propulsion systems the number of engines required ranged from 2 for the General Electric GE90 to about 264 for the Williams FJ22; a more likely candidate for the distributed propulsion approach was the General Electric CF34, with about 14 engines required. The BWB approach has also been considered for transonic and supersonic cruise applications (e.g., ref. 8).

This current effort is coordinated with a configuration definition study by Boeing Phantom Works, to be performed June 2005-January 2006; engine cycle calculations were performed by NASA Glenn Research Center (GRC). The configuration defined by Boeing, described by Kawai (ref. 9), is a 170 passenger, 180,000 lb Take-Off Gross Weight (TOGW) airplane with short-field capability. A high-aspect-ratio slot nozzle is used in conjunction with a slotted airfoil with the nozzle exhaust pumping through the slot to increase circulation and lift. Twelve engines are used, partially embedded in the upper wing surface. Half of the fan flow from each engine is diverted to slot. Boeing selected engines with bypass ratio BPR = 5.7, and NASA also provided data for engines with BPR = 9.4. The layout of the engines on the wing is shown in figure 1.

Literature Review

An extensive review of the literature was undertaken and documented in reference 10. This review covered the various jet STOL systems investigated in the 1970s, with emphasis on engines designed specifically for STOL application. The methods of achieving powered lift are also reviewed, the main emphasis in those studies was on both Under-The-Wing Externally (UTW) and Over-The-Wing (OTW) Externally Blown Flap (EBF) systems, as well as the Augmentor Wing (AW). Some work was done on other concepts, such as the Internally Blow Flap (IBF), which has now become of interest. Since the use of thrust reversers was included in these concepts, including in some cases partial thrust reversal on approach, thrust reverser noise was found to be important, particularly for the 152-m (500-ft) sideline. The literature review focused particularly on the noise characteristics of these powered lift systems and the correlations and prediction models that were developed.

Noise Modeling

The prediction capability is built on the NASA FOOTPR code first described by Clark (ref. 11). The predictive modeling for jet noise has advanced considerably, and this work uses as a starting point the model of Stone, Krejsa and Clark (ref. 12) for unsuppressed and suppressed single- and dual-stream nozzles. For the augmentor wing, we use the model of Dunn and Peart (ref. 13). For the engine internal noise components we use NASA methods: Stone, Krejsa and Clark (ref. 14) for combustion noise; Heidmann (ref. 15) for fan and compressor noise; and Krejsa and Valerino (ref. 16) for turbine noise. In

performing this task, we extended the jet noise modeling capability in two areas: slot nozzle jet mixing and shock noise, including azimuthal angle effects, and wing shielding, as discussed below.

Slot Nozzle Jet and Shock Noise

Our recent activities on predicting noise for high bypass ratio engines has not included slot nozzles, and the most recent model we have in the FOOTPR system is that of the original ANOPP jet noise model of 1974 (ref. 17), which is rather crude in comparison to our current coaxial nozzle noise model (ref. 12). Therefore, we considered it worthwhile to extend reference 12 to cover slot nozzle cases, and to do this we incorporated two-dimensional nozzle aspect ratio effects from reference 18 along with slot nozzle effects relative to circular nozzle from reference 17. In the following discussion W denotes the slot nozzle width, H the slot nozzle height, and ϕ the azimuthal angle. The origin for this angle is the center of the nozzle exit plane, with the $\phi = 0°$ axis aligned with the nozzle long dimension W (typically broadside to the aircraft on the ground), and $\phi = 90$ deg is aligned with the short dimension H (directly under the aircraft at flyover. To account for aspect ratio (W/H) and azimuthal angle (ϕ) effects, the corner angle is defined as $\phi_{corner} = \tan^{-1}(H_{exit}/W_{exit})$ where the subscript exit denotes that it is the nozzle exit geometry to be used and not that of the throat. In reference 18 it was assumed that for each noise source, the noise reduction at any ϕ, relative to its maximum at $\phi = 90°$, is related to the simple distance ratio: the distance from the center of the exit plane to the nozzle edge in the direction of the observer divided by the corresponding length for $\phi = 90°$. The resulting geometric factor is calculated as follows:

$$GF(\phi, H/W) = \begin{cases} [(H_{exit}W_{exit})\cos\phi]^{-1} & \text{for } 0 < \phi < 90\ \phi_{corner} \\ (\sin\phi)^{-1} & \text{for } \phi \geq \phi_{corner} \end{cases} \tag{1}$$

Mixing Noise

For the mixing noise components, we use the spectral relation of reference 17, where for a slot nozzle the Strouhal number includes the ratio of hydraulic to equivalent diameter, $(D_h/D_{eq})^{0.4}$. We apply this factor to large scale mixing noise, transitional /intermediate mixing noise and small scale mixing noise. For large scale mixing noise we utilize the relation for GF developed in reference 18 for "merged" mixing noise; azimuthal directivity function Fcn_L is given by the following:

$$F_{cn_L} = \begin{cases} 0.0 & \text{for } \theta'_L \leq 120° \\ -7.5[(\theta'_L - 120)/60]\log GF(\phi, H/W) & \text{for } \theta'_L > 120° \end{cases} \tag{2}$$

For the transitional/intermediate and small scale mixing, the "premerged" relation of reference 18 is used:

$$F_{cn_T} = \begin{cases} -4.5(\theta'_T/90)^2 \log GF(\phi, H/W) & \text{for } \theta'_T \leq 90° \\ -[2.25(\theta'_T/90)^2 + 6.75(\theta'_T/120)^2]\log GF(\phi, H/W) & \text{for } 90 \leq \theta'_T \leq 100° \\ -13.0(\theta'_T/120)^2 \log GF(\phi, H/W) & \text{for } \theta'_T > 100° \end{cases} \tag{3}$$

$$F_{cn_S} = (\text{same relations with } \theta'_S \text{ instead of } \theta'_T) \tag{4}$$

Shock Noise

In reference 18 no azimuthal angle or aspect ratio effects were found for external shock noise, so we retain that assumption. The characteristic dimension for annular nozzle shock noise in reference 12 is hydraulic diameter, and we retain that assumption for slot nozzle shock noise.

Results

With no trajectory data yet available, we drew on experience from the High Speed Civil Transport Program and made the assumption that on the 500 ft sideline the maximum noise would occur at an azimuthal angle $\phi = 25°$, resulting in a 552 ft slant range at closest approach. Calculations are performed first for a slot nozzle pressure ratio slightly below sonic, slot nozzle pressure ratio SNPR = 1.85. The total and component OASPL directivities on the 500 ft sideline is shown in figure 2; large scale mixing is the dominant source. Total and component spectra at directivity angles θ of 30, 60, 90, 120, and 140° are shown in figure 3. Because the small and transitional scale mixing contribute at higher frequency, they will contribute significantly to the perceived noise level at $\theta = 90°$ and in the forward quadrant. Next the model was exercised for SNPR = 1.91, slightly above sonic. As shown in figure 4, the OASPL is significantly increased in the forward quadrant (7 dB at $\theta = 30$) even though the rear quadrant levels are increased by only about 1 dB. The spectral plots for this case, shown in figure 5, illustrate that it is shock noise, which has caused this problem. At $\theta = 30$, shock noise is more than 20 dB above mixing noise at its peak. Based on these findings, NASA and Boeing agreed that nozzle pressure ratios should be kept sub-critical.

Shielding Correlation

To describe the total jet noise situation for the BWB aircraft we must also bring in the jet noise from the engine nozzle, for which our current coaxial jet noise model is appropriate. However, neither the coaxial or slot nozzle model has a wing shielding relation, so that became the next needed development. Fortunately, the coaxial jet noise model does include axial source location relations for peak-frequency noise as a function of directivity angle θ. Using the Strouhal relations for slot nozzles discussed in the slot nozzle progress report, this model can also be applied to the slot nozzle. A recurring feature has been groups of engines feeding one slot nozzle, so our relations feature the ability to handle both nozzle types on the same configuration at the same time. Clark (ref. 11) had a relationship for shielding, but only for the relative effects of ϕ and θ. Reshotko, et al. (ref. 19) reported on the shielding effects for a CTOL-OTW configuration for $\phi = 90°$ and $\theta = 120°$, for 10 to 20° and 30 to 60° flap positions.

We tried to develop a somewhat phenomenological approach and assumed that with the highly integrated configurations we're dealing with the 10 to 20° flap data were most appropriate. We assumed that the correlating parameter would be source location relative to the trailing edge divided by wavelength. We ran the conical nozzle model (ref. 12) for this case and found that large-scale mixing was the dominant source up to 800 Hz, with small-scale mixing dominant at higher frequencies (fig. 6). The model currently only gives X_{Sor} for the peak frequency noise, so we made the assumption that at each angle X_{Sor} varies in a logarithmic fashion:

$$X_{Sor}(f) = X_{Sor(f_{pk})}\,[1 - \log(f_{pk}/f)], \text{but not} < 0 \tag{5}$$

So X_S as a function of f (or alternatively wavelength λ) was obtained by patching these two sets of values at 800 Hz, by setting $X_{Sor} = (X_{Sor,L} + X_{Sor,S})/2$.

We read the experimental shielding values from figure 34 of the reference 19 and plotted the points thus picked off versus the effective shielding-length-to-wavelength ratio, $(X_{Sor} - X_{te})/\lambda$, where X_{te} is the distance from the nozzle exit to the wing trailing edge. Negative values for $(X_{Sor} - X_{te})/\lambda$ are found at low

frequency, indicating that the source location is beyond the tip of the last flap segment. Therefore, the effect of the wing is plotted against $[1 + (X_{Sor} - X_{te})/\lambda]$ on a logarithmic scale in figure 7. The experimental data (especially considering the difficulty in reading these numbers from a small chart) exhibit a rather linear relationship with the correlating parameter down to the lowest Strouhal number on the reference chart, 0.3, where the suppression is – 3.3 dB. It seems perfectly reasonable that at low frequency, in spite of shielding there is a noise increase due to the presence of a surface in the near field, even without jet impingement on the wing. We arbitrarily decided that this noise increase should be limited to 6.0 dB (pressure doubling). The correlation shown in figure 7 is used along with the ϕ and θ variations suggested by Clark (ref. 11) in developing a shielding module for EWP configurations.

Shielding Calculation

In the previous section we developed a correlation of the shielding effects for a CTOL-OTW configuration for $\phi = 90°$ and $\theta = 120°$, for 10 to 20° flap configuration from the data of Reshotko et al. (ref. 19). We correlated the shielding and low-frequency amplification as a function of the source location relative to the trailing edge divided by wavelength, $(X_S - X_{te})/\lambda$. To apply this correlation at other angles, we considered first the effect of azimuthal angle ϕ, and assumed that $\Delta_{shld}(\phi) = \Delta_{shld}(\phi = 90°) + 5 \log(1 + \cos\phi)$. The effect of directivity angle θ was also assumed to have a simple form, that $\Delta_{shld}(\phi, \theta'_{cor}) = \Delta_{shld}(\phi, \theta'_{cor} = 90°) + 10 \log(1 + \sin\theta'_{cor}) - 3.013$. We limited the shielding term so that $\Delta_{shld}(\phi, \theta'_{cor}) \geq -6.0$ as mentioned above.

Samples of the shielding effects calculated by this model at $\phi = 25°$ and $\theta = 90°$ are shown in figure 8 for three configurations: the engine nozzle (fig. 8 (a)), the engine nozzle with chevrons (design scaled from GRC/GE Configuration 3IC, ref. 20) (fig. 8 (b)) and the IBF slot nozzle (fig. 8 (c)).

Component/Subcomponent Noise Prediction

Engine Nozzle

Using these shielding relations and the coaxial nozzle relations of reference 12, we computed the engine jet noise for Boeing's candidate BWB configuration, under the assumption that the peak sideline noise would occur as the plane reaches an azimuthal angle $\phi = 25°$ on the 500 ft sideline, yielding a closest-approach slant range of 168 m (551.7 ft). To roughly account for ground reflections, 3.0 dB are added to the free-field levels. The current calculations are for coaxial nozzle without chevrons or center plug. The 152-m (500-ft) sideline OASPL directivities for total engine jet noise and its subcomponents, large-scale mixing, transitional/intermediate-scale mixing and small-scale mixing are shown in figure 9. Because of the high core jet velocity, $V_{j,} = 1765$ ft/sec, the strongest component at most angles is the transitional/intermediate scale mixing. This can also be seen on a spectral basis in figure 10 at directivity angles $\theta = 30, 60, 90, 120, 140$, and 160° in figure 10(a) to (f).

Validation of Nozzle Jet Noise Model

To validate these calculations, the predictive model is compared with experimental GRC/General Electric (GE) model experimental results (ref. 20) for similar conditions. For the model test the BPR = 4.8 (Configuration 3BB), while for the BWB case the *nozzle* BPR = 2.9 even though the *engine* BPR = 5.8, with half the fan flow directed to the slot nozzle. The model nozzle had a center plug (and plug separation noise), in contrast to the BWB configuration. Also differing somewhat, the model tests were at a simulated flight Mach number $M_a = 0.28$, while the BWB prediction is at $M_a = 0.20$. The jet velocities are matched fairly well: $V_{j,I} = 1699$ ft/sec (model) and 1629 (BWB); $V_{j,O} = 1092$ ft/sec (model) and 1068 (BWB); $V_{mix} = 1198$ (model) and 1212 (BWB). Comparison of experimental model results and predicted OASL directivity for Configuration 3BB, reading 396, is shown in figure 11. Note that this plot is a

constant radius, rather than the sideline pattern shown earlier. The agreement is very good except at the most aft directivity angles, where we suspect that the shear layer correction applied to the experimental data should be modified to account for the finite shear layer thickness. Spectral comparisons are shown at directivity angles θ = 60, 90, 120, 140, and 160° in figure 12 (a) to (e). Not only are these plots at constant radius rather than sideline, they are free-field and lossless. The good agreement seen here validate that the predictive model works well for a somewhat similar configuration and set of conditions.

Engine Nozzle With Chevrons

Since Boeing has suggested that chevrons on the fan and core streams might be helpful, we assessed this option using a chevron design based on Configuration 3IC of the GRC/GE test series (ref. 20). OASPL directivity is shown in figure 13; reductions in large-scale and transitional/intermediate-scale mixing noise can be seen at all angles, and the small increase (1.7 dB) in small-scale mixing noise does not significantly impact the total noise reduction of close to 4 dB. The corresponding predicted spectra at directivity angles θ = 30, 60, 90, 120, 140, and 160° are shown in figure 14 (a) to (f). Significant reductions due to the chevrons are seen over most of the frequency range; the slight increase in small-scale mixing noise does not cause a significant impact.

IBF slot nozzle

For the slot nozzle, fed by half the fan flow of four engines, at the somewhat lower exhaust velocity, V_j = 1023 ft/sec, the large-scale mixing is the strongest source. The somewhat ragged directivity relations (fig. 15) for transitional/intermediate and small-scale mixing noise are due to the direct use of the aspect ratio and azimuthal angle effects directly from the two-dimensional mixer ejector relations developed for the High-Speed Civil Transport (ref. 18). The corresponding predicted spectra at directivity angles θ = 30, 60, 90, 120, 140, and 160° are shown in figure 16 (a) to (f).

Since the slot nozzle relation does not include a jet/flap noise term, we thought it appropriate to treat the configuration as an AW at a 40° flap angle for comparison with the results of the shielded slot nozzle. This prediction is done using the Dunn and Peart predictive model (ref. 13). The results are shown in figure 17 with the shielded slot nozzle predictions shown for comparison. Near the peak, the slot nozzle prediction gives higher OASPLs. The SPL spectra are shown at directivity angles θ = 30, 60, 90, 120, 140, and 160° in figure 18. In general the slot nozzle assumption yields higher noise at low frequency and less noise at high frequency than the AW assumption, and the differences are large at the more aft angles. However, when we consider the impact on metrics, in this case the 500-ft sideline noise shown in figure 19, the differences are not so great, and the slot nozzle assumption gives only 0.5 EPNdB higher EPNL than the AW assumption. Neither of these approaches is well validated by comparisons with recent, high-quality experimental data, so it is encouraging that the end results are similar. With caution, we model the IBF with the shielded slot nozzle relations in subsequent calculations.

PNL/EPNL Predictions for 4-Engine/1-Slot Cluster

In the earlier phases of their study (ref. 21) Boeing's study focused on 3 clusters of 4 engines feeding 1 slot nozzle. PNL calculations were performed for a 4-engine, 1-slot cluster on Boeing's candidate early BWB configuration, under the assumption that the peak sideline noise would occur as the plane reaches an azimuthal angle ϕ = 25° on the 500 ft sideline, yielding a closest-approach slant range of 168 m (551.7 ft). We assumed that the view factor for a multi-engine cluster would be given by the simple relation:

$$\left.\begin{aligned} n_{eff} &= n_{total} && \text{for } \phi \geq 45° \\ n_{eff} &= 1 + (n_{total} - 1)(\phi / 45) && \text{for } \phi < 45° \end{aligned}\right\} \tag{6}$$

Where n_{eff} is the effective number of engines heard at the observer location, and n_{total} is the total number of engines. Since it is not clear whether the shielded slot nozzle assumption or the augmentor wing assumption, if either, best describes the proposed configurations, we explored both assumptions.

We've already shown (fig. 19) the differences between slot nozzle and AW assumptions on the early baseline aircraft with no nozzle suppression. It is clear that the unsuppressed configuration would not closely approach the 1970s 500-ft sideline goal of 95 PNdB maximum. Therefore, we consider the impact of nozzle exit chevrons on engine fan and core nozzles for the 4-engine/1-slot. The effect on engine nozzle spectra was shown earlier (figs. 9 and 10 compared with figs. 13 and 14). The PNLT time histories are compared in figure 20, using the shielded slot nozzle model for the IBF. The resulting EPNL is 99.6 EPNdB with the chevron nozzles, compared to 102.5 with unsuppressed nozzles. So the chevrons provide a suppression of 2.9 EPNdB. Note that this is for one 4-engine cluster, and the observer would also hear noise from the other 2 clusters now envisioned, adding 3 to 4.5 EPNdB.

Application of Predictive Model to Final Concept Design

Having shown the development of our predictive model and it's application to early design variations in the preceding sections, we present analyses of the final configuration, as shown in figure 1, here. We apply our predictive tools to several potential aircraft configurations to determine the acoustic impact of design variations and to illustrate the considerable potential of such aircraft to provide noise reduction benefits to the airport vicinity. We also assess the sensitivity of our calculations to some of the simplifications we make. In all cases we employ the "What you see is what you hear." approximation, i.e. the two engines at the center rear and the five engines on the side toward the observer are heard toward the side, while for flyover all engines are heard.

Baseline Unsuppressed BPR = 5.7 Engines on 152-m (500-ft) Sideline

The first configuration for which noise estimates are discussed is the baseline aircraft, with no suppression features except for the shielding provided by the engine/wing/flap configuration. We also investigate the impact of approximations we employ in the rest of this study. We first model the situation in more detail by considering the engines in three "clusters." Cluster 1 consists of the three engines closest to the sideline observer; engine nozzle shielding length (nozzle exit to trailing edge) 8.1 ft, and slot nozzle shielding length 6.6 ft. Cluster 2 consists of the next two engines, which have different shielding lengths; we use the geometric mean of 12.124 ft for the engine nozzles and 10.5 for the slot nozzle. Cluster 3 is the two center-most engines, with shielding lengths of 15.7 and 14.3 ft (constant) for the engines and slot, respectively. We then repeat these calculations using "lumped assumptions, assuming all the engine nozzles and all the slots can be accounted for using the geometric mean shielding lengths, 10.981 ft for engines and 9.334 ft for slots. The resulting Tone Corrected Perceived Noise Level (PNLT) time histories under these two sets of assumptions are shown in figure 20. Using the "cluster" approach (in red) the maximum PNLT is 109.0 PNdB at $\theta = 139.6°$, and the EPNL is 106.5 EPNdB. For the "lumped" approach (in blue) the peak PNLT is 108.4 PNdB at $\theta = 135.4°$, and the Effective Perceived Noise Level (EPNL) is 106.1 EPNdB. From this comparison, we conclude that at this early stage the "lumped" approach is sufficiently accurate, but in an actual development program each engine should be treated individually since even 0.1 dB is significant when approaching certification. It is also clear that, as suggested by our earlier exercises, some noise suppression approaches will have to be employed to approach the old STOL goal of 95 PNdB on a 500-ft sideline.

Spectral comparisons are shown for $\theta = 30, 60, 90, 120, 140$, and $160°$ for the both the "cluster" and "lumped" approximations in figure 21. The differences in shielding effects can readily be seen, even though the overall differences are not great. The annoyance spectra are compared at these angles in figure 22.

Since the sideline noise estimate does not closely approach the old STOL goal, our further analyses will focus on suppressed options, and we do not estimate the baseline noise for other measuring stations. Based on the results shown here, we perform the rest of our analyses using the "lumped" approach.

BPR = 5.7 Engines With Chevron Nozzles

Chevron nozzles have been shown to provide significant reduction in low frequency noise accompanied by relatively small increases in high frequency noise (e.g., ref. 20). The use of chevron nozzles also brings the noise generating regions closer to the nozzle exit plane, so that the effective shielding lengths are increased. To estimate the effect of chevrons we assumed that the chevron design would be scaled from that investigated in reference 20, on which our predictive model is based.

152-m (500-ft) Sideline

First we estimate the noise levels on the 500-ft sideline (using the lumped approach). The PNLT time history is shown in figure 23; the maximum PNLT is 106.3 PNdB at $\theta = 130.4°$ for the aircraft with chevron nozzles, and the EPNL is 103.4 EPNdB. Thus, the suppression achieved by the engine nozzle chevrons is 2.7 EPNdB. The unsuppressed PNLT time history is also shown for comparison; the reduction in peak PNL is 2.1 PNdB, and the more rapid roll-off after the peak provides a further reduction in EPNL. Spectral comparisons are shown for $\theta = 30$, 60, 90, 120, 140, and 160° in figure 24. The unsuppressed total noise spectrum is also shown for comparison. At low frequencies the noise reduction is due to the combination of reduced low frequency noise generation at the source and increased shielding. The reductions seen at higher frequencies illustrates that the improved shielding provides enough benefit to more than offset the slight increase in higher frequency noise generation. Even with the chevron benefit the old STOL sideline goal of 95 PNdB maximum on the 500-ft sideline is not met, but this is still a very quiet aircraft as will be shown by results at the FAR 36 measuring stations.

FAR-36 450-m (1476-ft) sideline

Going to the farther sideline distance of FAR-36 results in noise reduction that increases with increasing frequency, due to atmospheric attenuation. For this reason, we do not show the spectral plots here. The PNLT time history is shown in figure 25; the peak noise is 95.6 PNdB at $\theta = 130.6°$, and the EPNL is 96.9 EPNdB. The current regulatory level (Stage 3) at TOGW = 189,000 lb is 97.3 EPNdB, meaning that this design appears meets the requirement with a margin of 0.4 EPNdB. The level of 95.8 EPNdB at 150,000 lb was proposed in reference 4 to be consistent with the 1970s goal of 95 EPNdB. So the proposed airplane would exceed the sideline target by 0.9 EPNdB. Thus, even at this difficult sideline orientation, this aircraft is relatively quiet, meeting the Stage 3 noise rule with margin and closely approaching the proposed future noise rule. It is at the other locations where the benefit is expected to be greater.

FAR-36 Take-off Flyover

The measuring station is 650-m (21,325 ft) from brake release, where the altitude is 672 m (2,500 ft). With further reductions due to increased atmospheric attenuation, but with loss of engine-to-engine shielding the peak PNL is predicted to be 92.6 PNdB at $\theta = 130.3°$, and the EPNL is 94.7 EPNdB, as shown in figure 26. Note that there is a tone correction from 31.25 to 43.75 sec; this is artificial and due to the rapid roll-off due to atmospheric attenuation. The Stage 3 rule is 97.3 EPNdB, so the proposed new plane would be 2.6 EPNdB below the Stage 3 limit.

FAR-36 Approach

It is expected that turbomachinery noise will be quite important at this low power setting. However, we only have exhaust parameters available, so only engine nozzle and slot nozzle noise are calculated, and low noise levels are expected. The results are shown in figure 27; the peak noise is 50.7 PNdB at $\theta = 95.6°$, and the EPNL is 47.3 EPNdB. This is far below the current (Stage 3) limit of 101.0 EPNdB, but it is meaningless to calculate a traded noise level since turbomachinery noise is not included, but these calculations indicate a cumulative reduction of +0.4 + 2.6 +53.7 = 56.7 EPNdB. However, it is encouraging to note that the approach jet noise levels are very low, so if wing shielding and acoustic treatment are effective on the turbomachinery noise, very low approach noise is feasible.

BPR = 9.4 Engines With Chevron Nozzles

Since the engines with BPR = 5.7 do not appear to provide as great a noise reduction as hoped for, NASA is also considering higher bypass ratio engines also using chevron nozzles. NASA provided data to us for BPR = 9.4. (Note that even at this higher BPR, the effective BPR for the nozzle when half the fan flow is diverted to the slots is 4.7, compared to 2.85 for the baseline engines. Therefore the reduction in jet noise, while significant, is not dramatic as might be expected.)

152-m (500-ft) Sideline

First we estimate the noise levels on the 500-ft sideline (using the lumped approach). The PNLT time history is shown in figure 28, with the lower BPR result also shown for comparison. The peak noise of 104.3 PNdB (4.1 PNdB less than BPR = 5.7) is at $\theta = 130.4°$, while the EPNL is 101.6 EPNdB, 4.5 EPNdB less than for BPR = 5.7. This is a significant reduction. Spectral comparisons are shown in figure 29. The benefit of reduced bypass ratio is strongest at low frequency, but persists throughout the spectrum.

FAR-36 450-m (1476-ft) Sideline

Going to the farther sideline distance of FAR-36 results in noise reduction that increases with increasing frequency, due to atmospheric attenuation. For this reason, we do not show the spectral plots here. The PNLT time history is shown in figure 30. The peak noise of 93.8 PNdB (1.9 PNdB less than for the BPR = 5.7 case) occurs at $\theta = 129.4°$, and the EPNL is 95.3 (1.6 EPNdB less than at the lower BPR). The current regulatory level at TOGW = 189,000 lb is 97.3 EPNdB, so even at this difficult sideline orientation, this aircraft is relatively quiet, meeting the Stage 3 noise rule with a margin of 2.0 EPNdB. It is at the other locations where the benefit is expected to be greater.

FAR-36 Take-off Flyover

With further reductions due to increased atmospheric attenuation, but with loss of engine-to-engine shielding the peak PNLT is predicted to be 88.2 PNdB (compared with 92.6 PNdB at lower BPR) at $\theta = 130.3°$, and the EPNL is 90.2 EPNdB, representing a 4.5 EPNdB suppression relative to BPR = 5.7. The PNLT time history is shown in figure 31. Note that the PNLT calculation is influenced by artificial tone penalties due to the rapid roll-off due to atmospheric attenuation. The Stage 3 rule is 97.3 EPNdB, so the proposed new plane would be 7.1 EPNdB below the Stage 3 limit.

FAR-36 Approach

It is expected that turbomachinery noise will be quite important at this low power setting. As we showed at the lower BPR engine nozzle and slot noise is very low, and in reality turbomachinery noise would be controlling.

Thrust Reverser Noise on 152-m (500-Ft) Sideline

To get some indication of the possible importance of thrust reverser noise for such aircraft as these, we considered only the contributions of the fan and core reversers on the most outboard engine as an indicator, with full reverse thrust. Boeing has indicated that cascade thrust reversers would be used on both streams, and this is generally the quietest thrust reverser type. To simplify the problem we did the calculation for an aircraft speed of 80 ft/sec, whereas in reality it would vary from essentially touch-down speed to a very low speed where the engines would be throttled back strongly. Predicted thrust reversal noise spectra are shown in figure 32 at directivity angles θ = 30, 60, 90, 120, and 150°. The spectra at θ = 30° (fig. 32(a)) shows relatively low middle frequency noise due to the influence of propagation near the ground, the so-called extra ground attenuation (EGA). The differences in spectral shape from angle to angle are due to this phenomenon. It is clear that the fan reverser is louder than the core, due to its much higher mass flow rate. A pseudo-PNLT time history is shown in figure 33; it is not a true time history because of our constant speed assumption. The peak perceived noise is 105.7 PNdB at θ = 80°, and the effective perceived noise level is 101.9 EPNdB. Of course, thrust reversal noise is not regulated, and is unlikely to be, but there have been complaints about it from airport neighbors. The EPNL is essentially the same as for takeoff. At this early stage, planners should simply be aware of the potential issue that may arise.

Discussion

Since the internal engine component—fan, turbine and combustor—models have been checked against engine data recently, with minor adjustments they are ready to use, and with them complete propulsion system noise estimates for EWP aircraft can be now made. To do this full propulsion system noise assessment would require all the necessary data for the internal noise components, as well as trajectories with throttle settings, along with the nozzle data used so far. The models used to estimate source locations and shielding effects are rather crude, but could readily be improved if model data for the types of configurations of interest are obtained.

The relatively high noise contribution of the engine nozzle jets may be a serious issue with this type of configuration. This high engine nozzle noise is due to the high mixed jet velocity resulting from cutting the nozzle BPR in half to provide slot flow. We assessed the utility of nozzle exit chevrons and found they offered nearly 3 EPNdB reduction. However, the total projected EPNL does not appear to reach the old STOL goal of 95 EPNdB. But when we project our results to the 450-m sideline of FAR-36, we see noise benefits compared to current CTOL aircraft would still be quite significant. This is a STOL airplane that climbs quickly and perhaps descends steeply (likely at a reduced throttle setting as well), there would be a chance that the airplane might be significantly below the stage 3 rule's flyover and approach limits. This feature may go a long way in satisfying the stage 4 requirements that the airplane be (re stage 3 limits): –10 EPNdB, cumulative over all three points; and that it be –2 EPNdB, cumulative over any two points (which would likely be the flyover and approach points). Since we're about 6 EPNdB below the stage 3 sideline limit and stage 4 rules do not allow trades, another cumulative 4 EPNdB reduction at the other points (which should be quite feasible) would be needed for overall stage 4 certification.

Concluding Remarks

A prediction model for the noise characteristics of a Cruise-Efficient Short Take-Off and Landing (CESTOL) vehicle concept using an Embedded-Wing-Propulsion (EWP) system has been developed for exhaust noise; inlet noise still under development. Preliminary application to the current Boeing Blended Wing Body (BWB) airplane raises cautions concerning engine BPR; but chevrons on engine exhaust show significant promise; and compared to State-of-the-Art aircraft there are significant noise benefits.

In this report we present the acoustic performance characteristics of a Cruise-Efficient Short Take-Off and Landing (CESTOL) vehicle concept using an Embedded-Wing-Propulsion (EWP) system. To do this

we utilize the predictive model reported under Subtask 2. The airplane defined by Boeing in a parallel study is a 170 passenger, 189,000 lb Take-Off Gross Weight (TOGW) airplane with short-field capability, Take-Off Field Length of 2452 ft and Landing Field Length of 3477 ft. By contrast the STOL studies of the 1970s targeted 2,000 ft. Boeing has selected an Internally Blown Flap (IBF) configuration. A high-aspect-ratio slot nozzle fed by multiple engines is incorporated in conjunction with a slotted airfoil with half the fan nozzle exhaust pumping through the slot to increase circulation and lift. Twelve engines are partially embedded in the wing/body. The engine bypass ratio (BPR) selected by Boeing is 5.7; NASA is also investigating engines with BPR = 9.4.

We found that the baseline airplane without noise suppression devices would produce a peak tone-corrected perceived noise level of 108.4 PNdB at takeoff on the 500-ft sideline used in the STOL studies of the 1970s, with a corresponding effective perceived noise level of 106.1 EPNdB. Mixing enhancement chevrons on the engine fan and core noise were found to provide significant benefit; the peak noise is reduced to 106.3 PNdB and the EPNL is reduced to 103.4 EPNdB on the 500-ft sideline. In comparison with the current FAR-36 measuring points, the sideline noise is 96.8 PNdB, 0.5 EPNdB below Stage 3; the flyover noise is 94.7 EPNdB, 2.6 EPNdB below Stage 3; the approach noise is only 47.7 EPNdB, 53.3 EPNdB below Stage 3, but does not include turbomachinery noise, which is likely to be considerably higher. So it is clear that such an airplane might well develop into an attractive product. One possibility is to increase engine bypass ratio from the BPR = 5.7 baseline. NASA provided us with design data on BPR = 9.4 engines, and we found significant noise benefits; peak noise of 104.3 PNdB and EPNL = 101.6 EPNdB on the 500-ft sideline. At the FAR-36 locations the EPNL is 95.2 EPNdB (Stage 3 – 2.1) on the takeoff sideline and 90.2 EPNdB (Stage 3 – 7.1) at takeoff flyover; again the approach noise would be controlled by turbomachinery noise.

Aircraft of this type clearly have the potential with further development to offer a relatively quiet approach to utilizing smaller, more noise sensitive airports to relieve congestion and enable growth.

Appendix—Symbols

ANOPP	NASA Aircraft Noise Prediction Program
AW	Augmentor Wing
BPR	Bypass ratio, fan flow rate divided by core flow rate, dimensionless
BWB	Blended-Wing-Body
CARD	Civil Aviation Research and Development (study)
CESTOL	Cruise-Efficient Short Take-Off and Landing
CTOL	Conventional Take-Off and Landing
D	Diameter, ft (m)
DOT	Department of Transportation
EBF	Externally Blown Flap
EGA	Extra Ground Attenuation
EPNL	Effective Perceived Noise Level, EPNdB
EWP	Embedded-Wing Propulsion
f	Frequency, Hz
F_{cn}	Directivity function
FOOTPR	NASA GRC Fortran Noise Prediction Code
GE	General Electric
GF	Geometric factor for azimuthal angle and aspect ratio effects on jet noise, dimensionless (eq. 1)
GRC	NASA John H. Glenn Research Center at Lewis Field
H	Slot nozzle height, ft
IBF	Internally Blown Flap
M_a	Aircraft (flight or ground roll) Mach number, dimensionless
n_{eff}	Effective number of engines of a cluster heard by observer, dimensionless
n_{total}	Total number of engines in cluster, dimensionless
NASA	National Aeronautics and Space Administration
OASPL	Overall Sound Pressure Level, dB re 20 μPa
OTW	Over-The-Wing
PNL	Perceived Noise Level, PNdB
PNLT	Tone-Corrected Perceived Noise Level, PNdB
QCSEE	Quiet, Clean Short-haul (earlier STOL) Experimental Engine Program
QSRA	Quiet STOL Research Aircraft
RAC	Revolutionary Aeropropulsion Concepts
SNPR	Slot nozzle pressure ratio, dimensionless
SPL	Sound Pressure Level, dB re 20 μPa
STOL	Short Take-Off and Landing
TOGW	Take-Off Gross Weight, lb
USB	Upper-Surface-Blowing
UTW	Under-The-Wing
V	Velocity, ft/sec (m/sec)
W	Slot nozzle width, ft
X	Axial distance relative to nozzle exit plane

Δ_{shld}	Shielding SPL difference, dB
θ	Directivity angle (with respect to engine inlet), deg
θ'	Effective directivity angle, θ ($V_{i \text{ or } j}$?/c_{amb})
λ	Wavelength of sound, ft (m)
ϕ	Azimuthal angle, deg

Subscripts

amb	Ambient property
corner	Corner of slot nozzle
eq	Equivalent
exit	Exit of nozzle
h	Hydraulic
I	Inner stream (core)
j	Jet
L	Large-scale mixing noise
mix	Fully-mixed (mass averaged)
O	Outer stream (fan)
pk	Peak of noise spectrum at each angle
S	Small-scale mixing noise
Sor	Source location
T	Transitional/intermediate-scale mixing noise
te	Trailing edge

References

1. Rulis, R.J., "STOL Noise Sources and Fan Noise Treatment," NASA SP–311, pp. 259–290, May 1972.
2. "Civil Aviation Research and Development Policy Study Report," NASA SP–265 (DOT SP–10–4), March 1971.
3. "Civil Aviation Research and Development Policy Study, Supporting Papers," NASA SP–266 (DOT–10–5), March 1971.
4. "Turbo-Taxi," Air & Space – Smithsonian, Vol. 20, No. 2, June–July 2005, p. 12.
5. Kinzie, K.W., Schein, D.B., and Solomon, W.D., Jr., "Experiments and Analyses of Distributed Exhaust Nozzles," AIAA–2002–2555, June 2002.
6. Ahuja, K.K., Gaeta, R.J., Hellman, B., Schein, D.B., and Solomon, W.D., Jr., "Distributed Exhaust Nozzles for Jet Noise Reduction," GTRI Report A6221/2001–1, NASA Grant NAG3–2352, December 31, 2001.
7. Kim, H.D. and Saunders, J.D., "Embedded Wing Propulsion Conceptual Study," (Conf. Paper?), 2004/2005.
8. Molloy, J.K., Grantham, W.D., and Neubauer, M.J., Jr., "Noise and Economic Characteristics of an Advanced Blended Supersonic Transport Concept," NASA TP–2073, September 1982.
9. Kawai, R., "Quiet Cruise Efficient Short Take-Off and Landing Subsonic System, Boeing Technology Phantom Works, Huntington Beach, CA, Report to NASA Glenn Research Center, Contract NAS3–01140, Task Order #28, NASA CR to be published, 2006.
10. Stone, J.R. and Krejsa, "Initial Noise Assessment of an Embedded-Wing-Propulsion Concept Vehicle, Subtask 1.1—Vehicle Acoustic Requirements: Past Experience," Diversitech Report to NASA Glenn Research Center, Purchase Order No.: NNC05VD49P, June 27, 2005.
11. Clark, B.J., "Computer Program to Predict Aircraft Noise Levels," NASA TP–1913, September 1981.
12. Stone, J.R., Krejsa, E.A., and Clark, B.J., "Jet Noise Modeling for Suppressed and Unsuppressed Aircraft in Flight," MTC Report to NASA GRC, Contract NAS3–00178, Task No. 10, Final Report, October 2003.
13. Dunn, D.G. and Peart, N.A., "Aircraft Noise Source and Contour Estimation," Boeing Commercial Airplane Co. Document D6–60233, Contract NAS2–6969, NASA TP–1412, 1973.
14. Stone, Krejsa, E.A., and Clark, B.J., "Enhanced Core Noise Modeling for Turbofan Engines," MTC Report to Glenn Research Center Contract NAS3–00178, Task Order 15, December 30, 2004.
15. Heidmann, M.F., "Interim Prediction Model for Fan and Compressor Source Noise," NASA TM X–71763, 1979.
16. Krejsa, E.A. and Valerino, M.F., "Interim Prediction Method for Turbine Noise," NASA TM X–73566, 1976.
17. Stone, J.R., "Interim Prediction Method for Jet Noise," NASA TM X–71618, November 1974.
18. Stone, J.R., Clark, B.J., and Krejsa, E.A., "2-D Mixer Ejector Nozzle Noise Analyses and Prediction Code Development," Modern Technologies Corporation Report to General Electric, Purchase Order No. 200–1Q–1BN44510, Contract NAS3–27235, December 1999. (Subject to Limited Exclusive Rights restrictions until December 2004.)
19. Reshotko, M., Goodykoontz, J.H., and Dorsch, R.G., "Engine-Over-the-Wing Noise Research," J. Aircraft, Vol. 11, No. 4, April 1974, pp. 195–196. (Also NASA TM–68246, 1973).
20. Janardan, B.A., Hoff, G.E., Barter, J.W., Martens, S., and Gliebe, P.R. (GEAE), and Mengle, V., and Dalton, W.N. (Allison Engine Co.), "AST Critical Propulsion and Noise Reduction Technologies for Future Commercial Subsonic Engines—Separate-Flow Exhaust System Noise Reduction Evaluation," Final Report: NAS3–27720, Area of Interest 14.3, General Electric Report R98AEB152, May 1998.
21. Richard W. Shaw (Program Manager) "Revolutionary Aero-Space Engine Research—A Summary Report of Work Element 1," Contract NAS3–01140, Revolutionary Aero-Space Engine Research, Task Order # 28, July 15, 2005.

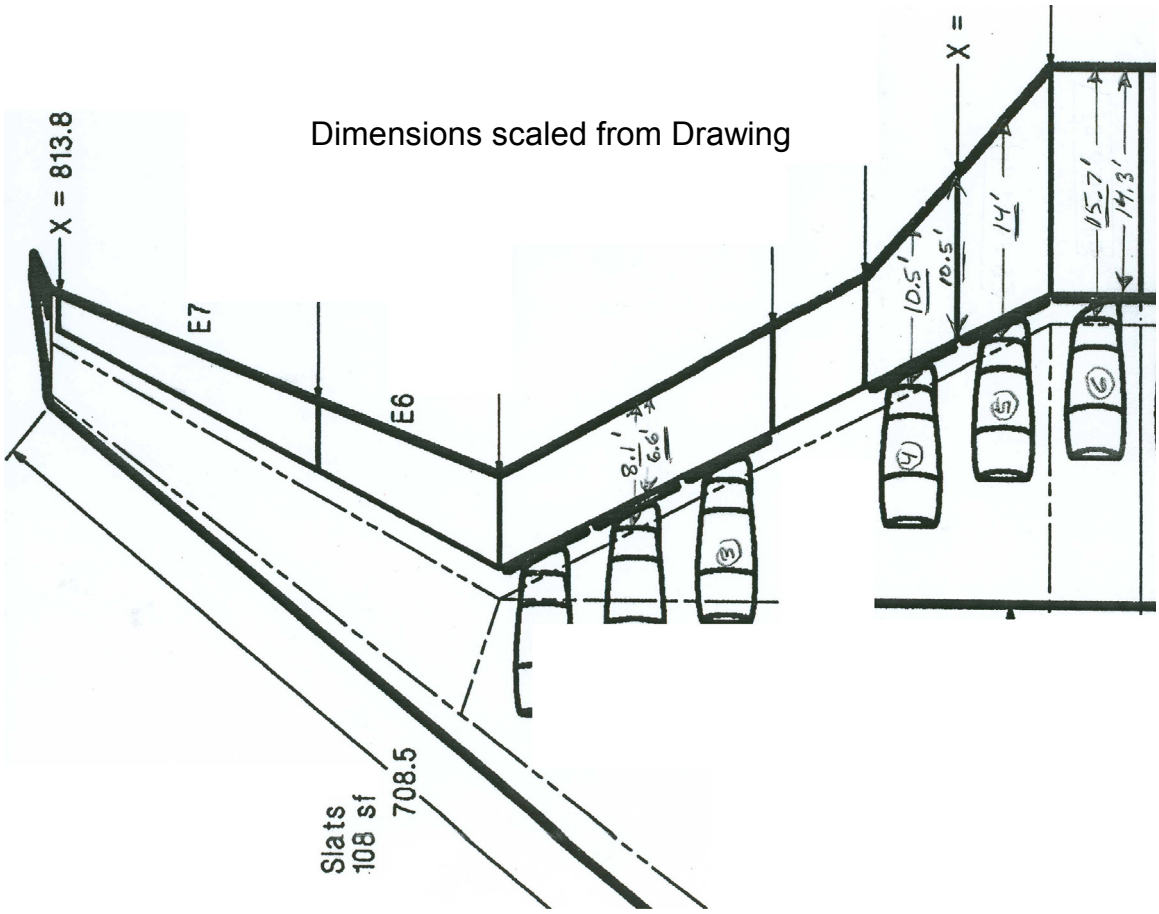

Figure 1 - Engine/Wing/Flap Geometry. (Engine and slot nozzle distances from trailing edge handwritten in ft.)

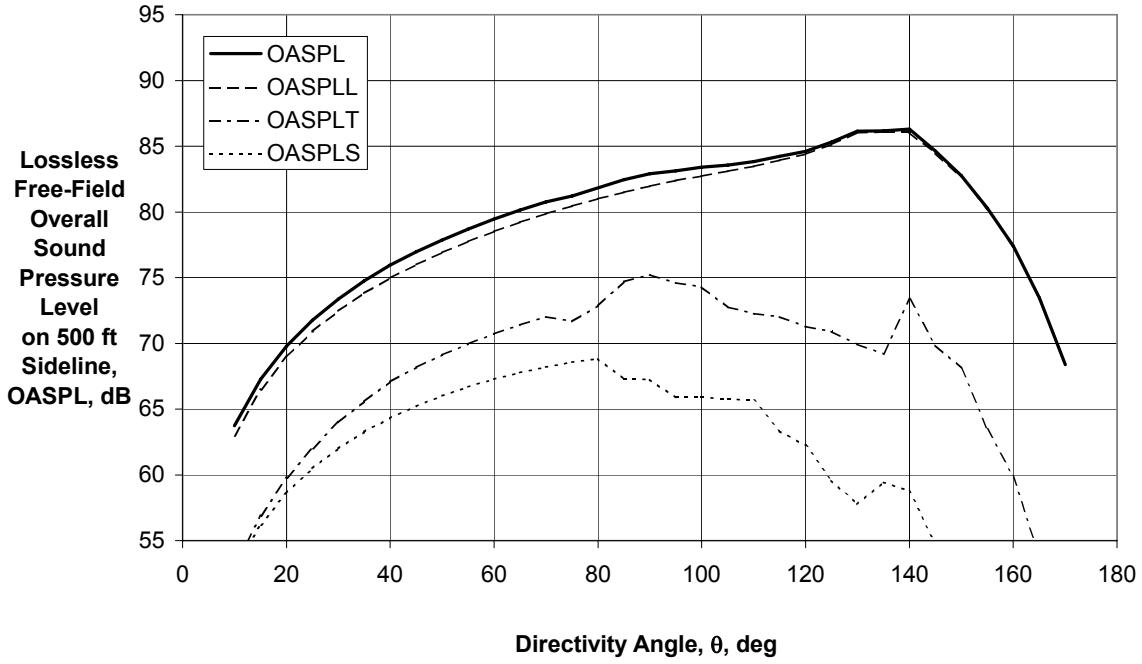

Figure 2 - Predicted Component and Total Noise Directivities for Slot Nozzle with SNPR = 1.85, M_a = 0.25 and ϕ = 25 deg

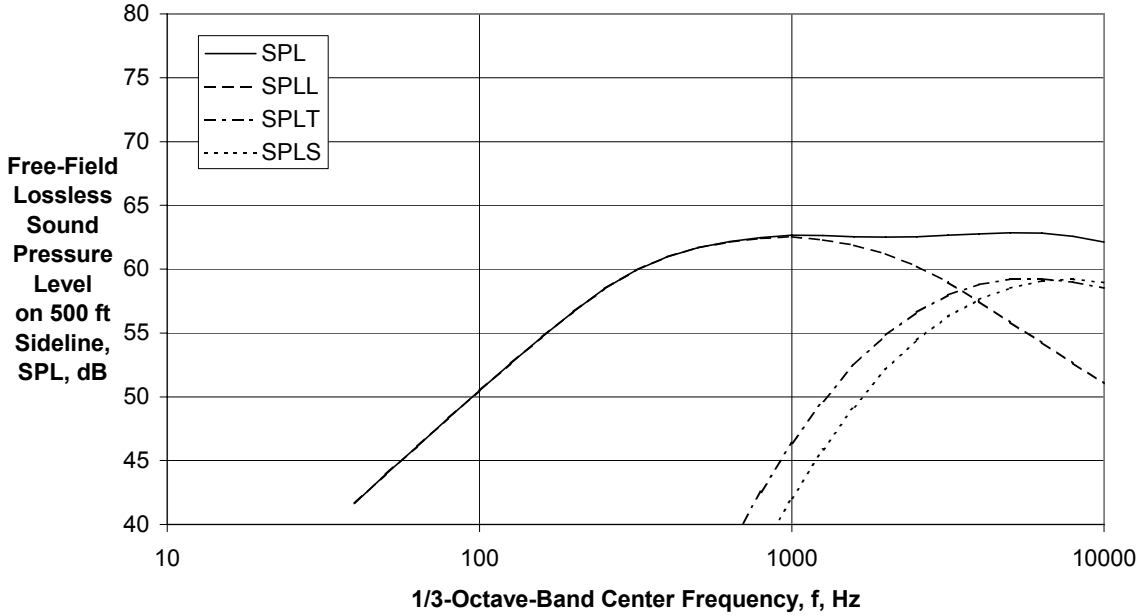

(a) Directivity Angle θ = 30 deg

Figure 3 - Predicted Component and Total Noise Spectra for Slot Nozzle with SNPR = 1.85, M_a = 0.25 and ϕ = 25 deg

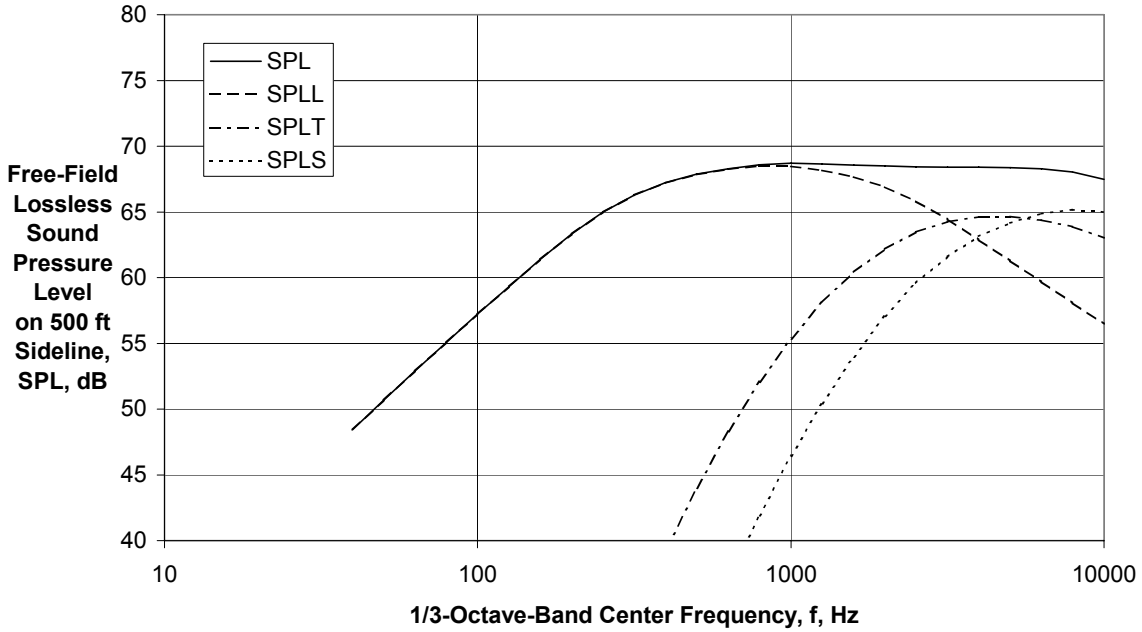

(b) Directivity Angle θ = 60 deg

Figure 3 - Predicted Component and Total Noise Spectra for Slot Nozzle with SNPR = 1.85, M_a = 0.25 and ϕ = 25 deg

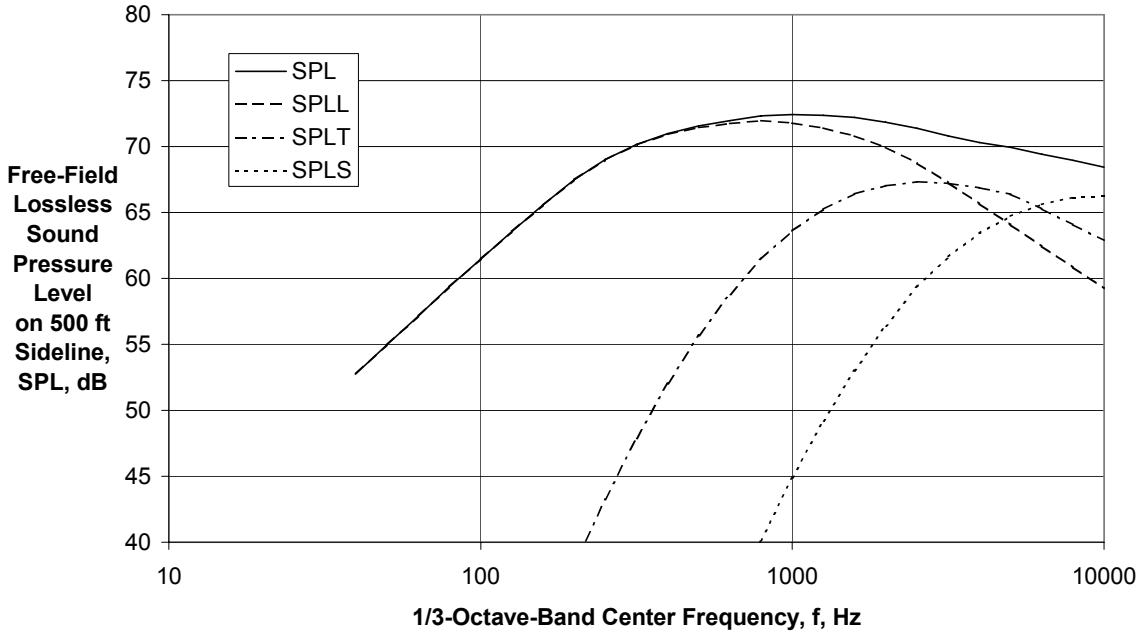

(c) Directivity Angle θ = 90 deg

Figure 3 - Predicted Component and Total Noise Spectra for Slot Nozzle with SNPR = 1.85, M_a = 0.25 and ϕ = 25 deg

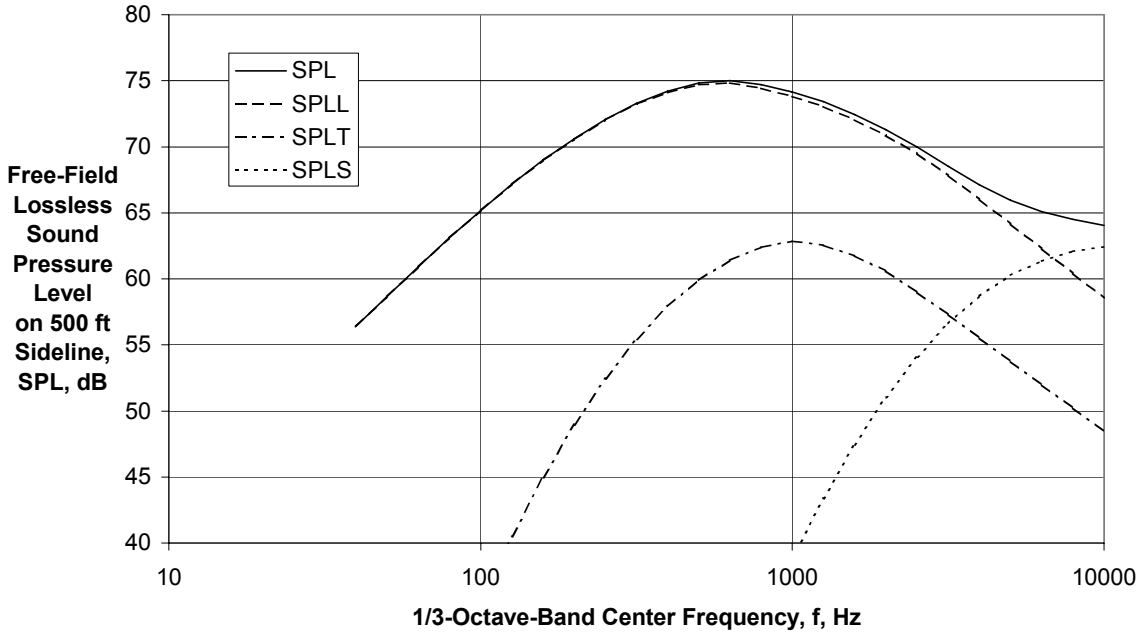

(d) Directivity Angle θ = 120 deg

Figure 3 - Predicted Component and Total Noise Spectra for Slot Nozzle with SNPR = 1.85, M_a = 0.25 and ϕ = 25 deg

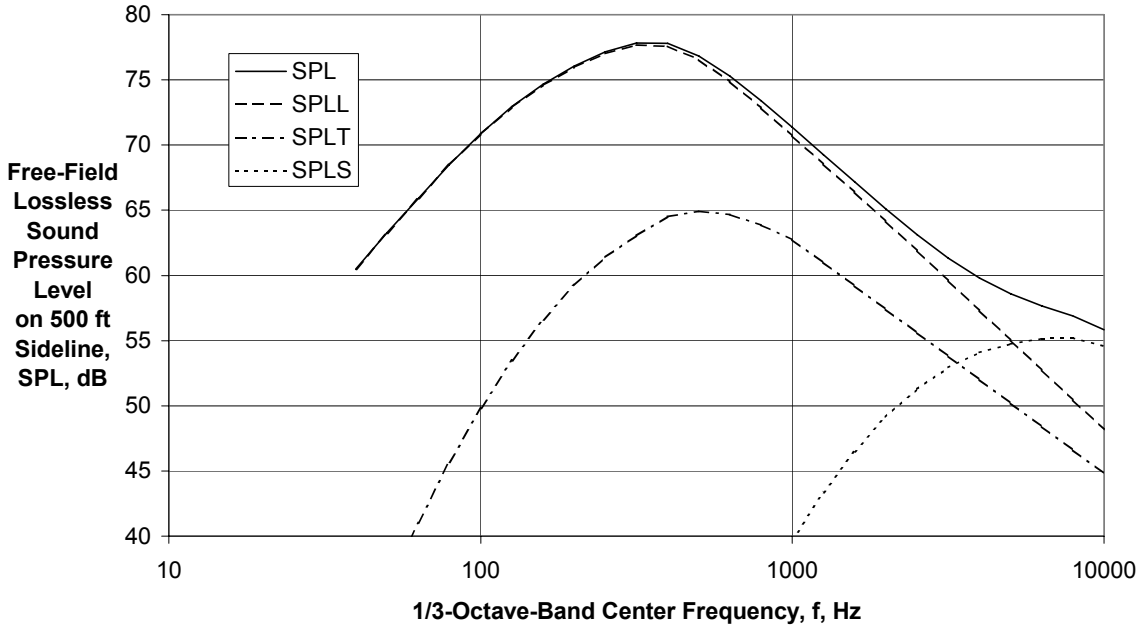

(e) Directivity Angle θ = 140 deg

Figure 3 - Predicted Component and Total Noise Spectra for Slot Nozzle with SNPR = 1.85, M_a = 0.25 and ϕ = 25 deg

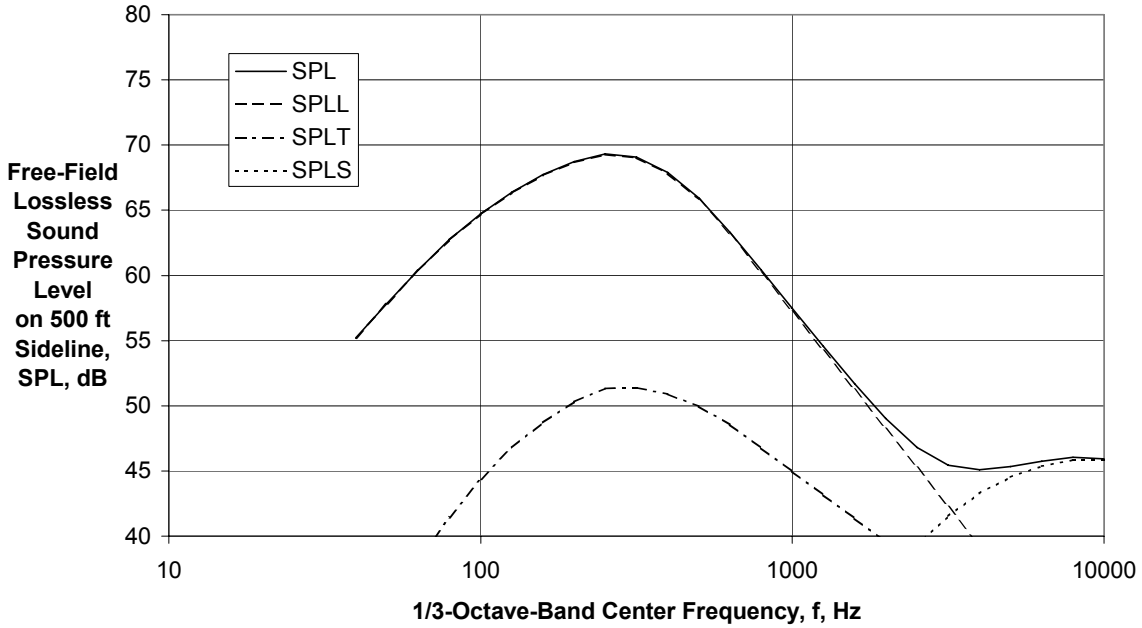

(f) Directivity Angle θ = 160 deg

Figure 3 - Predicted Component and Total Noise Spectra for Slot Nozzle with SNPR = 1.85, M_a = 0.25 and ϕ = 25 deg

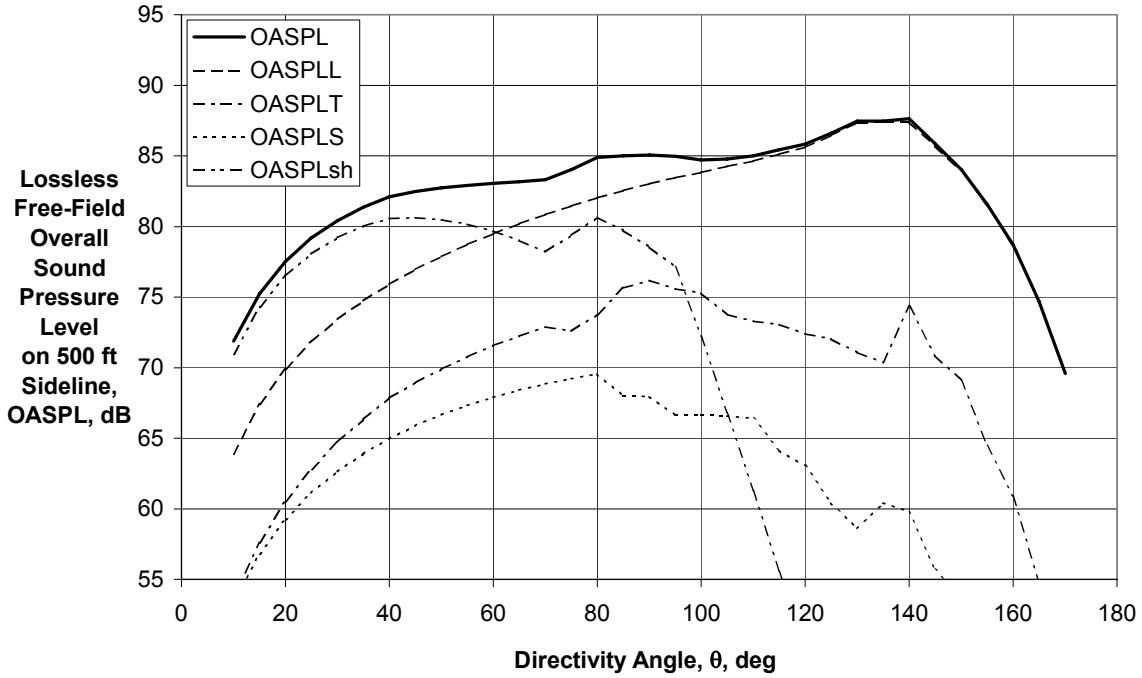

Figure 4 - Predicted and Component Total Directivities for Slot Nozzle with SNPR = 1.91, M_a = 0.25, ϕ = 25 deg

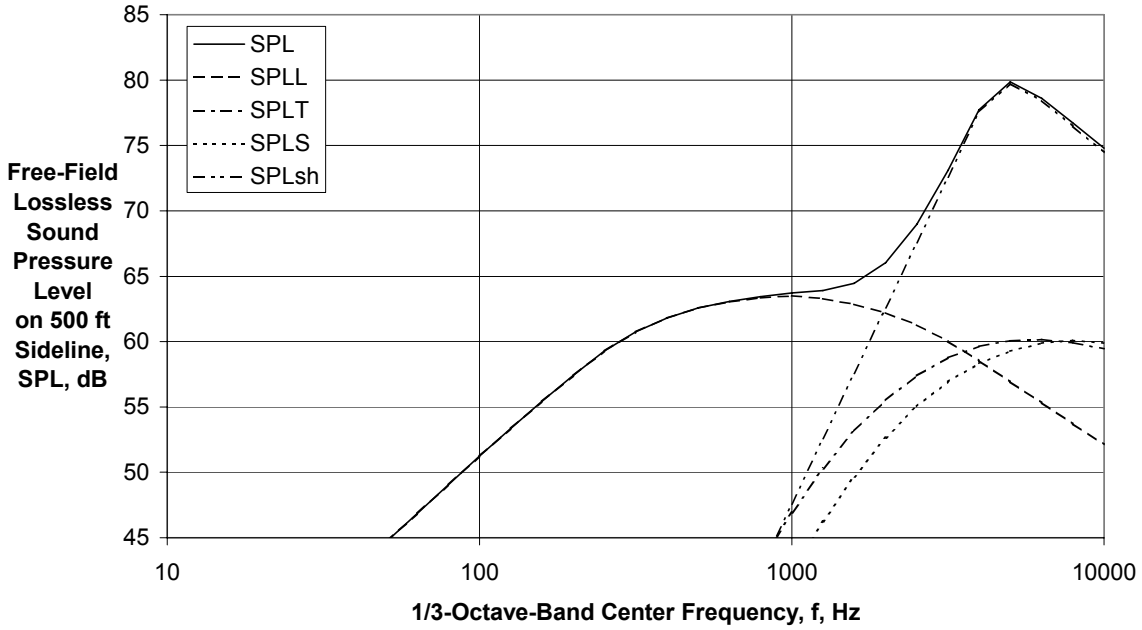

(a) Directivity Angle θ = 30 deg

Figure 5 - Predicted Component and Total Spectra for Slot Nozzle at SNPR = 1.91, M_a = 0.25, ϕ = 25 deg

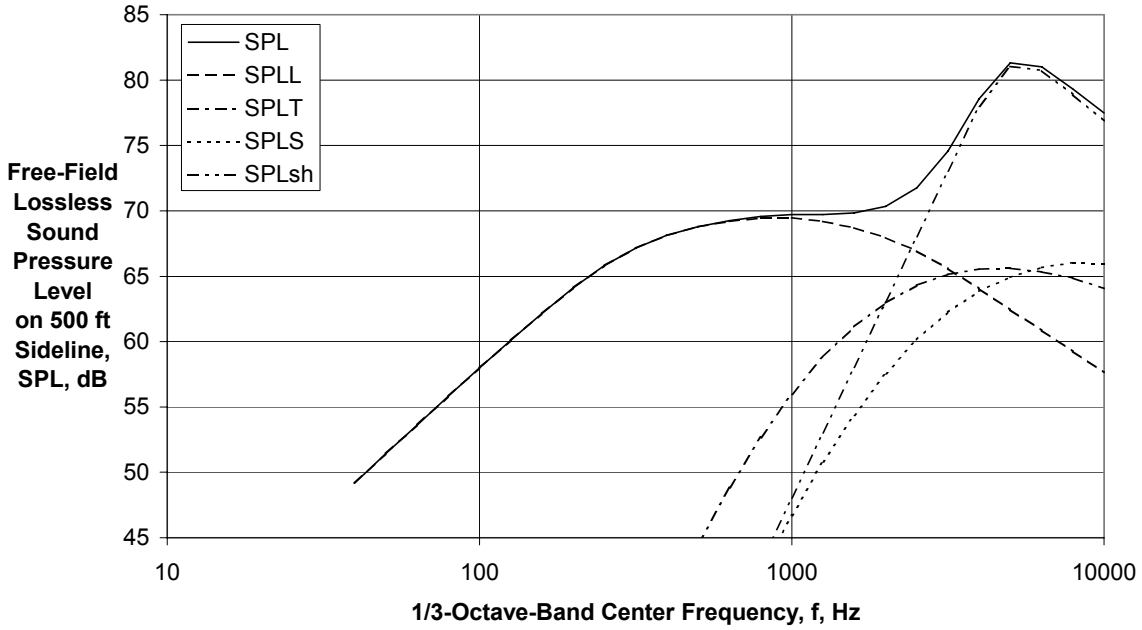

(b) Directivity Angle θ = 60 deg

Figure 5 - Predicted Component and Total Spectra for Slot Nozzle at SNPR = 1.91, M_a = 0.25, ϕ = 25 deg

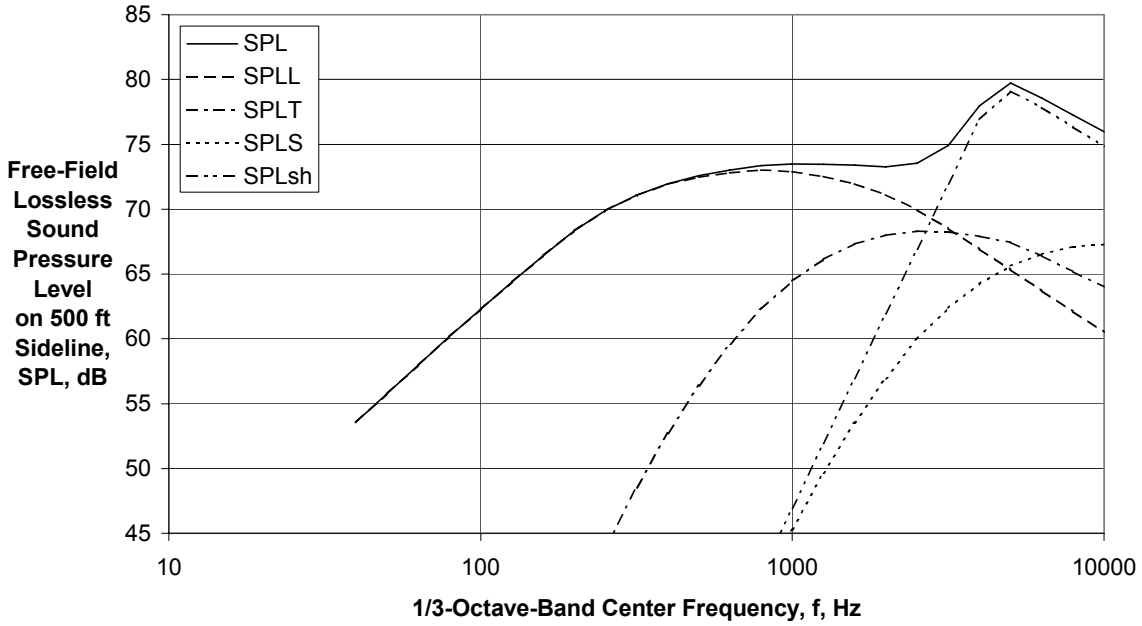

(c) Directivity Angle θ = 90 deg

Figure 5 - Predicted Component and Total Spectra for Slot Nozzle at SNPR = 1.91, M_a = 0.25, ϕ = 25 deg

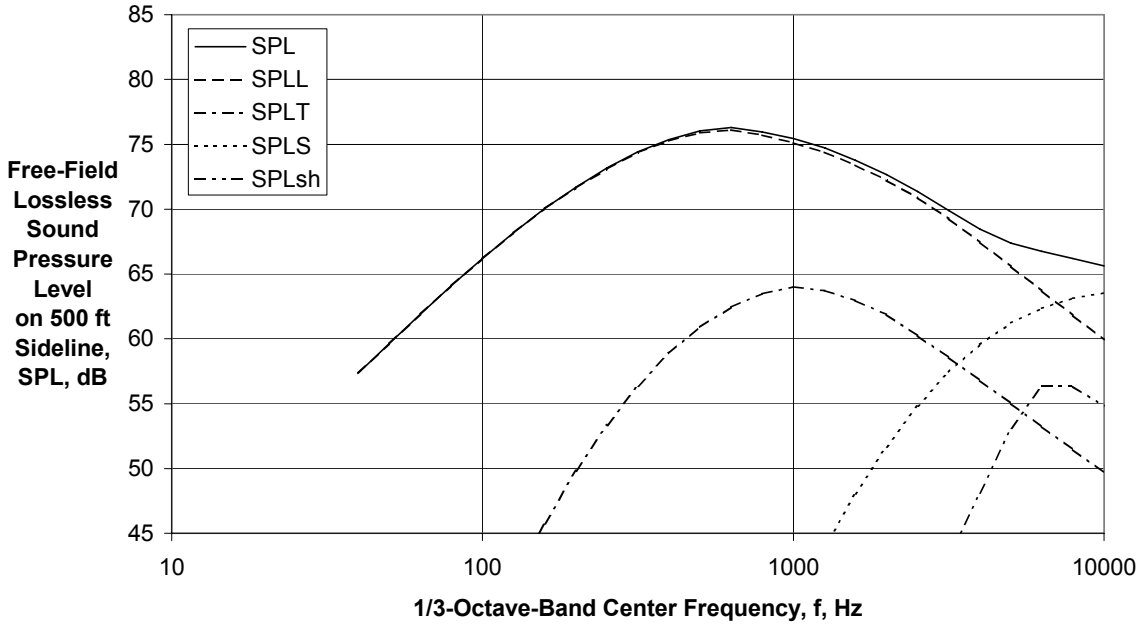

(d) Directivity Angle θ = 120 deg

Figure 5 - Predicted Component and Total Spectra for Slot Nozzle at SNPR = 1.91, M_a = 0.25, ϕ = 25 deg

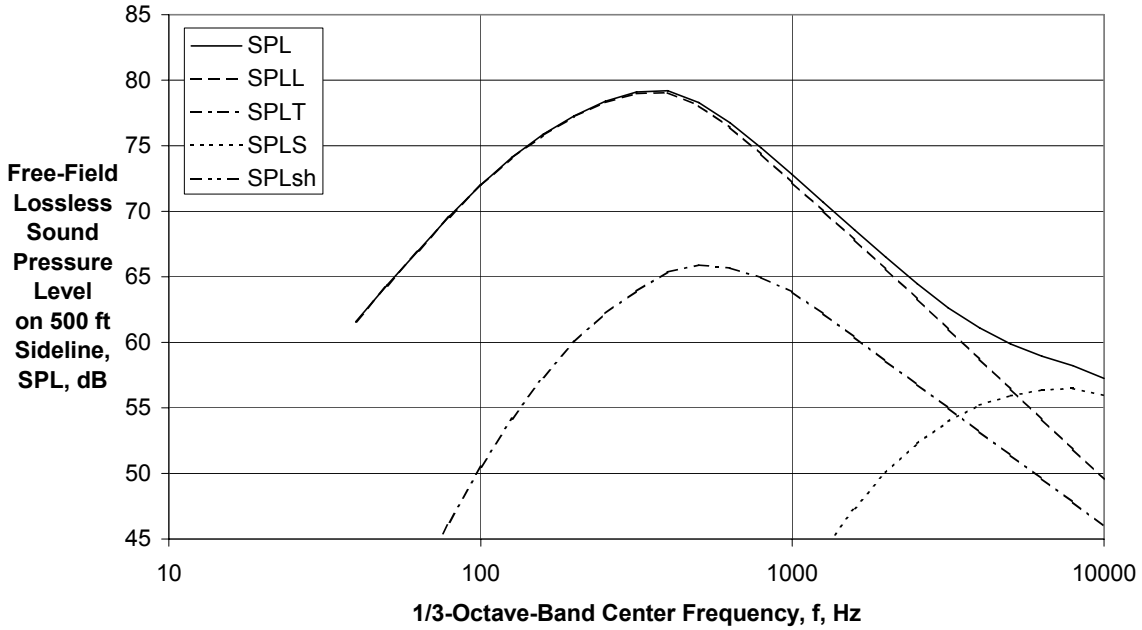

(e) Directivity Angle θ = 140 deg

Figure 5 - Predicted Component and Total Spectra for Slot Nozzle at SNPR = 1.91, M_a = 0.25, ϕ = 25 deg

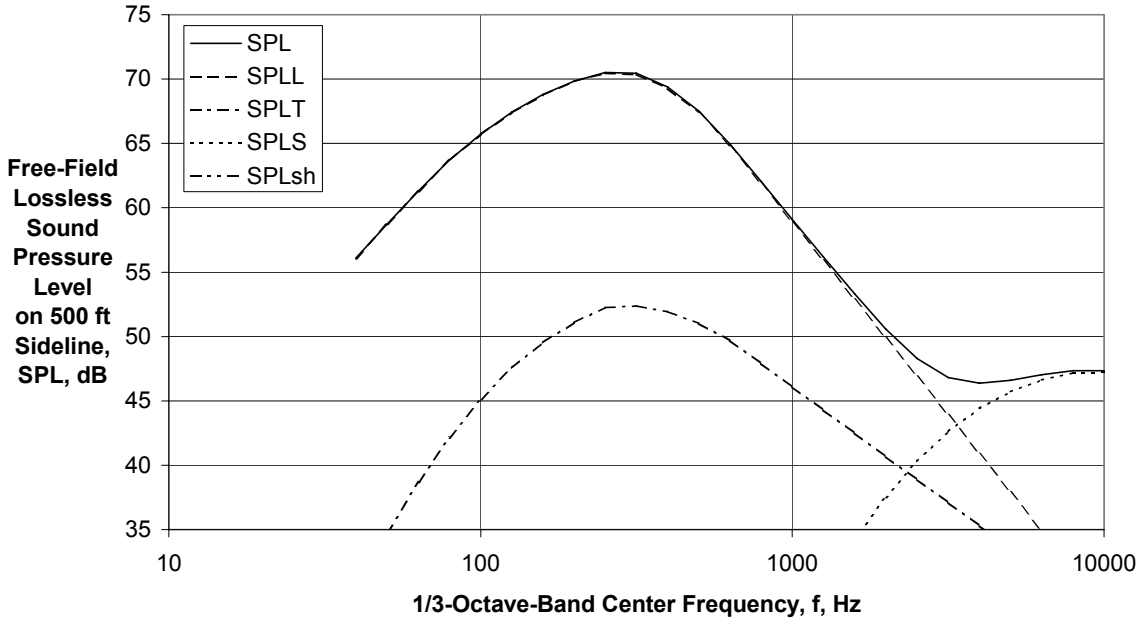

(f) Directivity Angle θ = 160 deg

Figure 5 - Predicted Component and Total Spectra for Slot Nozzle at SNPR = 1.91, M_a = 0.25, ϕ = 25 deg

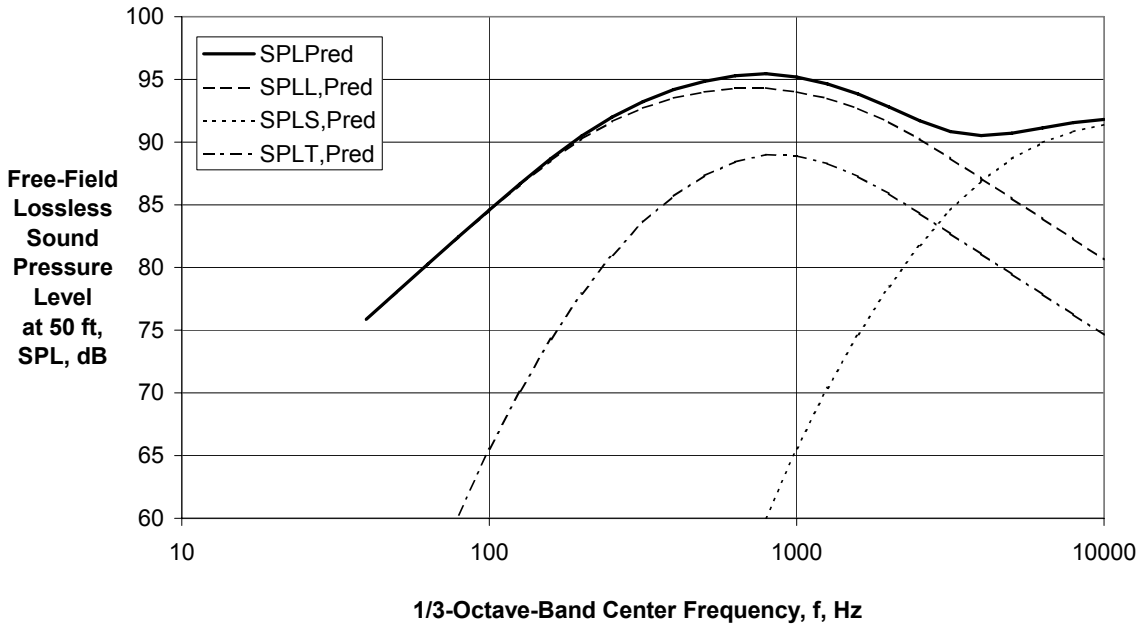

Figure 6 - Component and Total Predicted Spectra for 13-inch-Diameter Conical Nozzle of Reshotko, et al. (1973, Ref. 19) at θ = 120 deg and V_j = 985 ft/sec

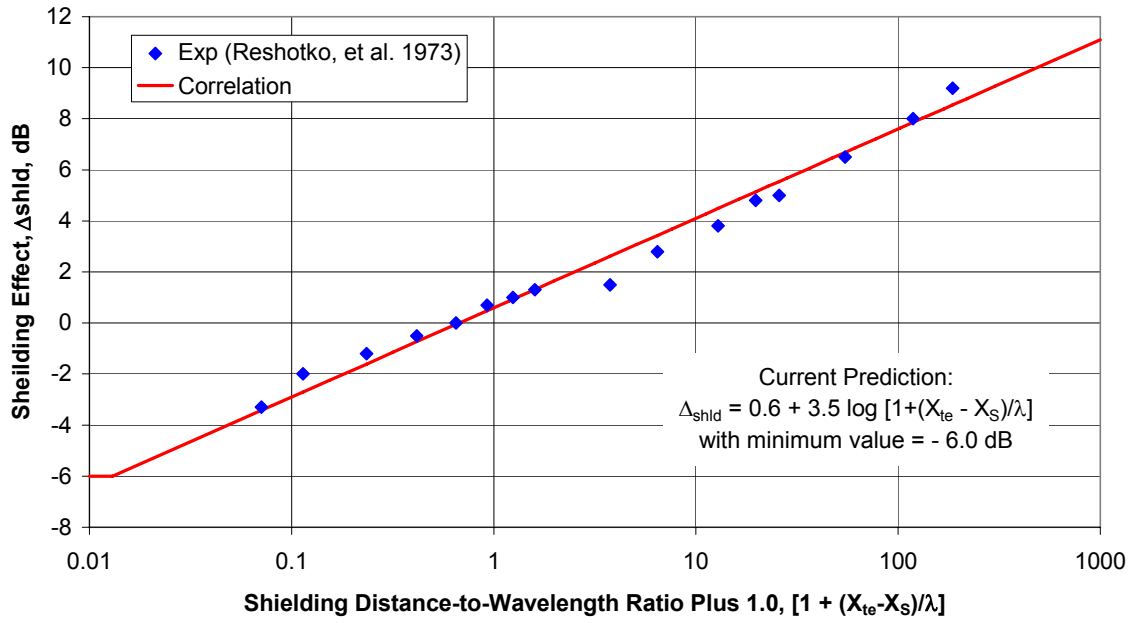

Figure 7 - Shielding vs. Shielding Distance to Wavelength Ratio Plus 1.0 at θ =120 deg and ϕ = 90 deg (Flyover) at Negative and Small (X_S-X_{te})/λ

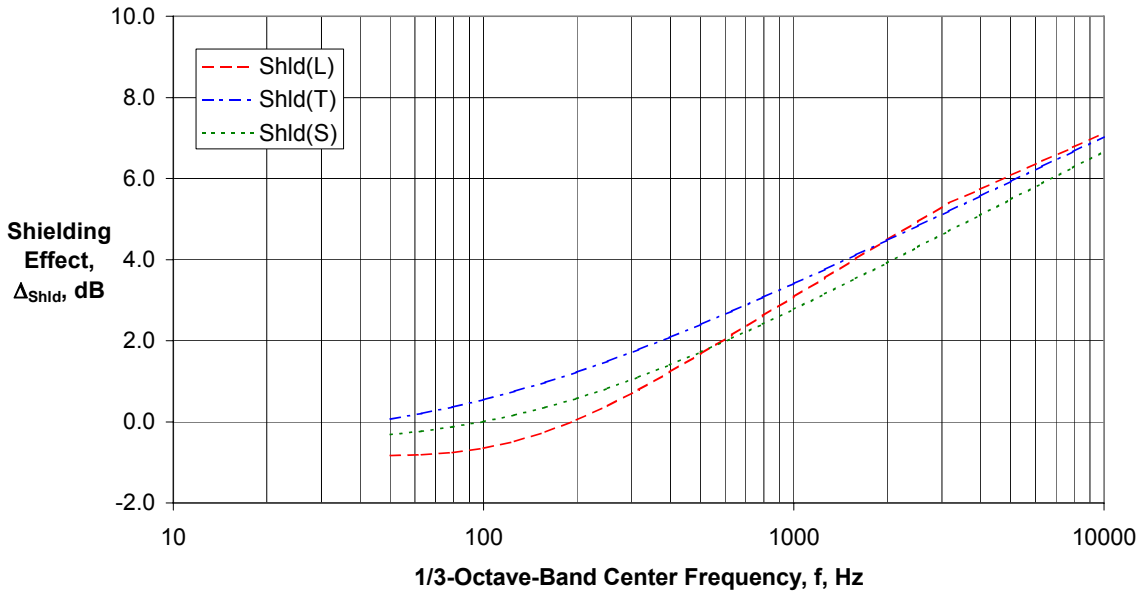

(a) Unsuppressed Engine Nozzle

Figure 8 - Calculated Wing Shielding Effects at Directivity Angle θ = 90 and Azimuthal Angle ϕ = 25 deg for BWB Airplane with Semi-Embedded Wing Propulsion

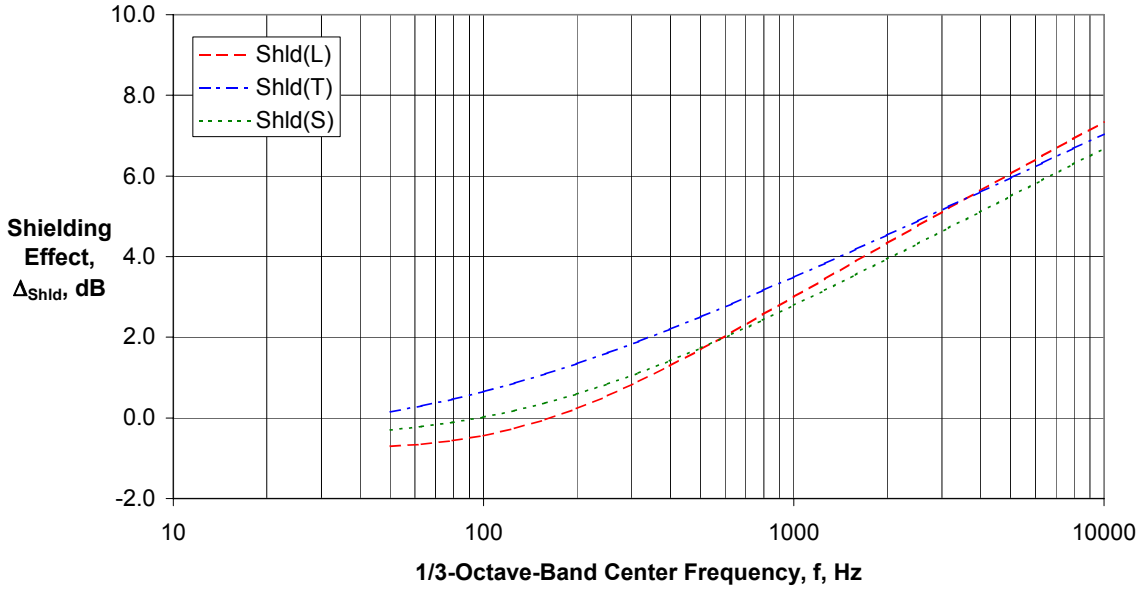

(b) Engine Nozzle with Chevrons

Figure 8 - Calculated Wing Shielding Effects at Directivity Angle θ = 90 and Azimuthal Angle ϕ = 25 deg for BWB Airplane with Semi-Embedded Wing Propulsion

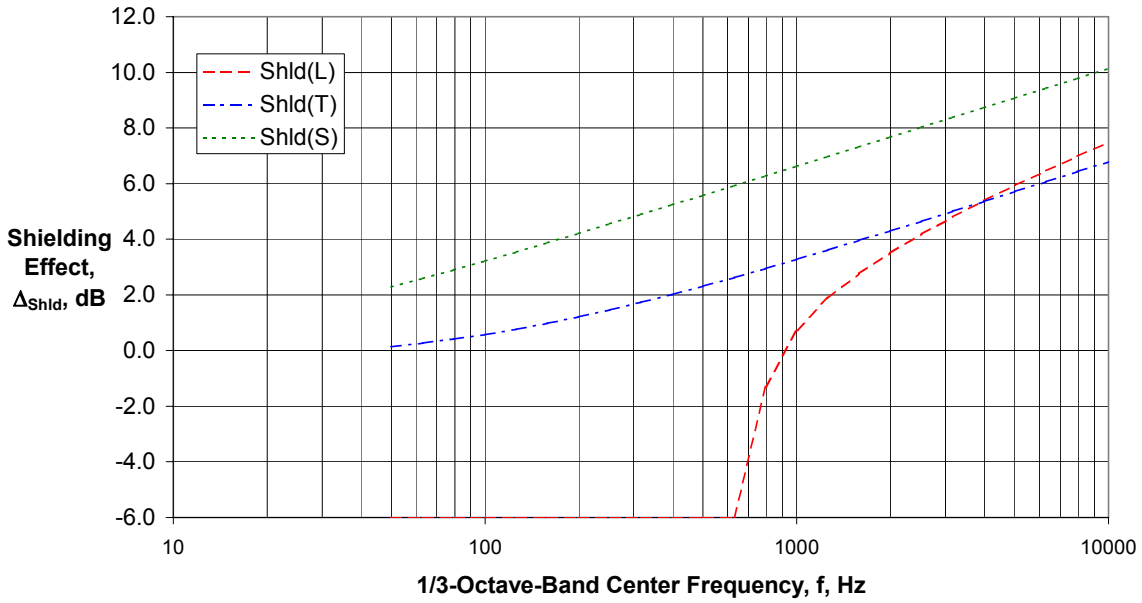

(c) IBF Slot Nozzle

Figure 8 - Calculated Wing Shielding Effects at Directivity Angle θ = 90 and Azimuthal Angle ϕ = 25 deg for BWB Airplane with Semi-Embedded Wing Propulsion

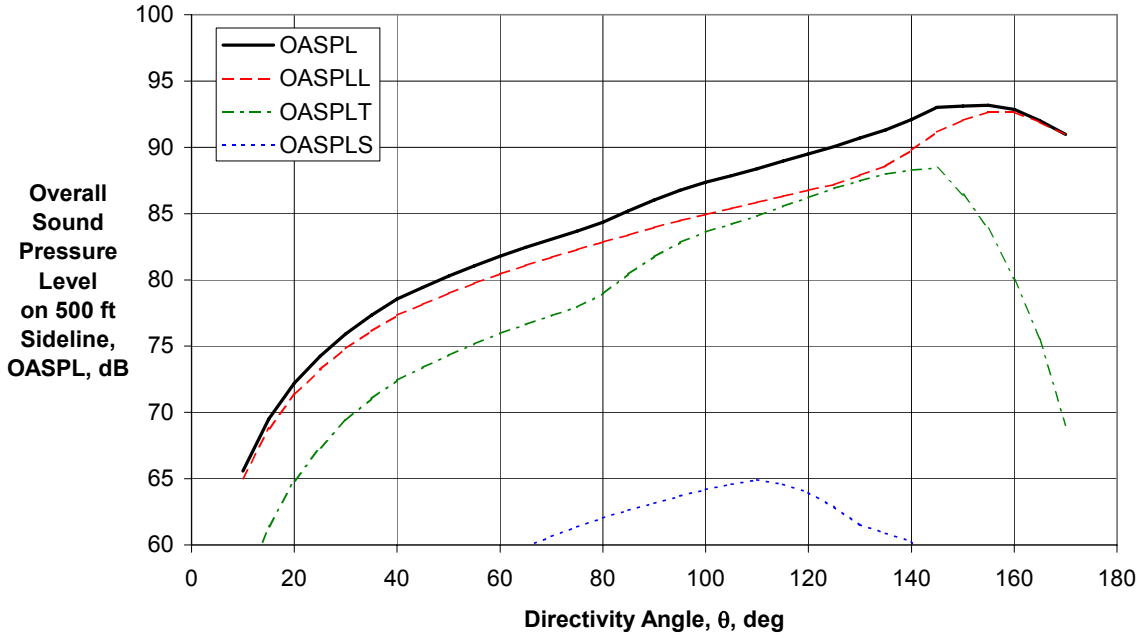

Figure 9 - Predicted Component and Total Coaxial Jet Noise Directivities for V_{mix}/c_{amb} = 1.085; M_a = 0.2, ϕ = 25 deg (BWB-CESTOL-EWP)

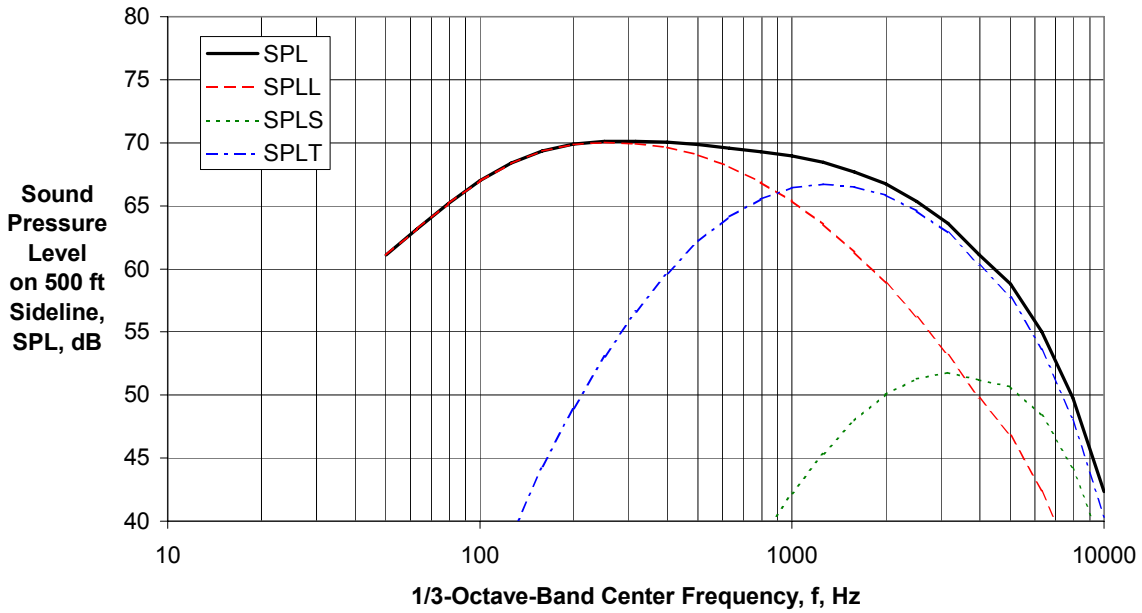

(a) Directivity Angle θ = 30 deg

Figure 10 - Predicted Component and Total Engine Coaxial Jet Noise Spectra for V_{mix}/c_{amb} = 1.085, M_a = 0.2, ϕ = 25 deg (BWB-CESTOL-EWP)

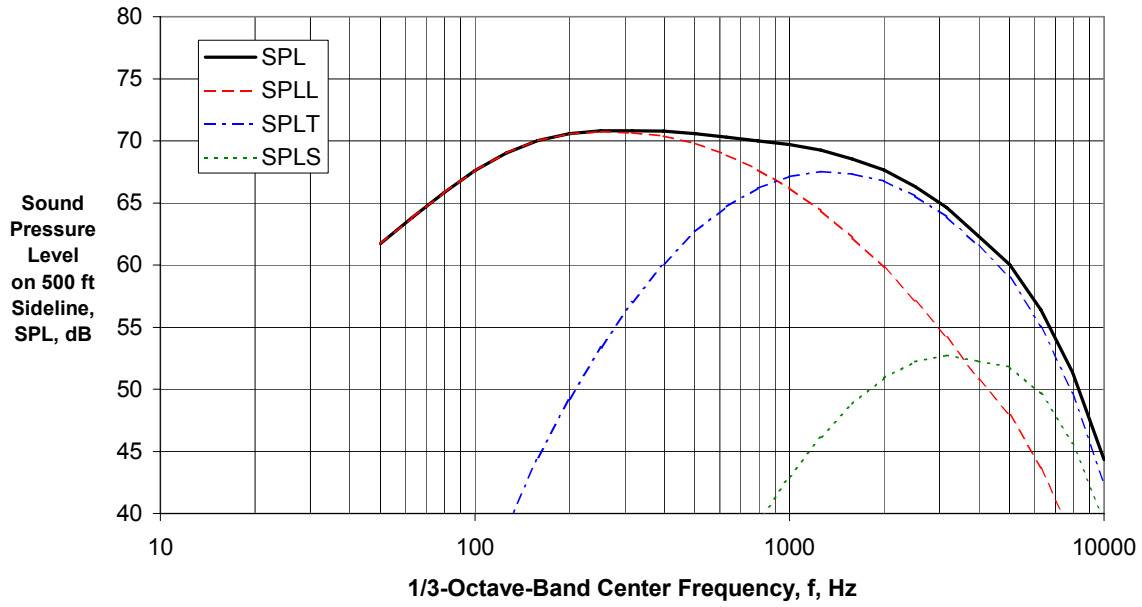

(b) Directivity Angle θ = 60 deg

Figure 10 - Predicted Component and Total Engine Coaxial Jet Noise Spectra for V_{mix}/c_{amb} = 1.085, M_a = 0.2, ϕ = 25 deg (BWB-CESTOL-EWP)

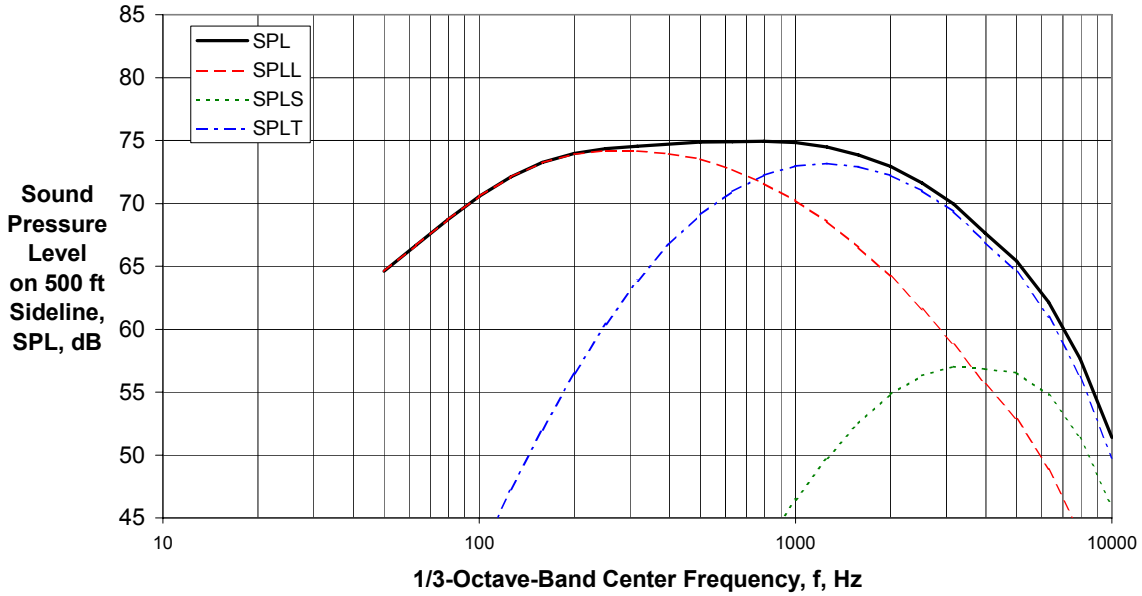

(c) Directivity Angle θ = 90 deg

Figure 10 - Predicted Component and Total Engine Coaxial Jet Noise Spectra for V_{mix}/c_{amb} = 1.085, M_a = 0.2, ϕ = 25 deg (BWB-CESTOL-EWP)

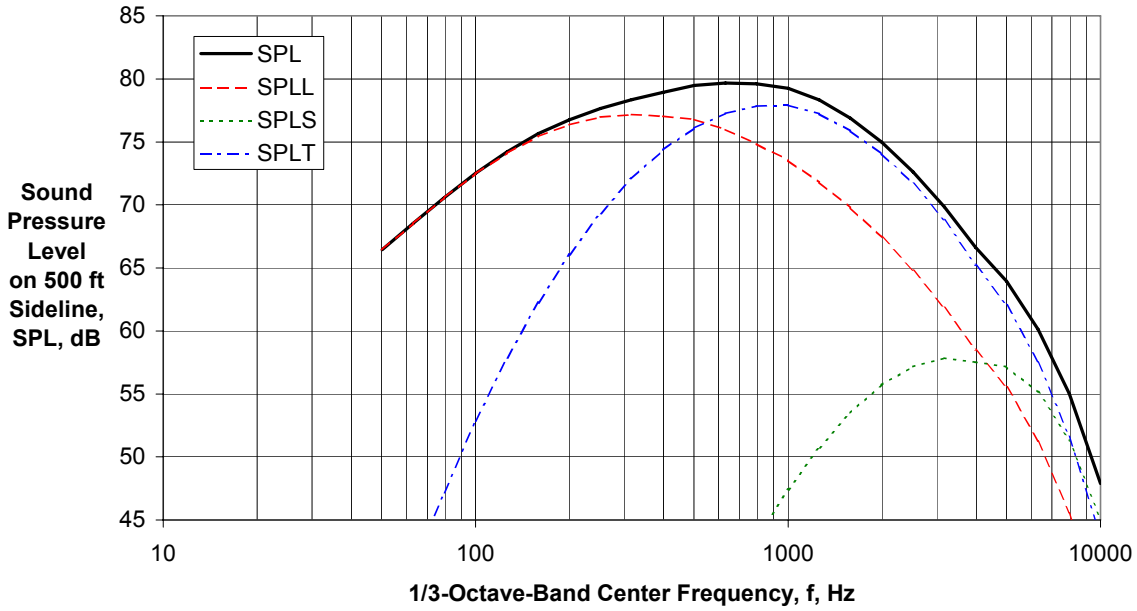

(d) Directivity Angle θ = 120 deg

Figure 10 - Predicted Component and Total Engine Coaxial Jet Noise Spectra for V_{mix}/c_{amb} = 1.085, M_a = 0.2, ϕ = 25 deg (BWB-CESTOL-EWP)

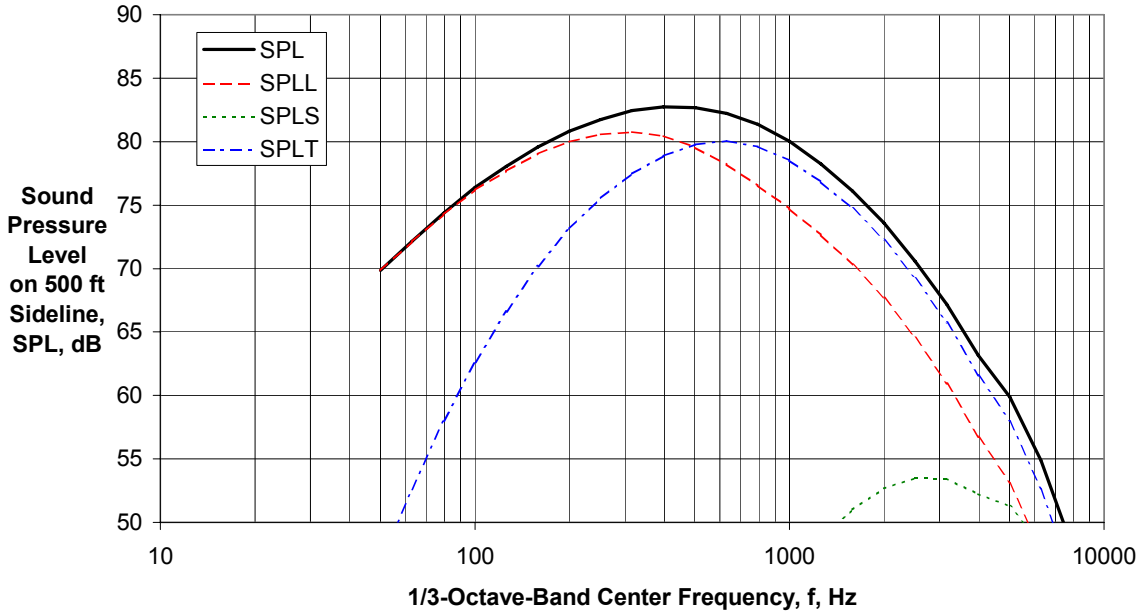

(e) Directivity Angle θ = 140 deg

Figure 10 - Predicted Component and Total Engine Coaxial Jet Noise Spectra for V_{mix}/c_{amb} = 1.085, M_a = 0.2, ϕ = 25 deg (BWB-CESTOL-EWP)

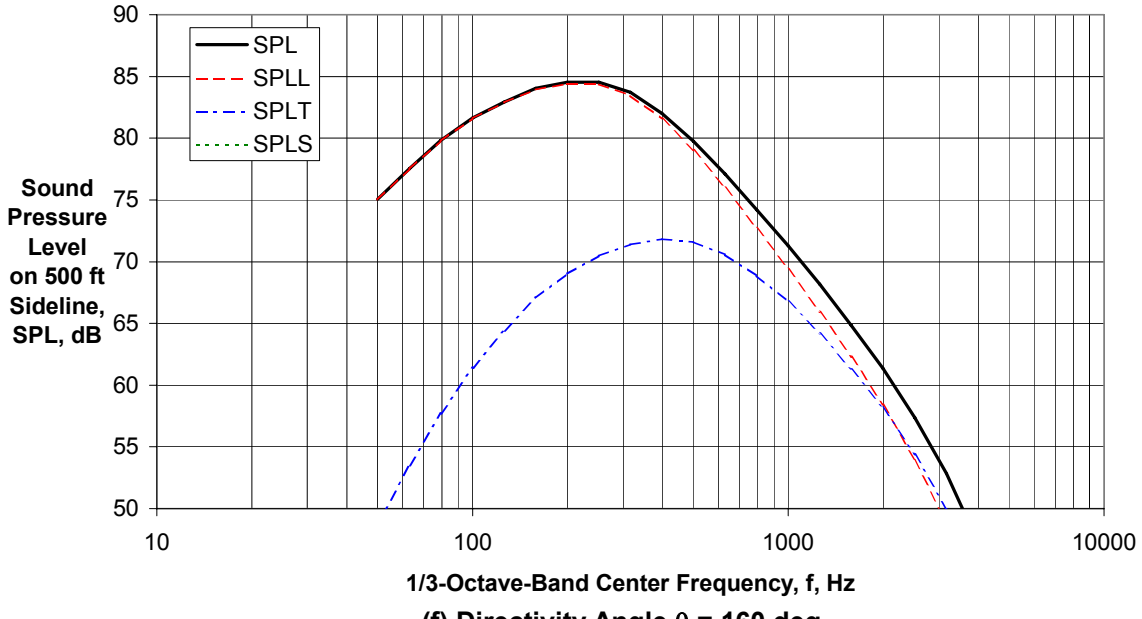

(f) Directivity Angle θ = 160 deg

Figure 10 - Predicted Component and Total Engine Coaxial Jet Noise Spectra for V_{mix}/c_{amb} = 1.085, M_a = 0.2, ϕ = 25 deg (BWB-CESTOL-EWP)

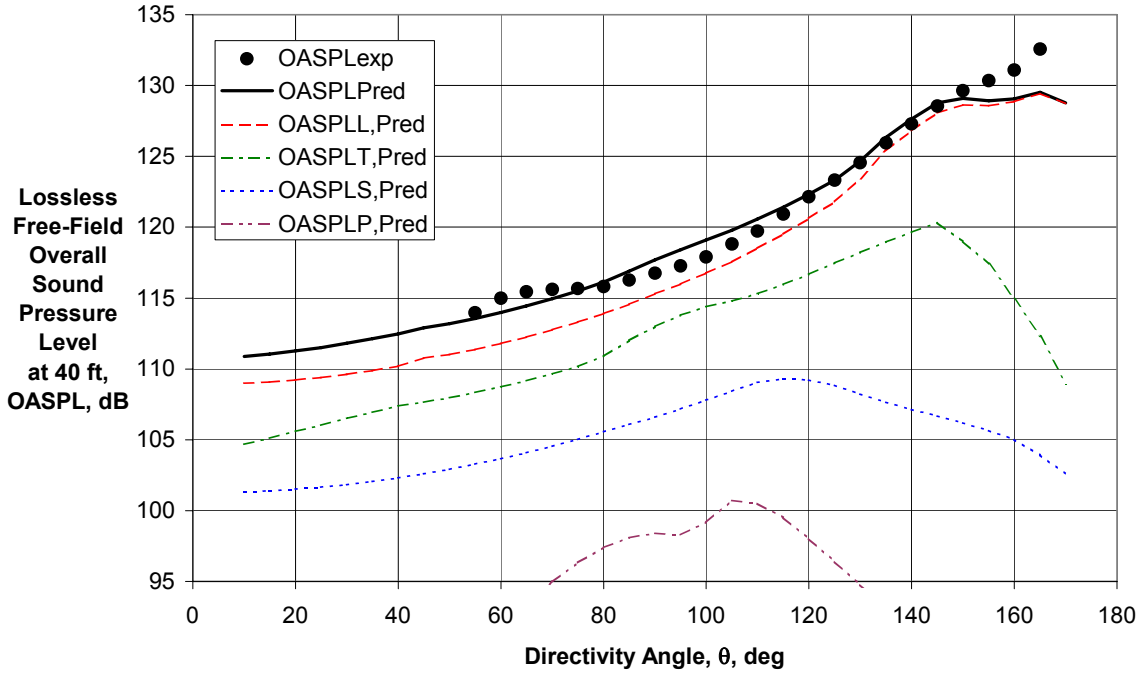

Figure 11 - Comparison of Experimental and Predicted OASPL Directivities for V_{mix}/c_{amb} = 1.086, M_a = 0.28 (Conf. 3BB, Rdg. 396)

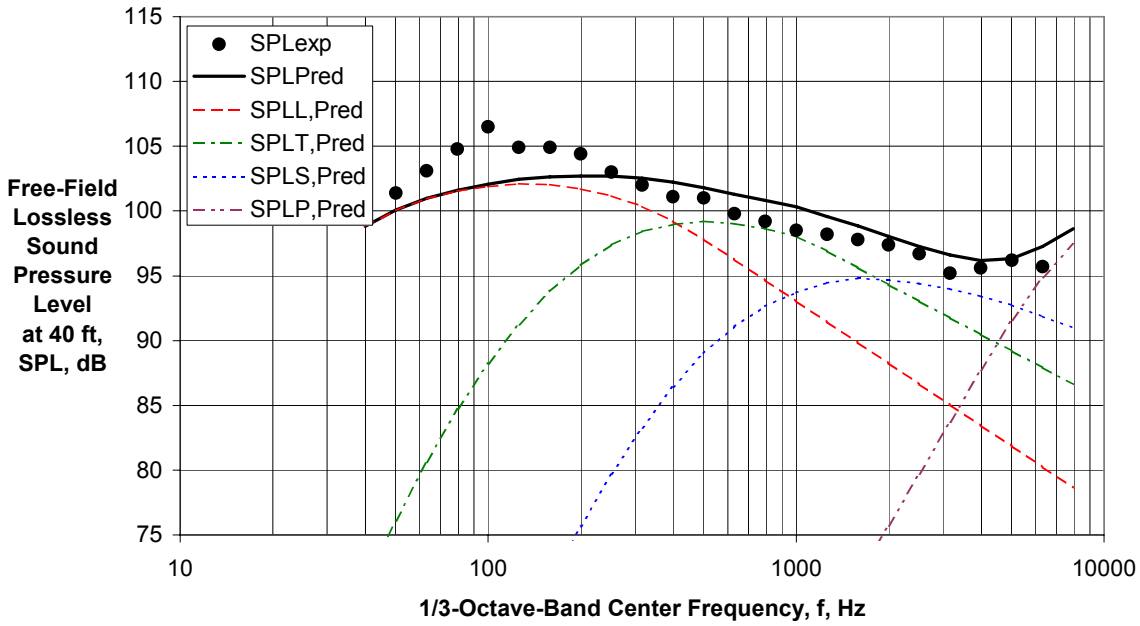

(a) Directivity Angle θ = 60 deg

Figure 12 - Comparison of Experimental and Predicted Spectra for V_{mix}/c_{amb} = 1.086, M_a = 0.28 (Conf. 3BB, Rdg. 396)

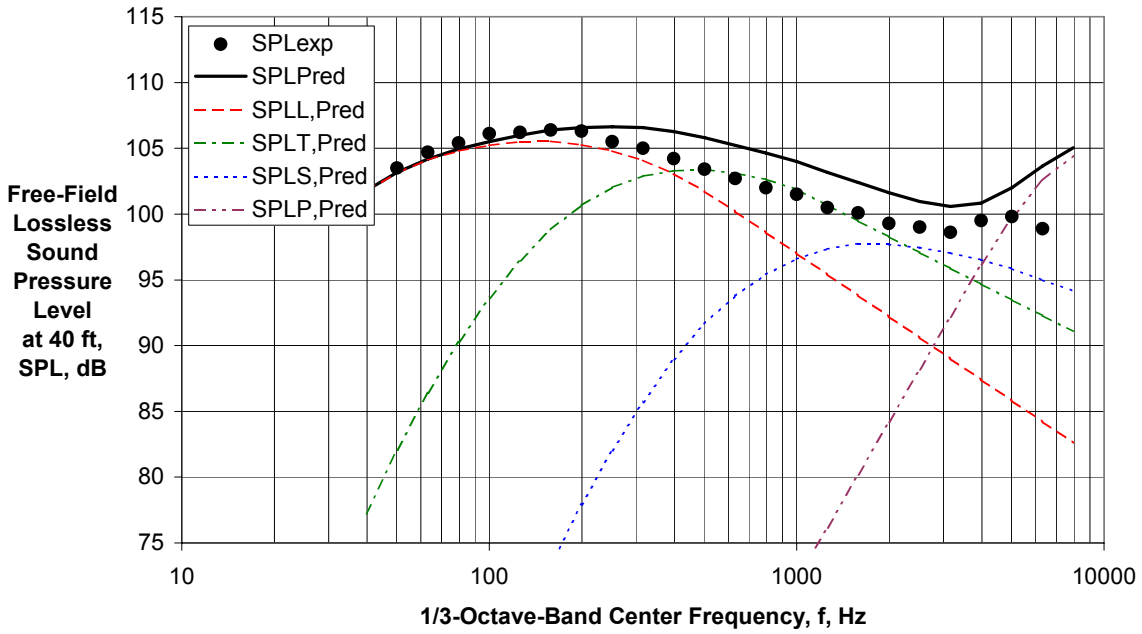

(b) Directivity Angle θ = 90 deg

Figure 12 - Comparison of Experimental and Predicted Spectra for V_{mix}/c_{amb} = 1.086, M_a = 0.28 (Conf. 3BB, Rdg. 396)

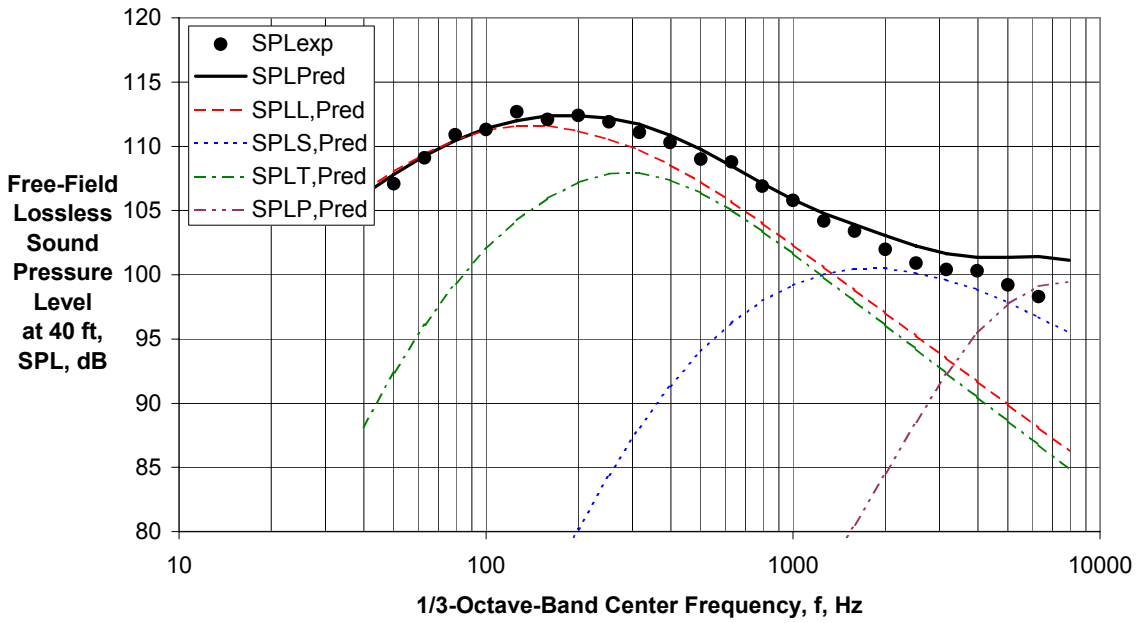

(c) Directivity Angle θ = 120 deg

Figure 12 - Comparison of Experimental and Predicted Spectra for V_{mix}/c_{amb} = 1.086, M_a = 0.28 (Conf. 3BB, Rdg. 396)

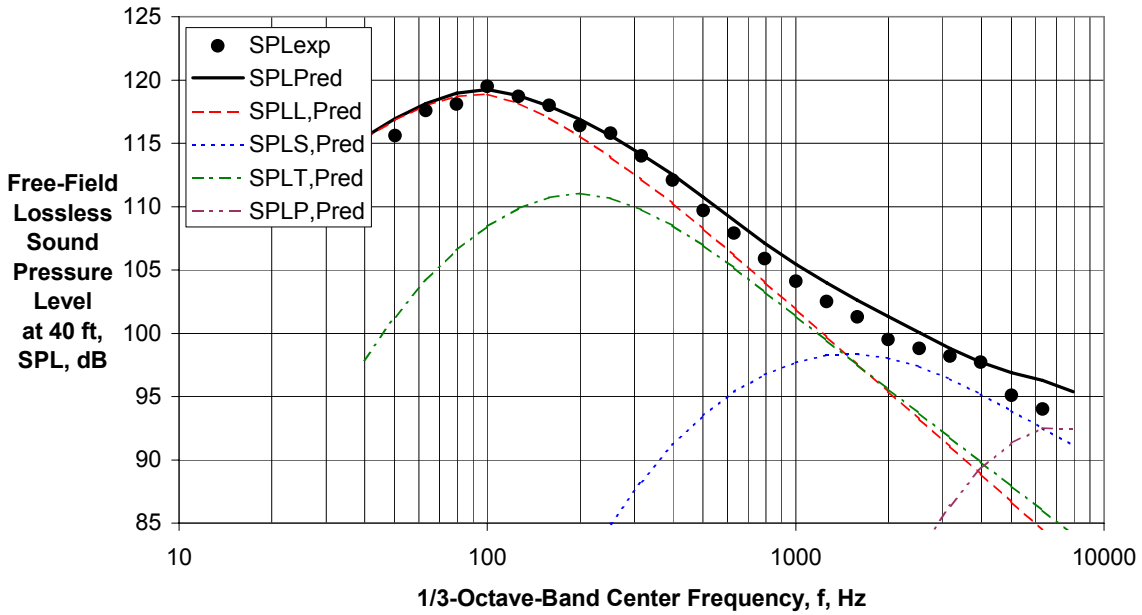

(d) Directivity Angle θ = 140 deg

Figure 12 - Comparison of Experimental and Predicted Spectra for V_{mix}/c_{amb} = 1.086, M_a = 0.28 (Conf. 3BB, Rdg. 396)

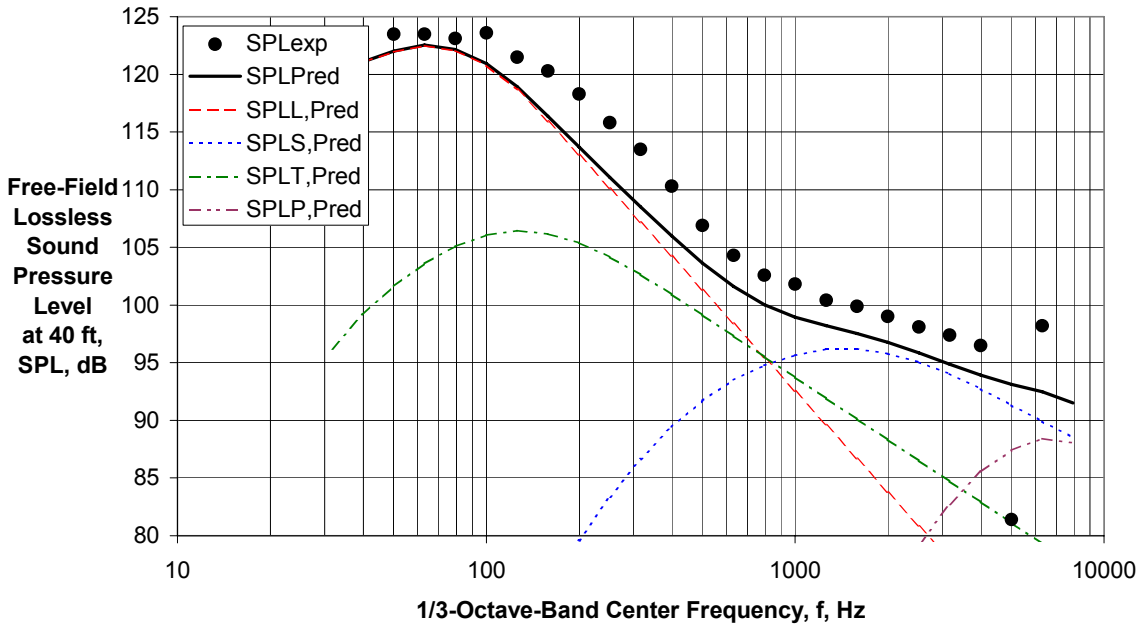

(e) Directivity Angle θ = 160 deg

Figure 12 - Comparison of Experimental and Predicted Spectra for V_{mix}/c_{amb} = 1.086, M_a = 0.28 (Conf. 3BB, Rdg. 396)

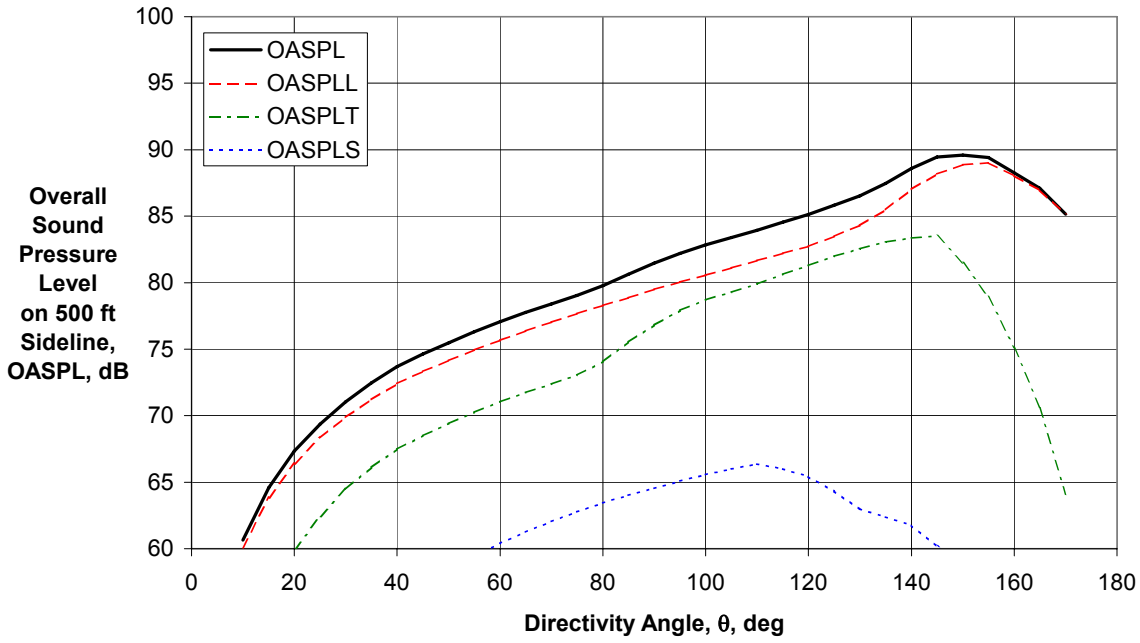

Figure 13 - Predicted Component and Total Engine Coaxial Chevron Nozzle Jet Noise Directivities for V_{mix}/c_{amb} = 1.085, M_a = 0.2, ϕ = 25 deg (BWB-CESTOL-EWP)

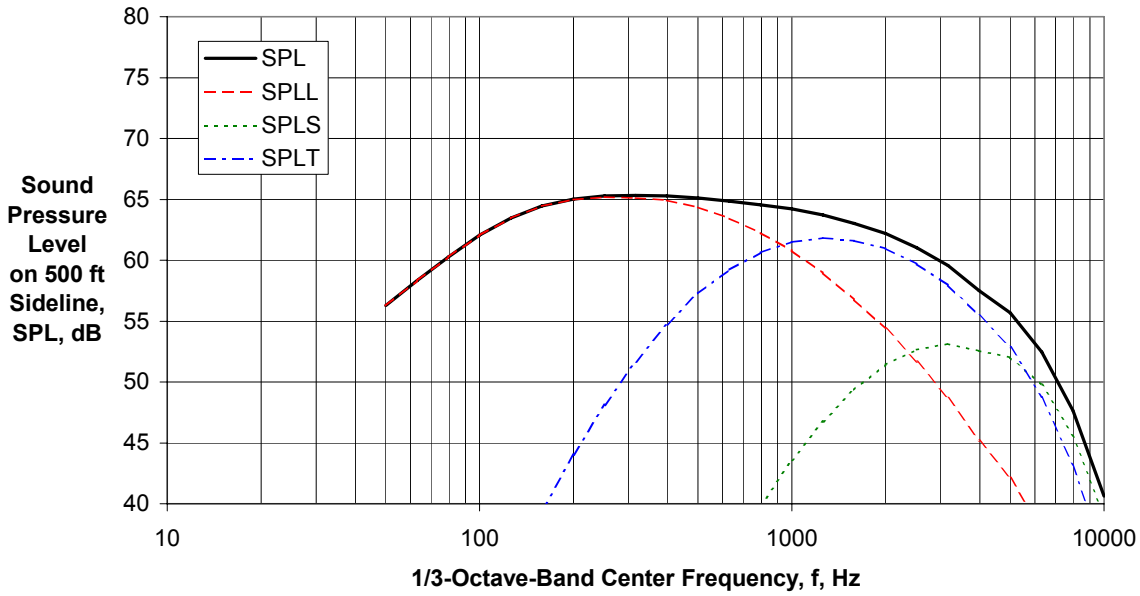

(a) Directivity Angle θ = 30 deg

Figure 14 - Predicted Component and Total Engine Coaxial Chevron Nozzle Jet Noise Spectra for V_{mix}/c_{amb} = 1.085, M_a = 0.2, ϕ = 25 deg (BWB-CESTOL-EWP)

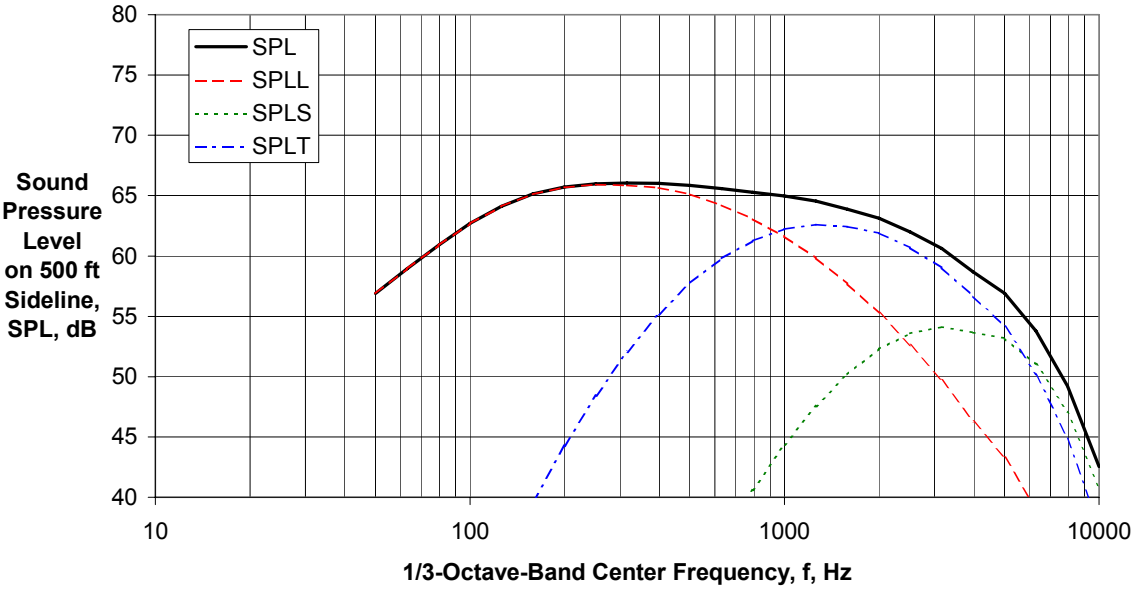

(b) Directivity Angle θ = 60 deg

Figure 14 - Predicted Component and Total Engine Coaxial Chevron Nozzle Jet Noise Spectra for V_{mix}/c_{amb} = 1.085, M_a = 0.2, ϕ = 25 deg (BWB-CESTOL-EWP)

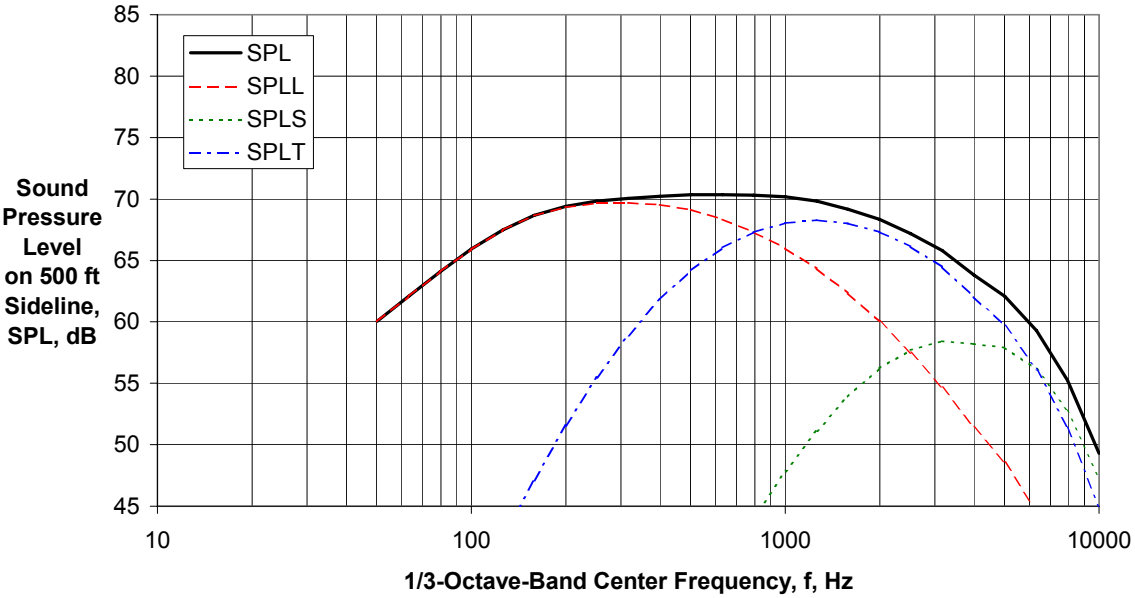

(c) Directivity Angle θ = 90 deg

Figure 14 - Predicted Component and Total Engine Coaxial Chevron Nozzle Jet Noise Spectra for V_{mix}/c_{amb} = 1.085, M_a = 0.2, ϕ = 25 deg (BWB-CESTOL-EWP)

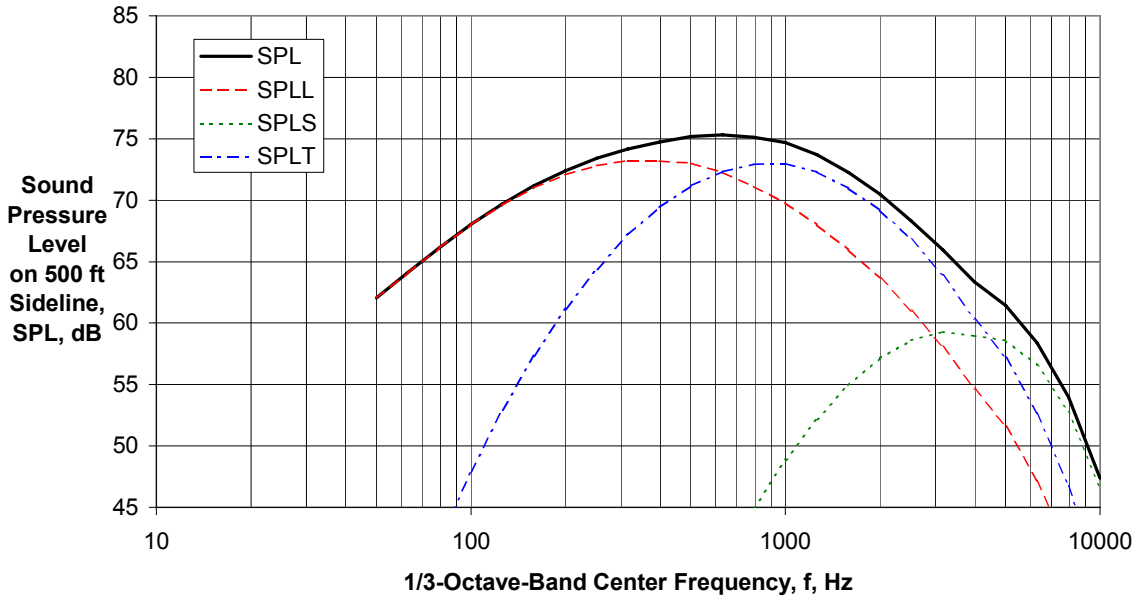

(d) Directivity Angle θ = 120 deg

Figure 14 - Predicted Component and Total Engine Coaxial Chevron Nozzle Jet Noise Spectra for V_{mix}/c_{amb} = 1.085, M_a = 0.2, ϕ = 25 deg (BWB-CESTOL-EWP)

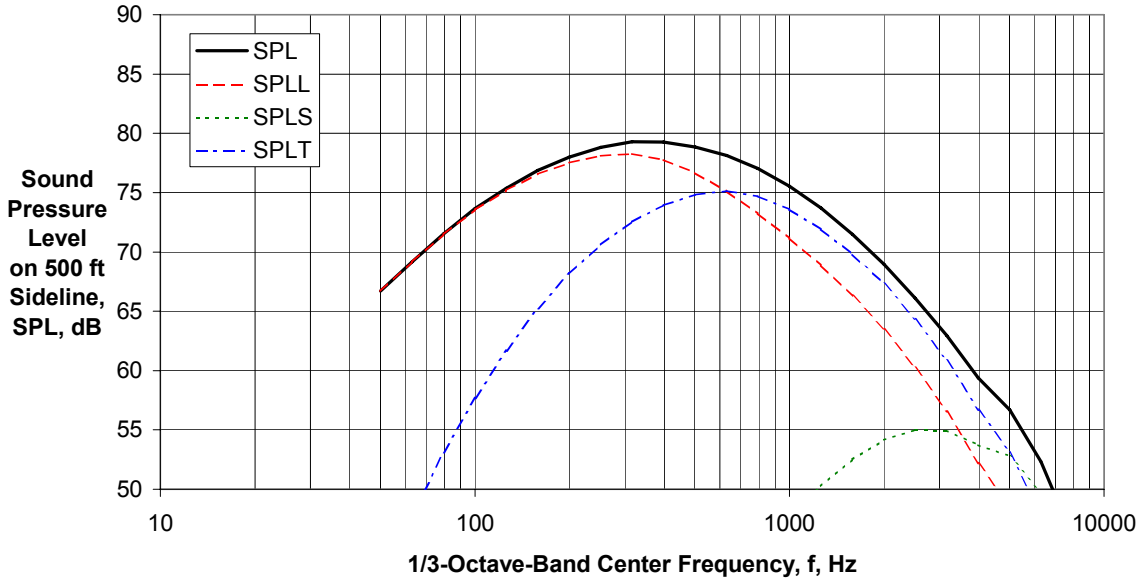

(e) Directivity Angle θ = 140 deg

Figure 14 - Predicted Component and Total Engine Coaxial Chevron Nozzle Jet Noise Spectra for V_{mix}/c_{amb} = 1.085, M_a = 0.2, ϕ = 25 deg (BWB-CESTOL-EWP)

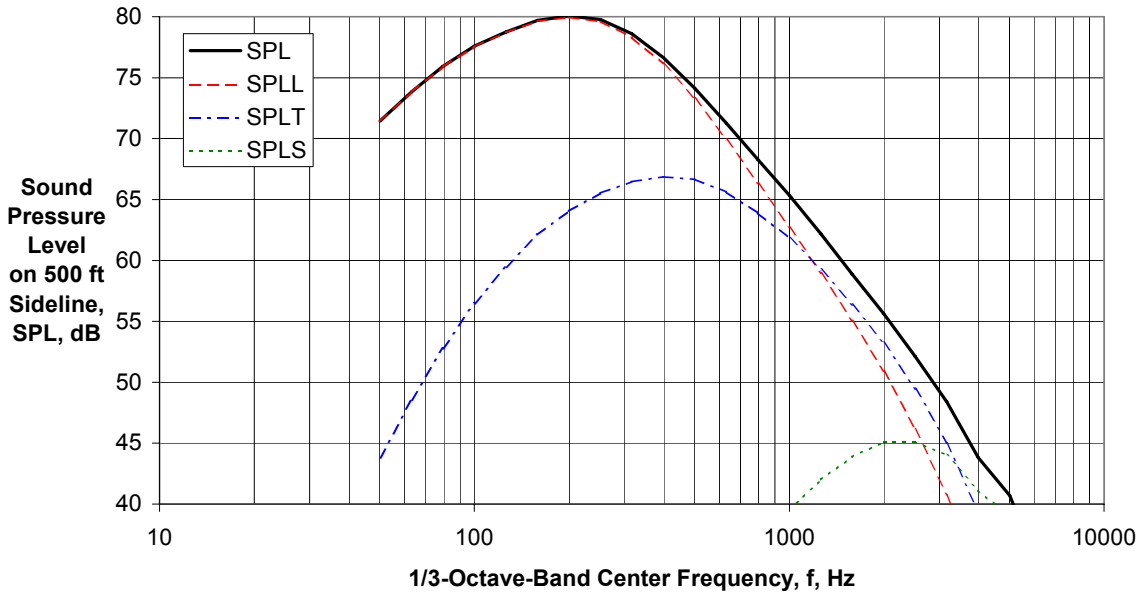

(f) Directivity Angle θ = 160 deg

Figure 14 - Predicted Component and Total Engine Coaxial Chevron Nozzle Jet Noise Spectra for V_{mix}/c_{amb} = 1.085, M_a = 0.2, ϕ = 25 deg (BWB-CESTOL-EWP)

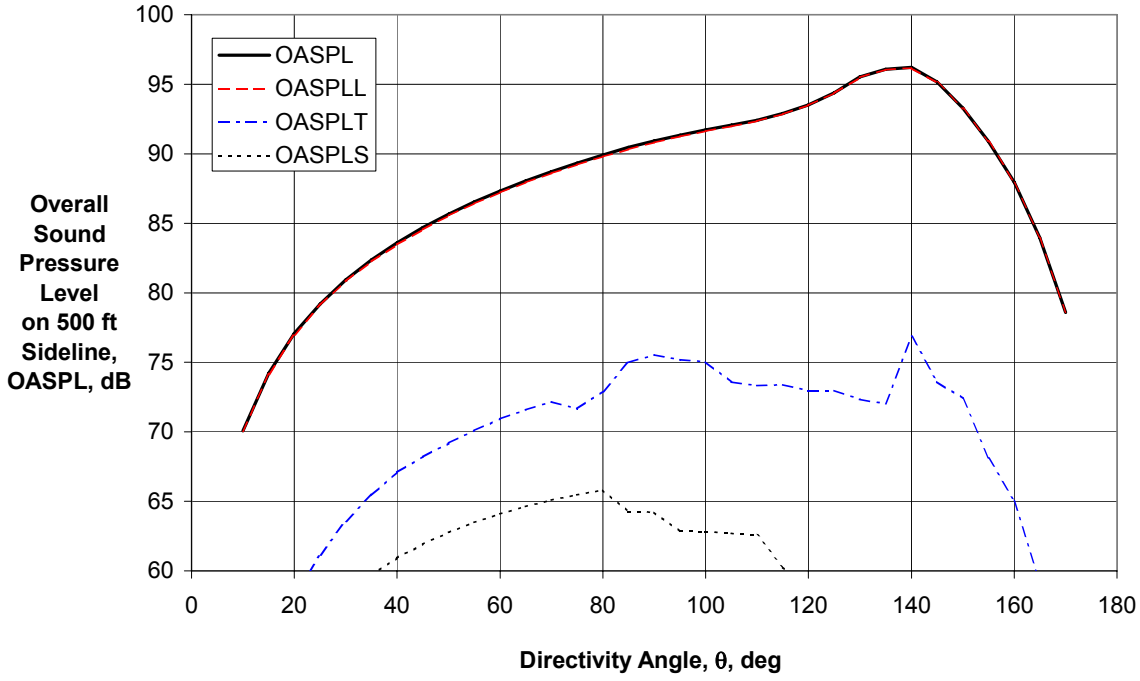

Figure 15 - Predicted Component and Total OASPL Directivities for IBF Slot Nozzle with SNPR = 1.69, M_a = 0.2, ϕ = 25 deg

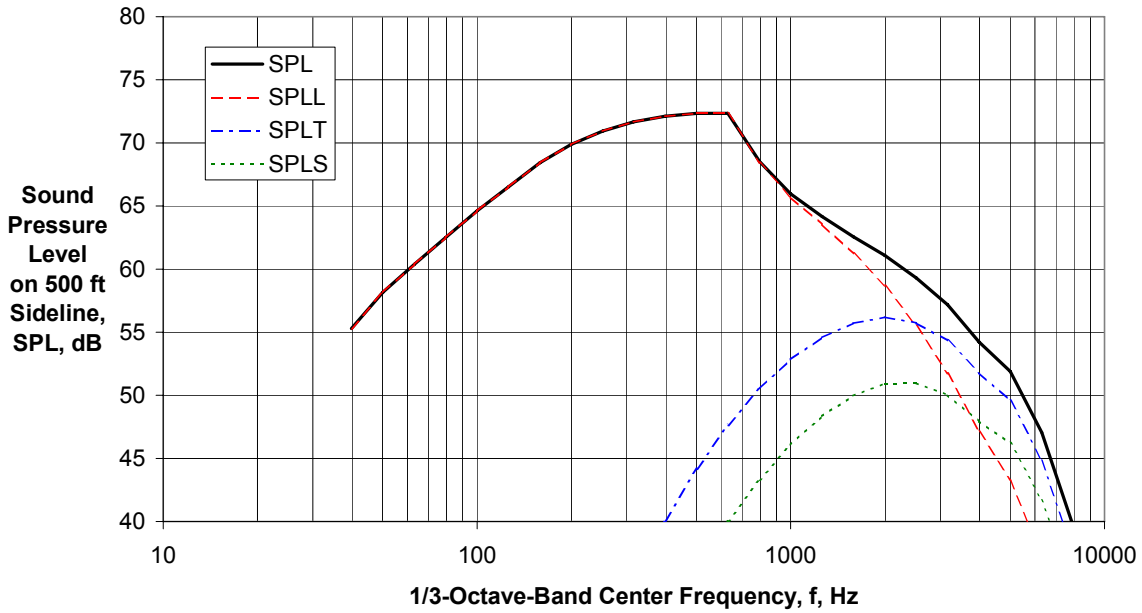

(a) Directivity Angle θ = 30 deg

Figure 16 - Predicted Component and Total Spectra for IBF Slot Nozzle with SNPR = 1.69, M_a = 0.2, ϕ = 25 deg

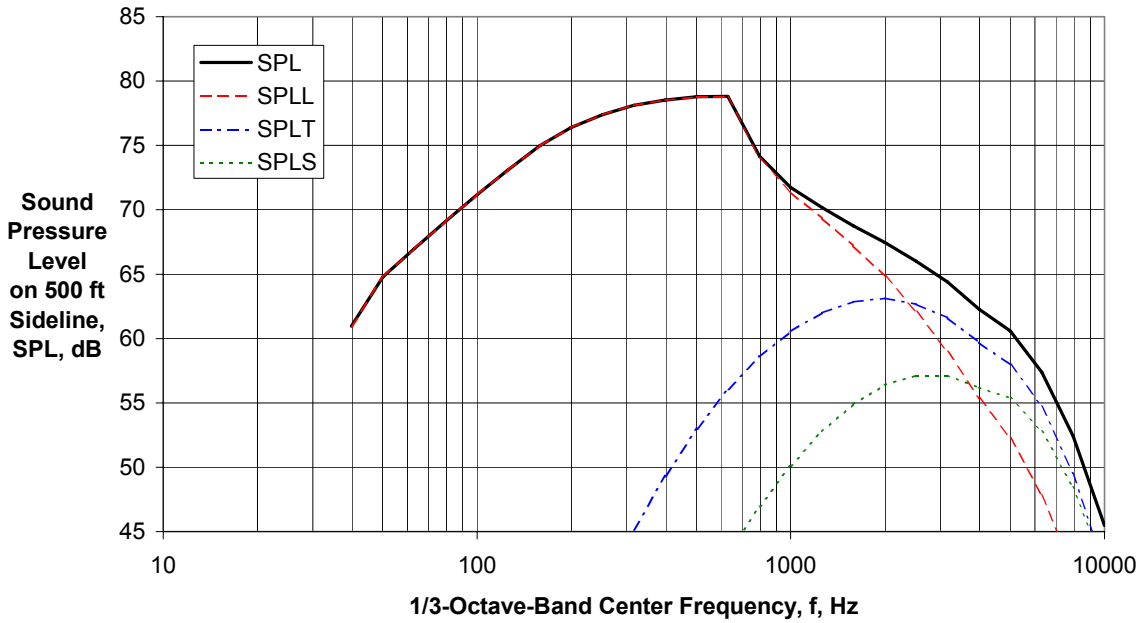

(b) Directivity Angle θ = 60 deg

Figure 16 - Predicted Component and Total Spectra for IBF Slot Nozzle with SNPR = 1.69, M_a = 0.2, ϕ = 25 deg

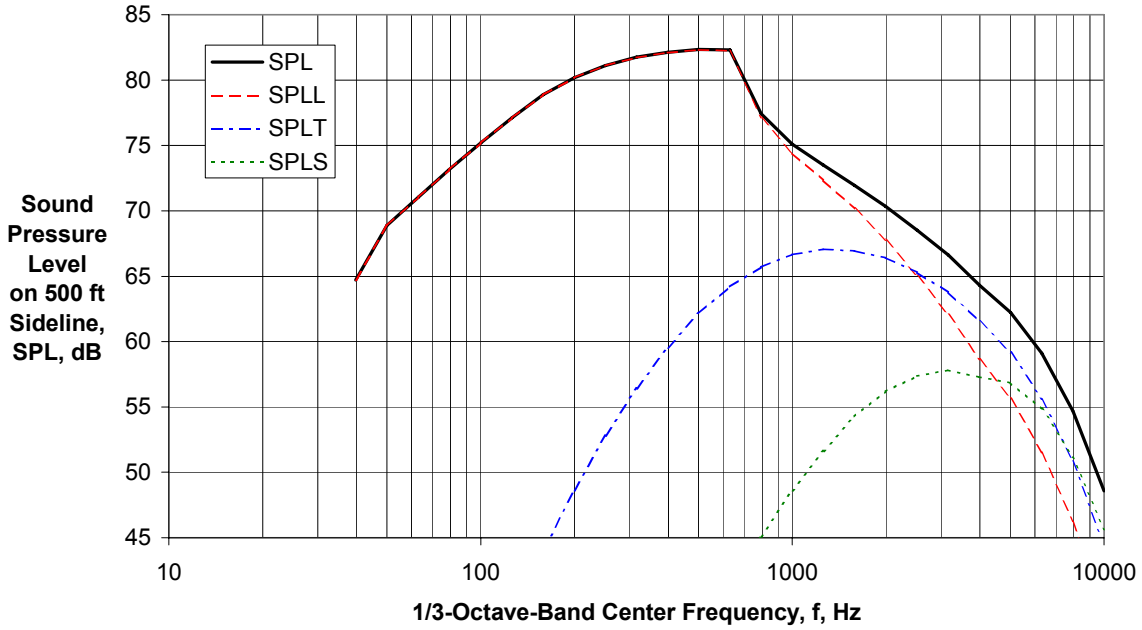

(c) Directivity Angle θ = 90 deg

Figure 16 - Predicted Component and Total Spectra for IBF Slot Nozzle with SNPR = 1.69, M_a = 0.2, ϕ = 25 deg

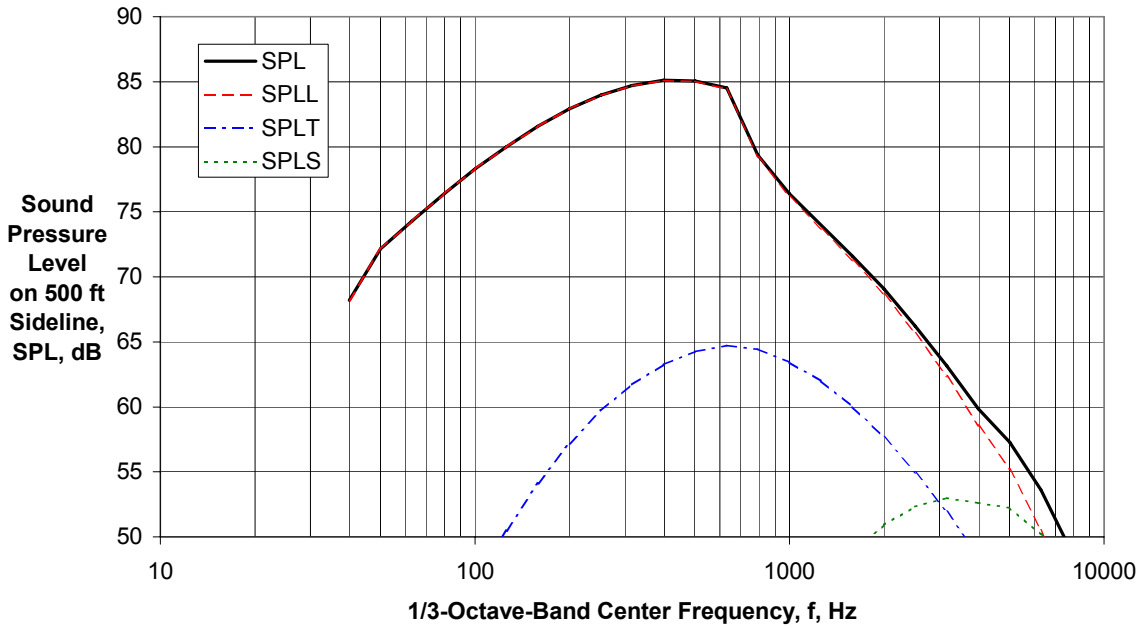

(d) Directivity Angle θ = 120 deg

Figure 16 - Predicted Component and Total Spectra for IBF Slot Nozzle with SNPR = 1.69, M_a = 0.2, ϕ = 25 deg

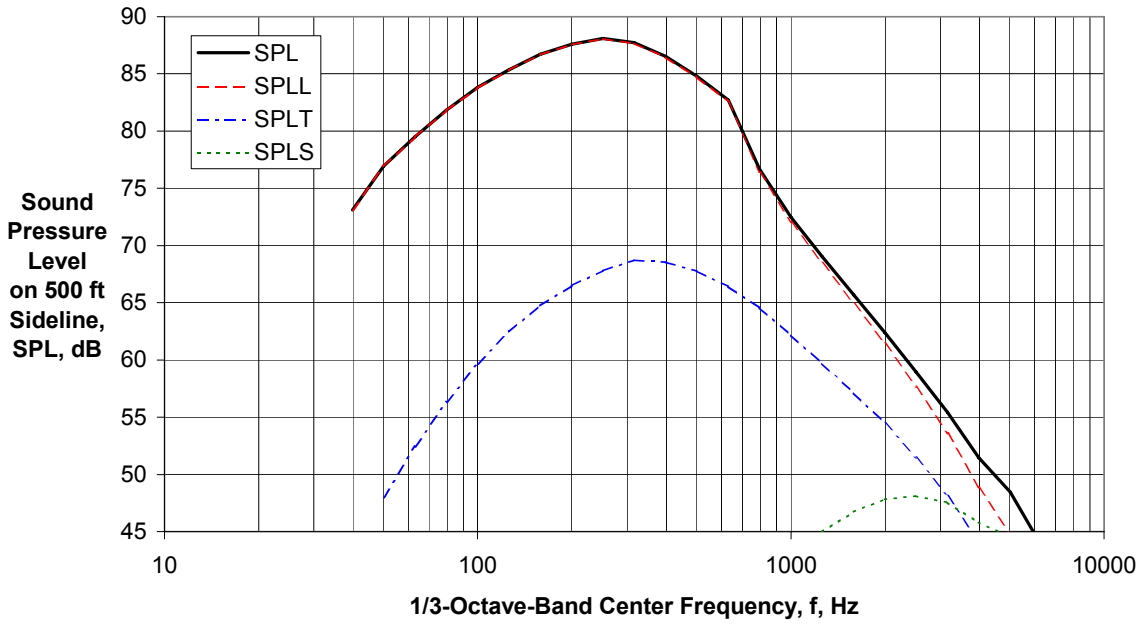

(e) Directivity Angle θ = 140 deg

Figure 16 - Predicted Component and Total Spectra for IBF Slot Nozzle with SNPR = 1.69, M_a = 0.2, ϕ = 25 deg

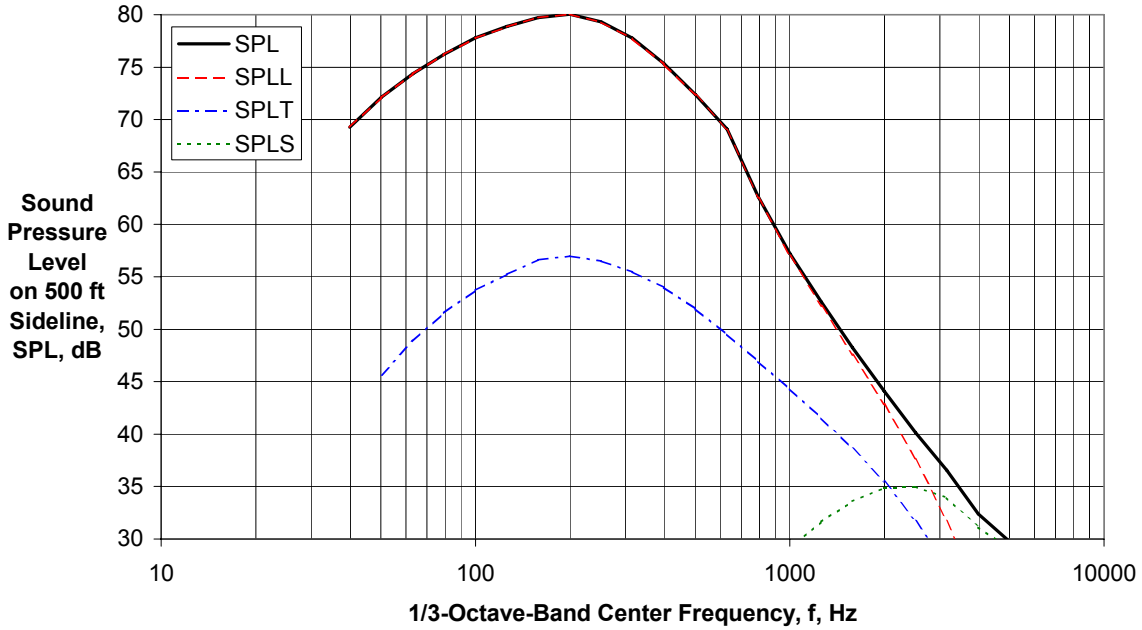

(f) Directivity Angle θ = 160 deg

Figure 16 - Predicted Component and Total Spectra for IBF Slot Nozzle with SNPR = 1.69, M_a = 0.2, ϕ = 25 deg

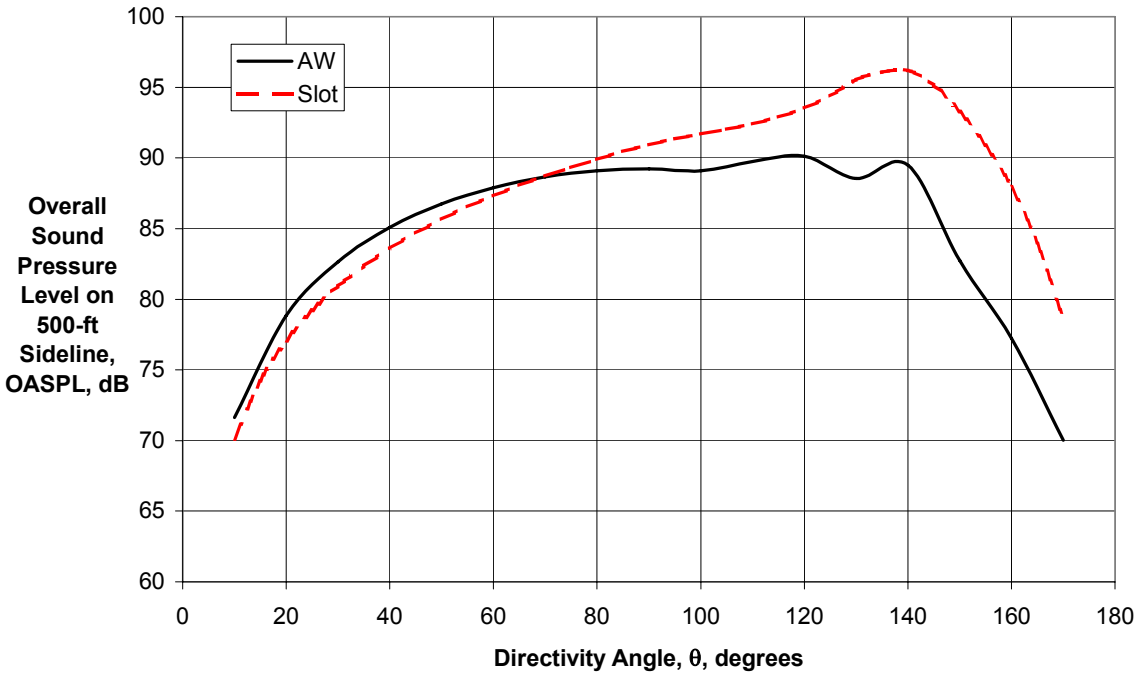

Figure 17 - 500-ft Sideline OASPL Directivity for Augmentor Wing (Dunn & Peart Prediction, Ref. 13) at BWB/IBF Slot Nozzle Conditions

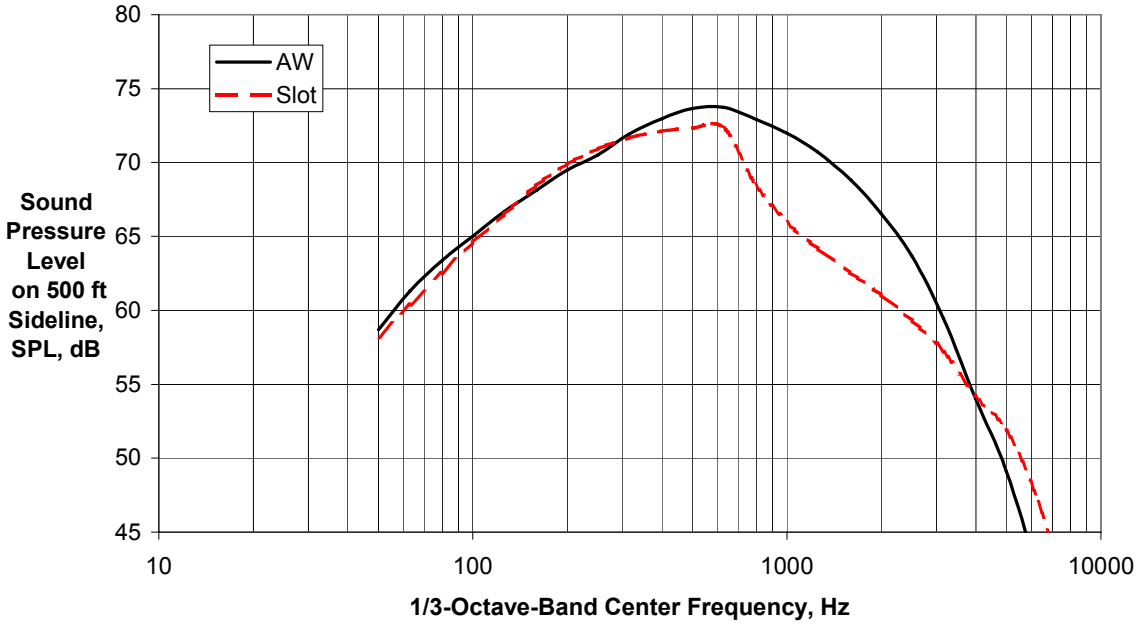

(a) Directivity Angle θ = 30 deg

Figure 18 - 500-ft Sideline SPL Spectra for Augmentor Wing (Dunn & Peart Prediction, Ref. 13) at BWB/IBF Slot Nozzle Conditions

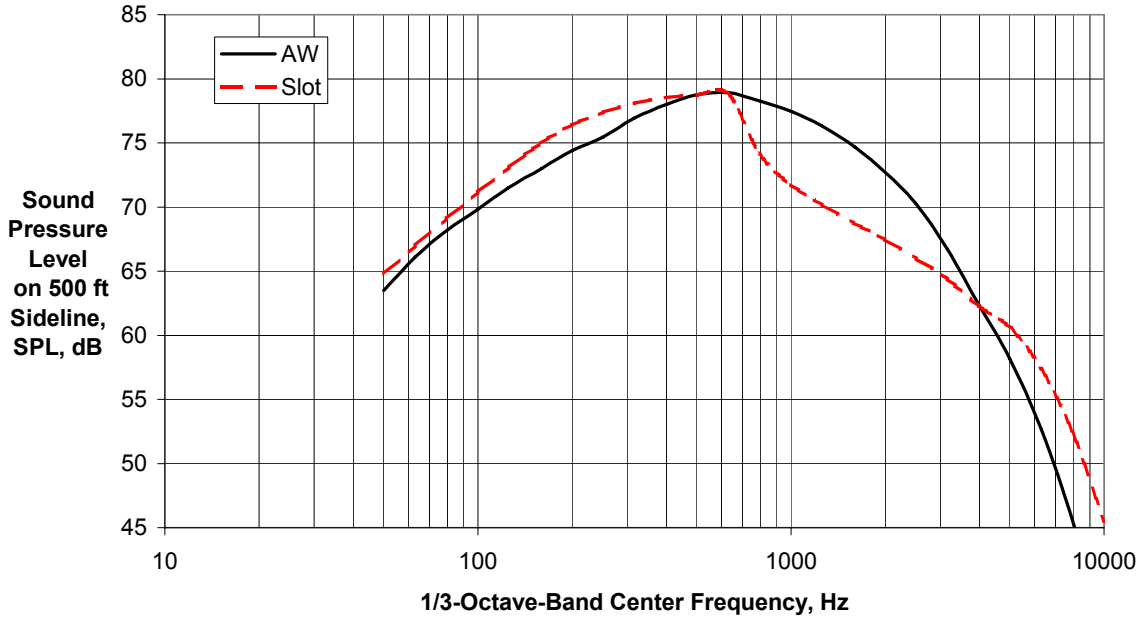

(b) Directivity Angle θ = 60 deg

Figure 18 - 500-ft Sideline SPL Spectra for Augmentor Wing (Dunn & Peart Prediction, Ref. 13) at BWB/IBF Slot Nozzle Conditions

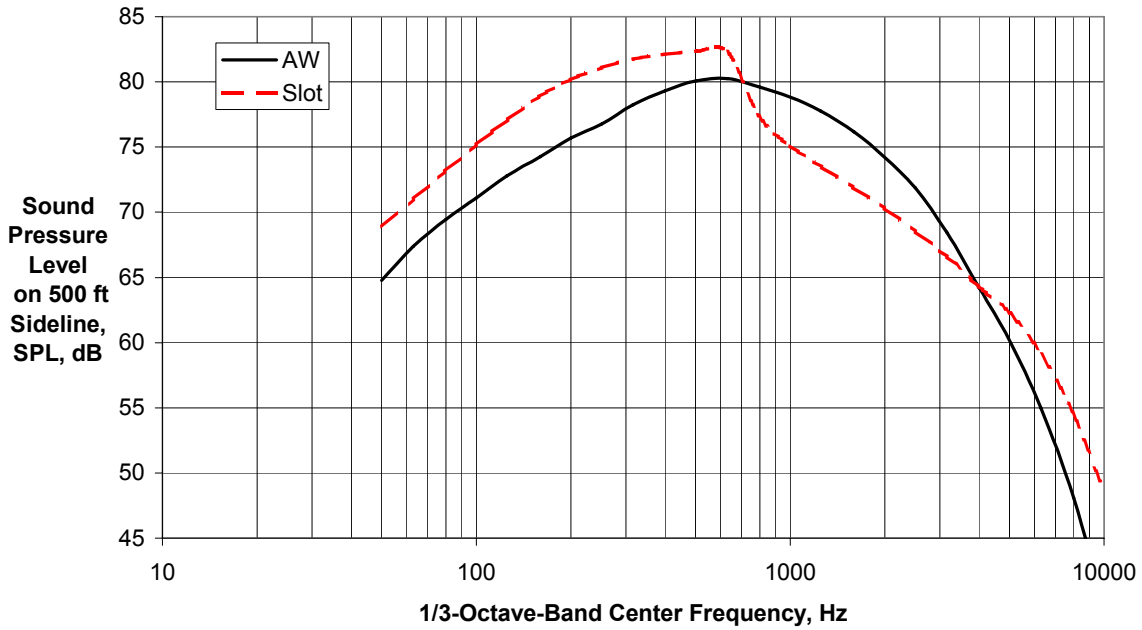

(c) Directivity Angle θ = 90 deg

Figure 18 - 500-ft Sideline SPL Spectra for Augmentor Wing (Dunn & Peart Prediction, Ref. 13) at BWB/IBF Slot Nozzle Conditions

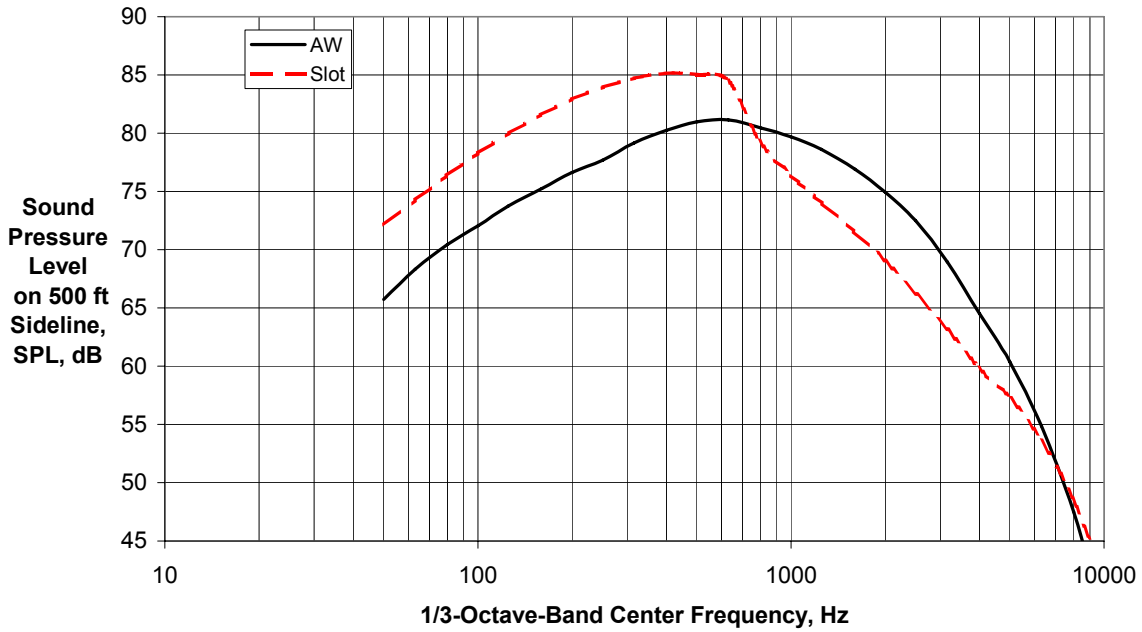

(d) Directivity Angle θ = 120 deg

Figure 18 - 500-ft Sideline SPL Spectra for Augmentor Wing (Dunn & Peart Prediction, Ref. 13) at BWB/IBF Slot Nozzle Conditions

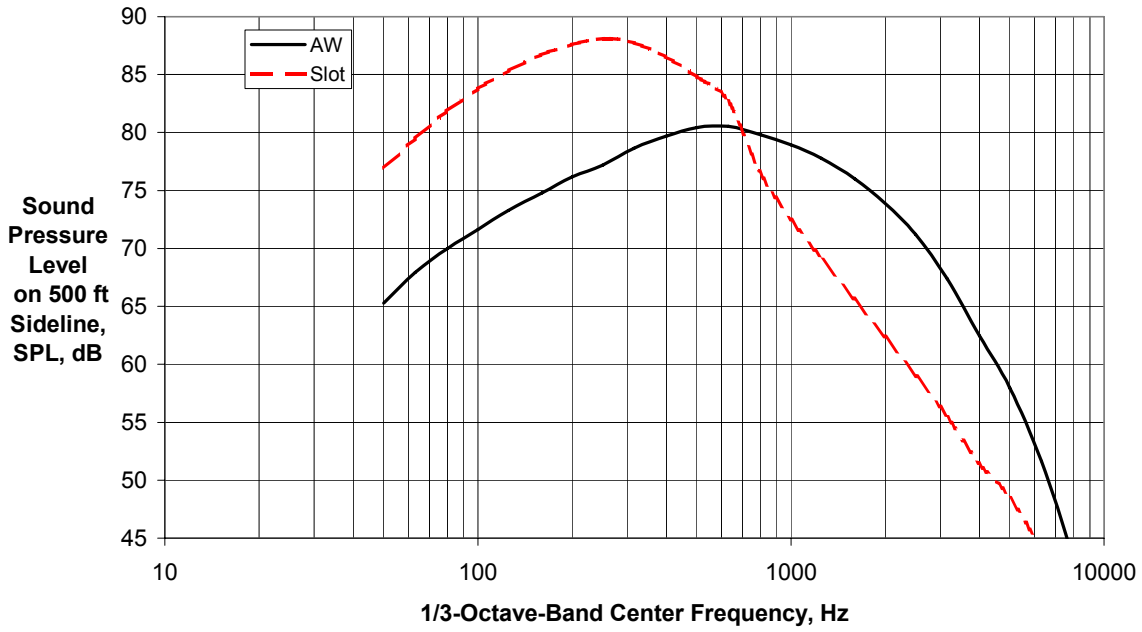

(e) Directivity Angle θ = 140 deg

Figure 18 - 500-ft Sideline SPL Spectra for Augmentor Wing (Dunn & Peart Prediction, Ref. 13) at BWB/IBF Slot Nozzle Conditions

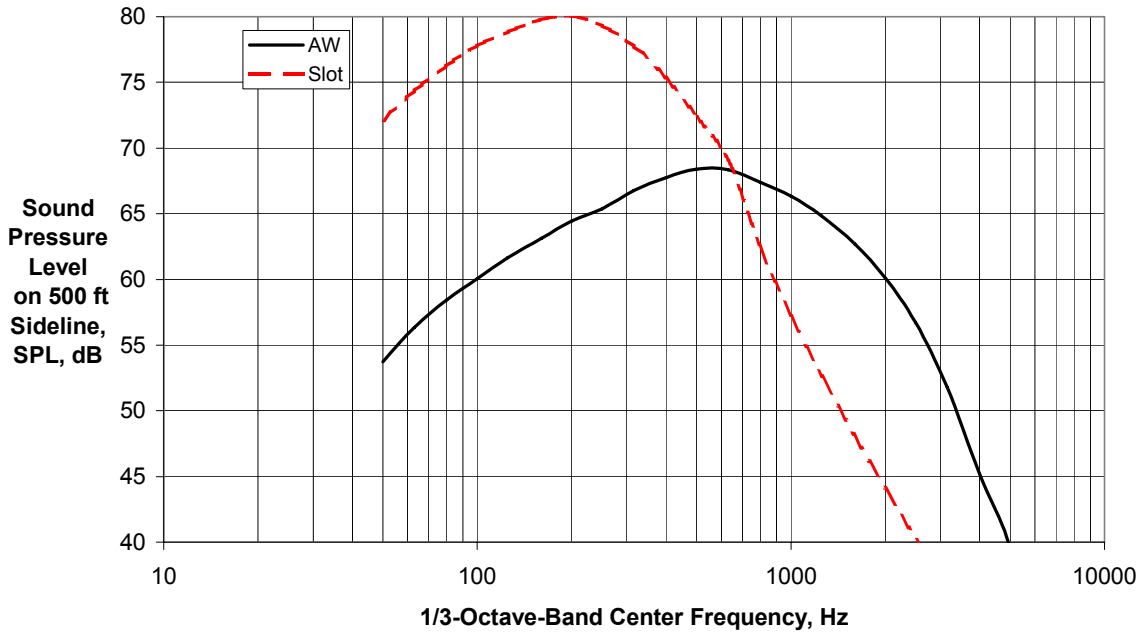

(f) Directivity Angle θ = 160 deg

Figure 18 - 500-ft Sideline SPL Spectra for Augmentor Wing (Dunn & Peart Prediction, Ref. 13) at BWB/IBF Slot Nozzle Conditions

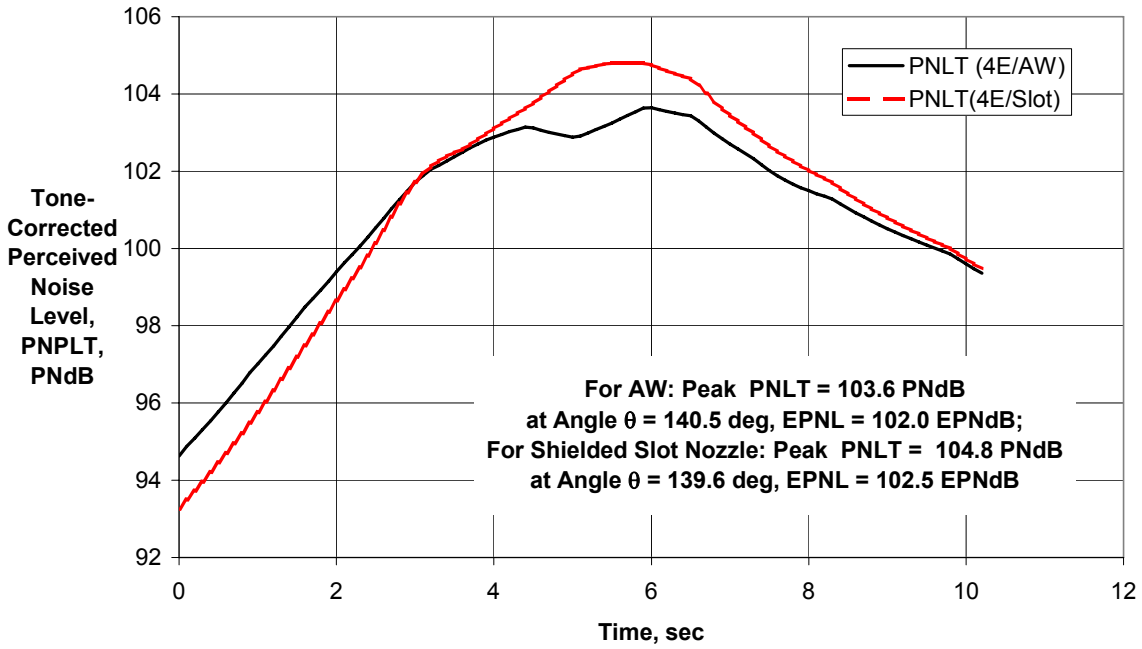

Figure 19 - PNLT distribution for 4-Engine/1-Augmentor BWB/IBF Airplane at Takeoff an 500-ft Sideline Compared With 4-Engine/1-Slot Assumption.

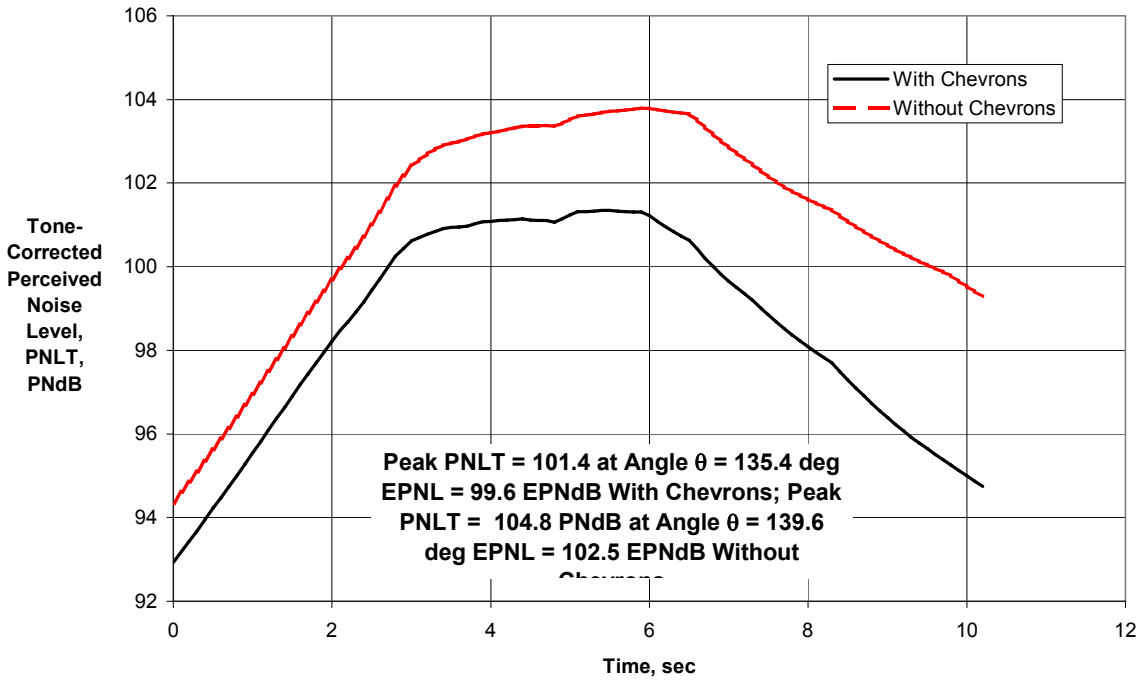

Figure 20 - PNLT Time History for 4-Chevron-Nozzle-Engine/1-Slot-BWB/IBF Airplane at Takeoff an 500-ft Sideline Compare With Unsuppressed Nozzles.

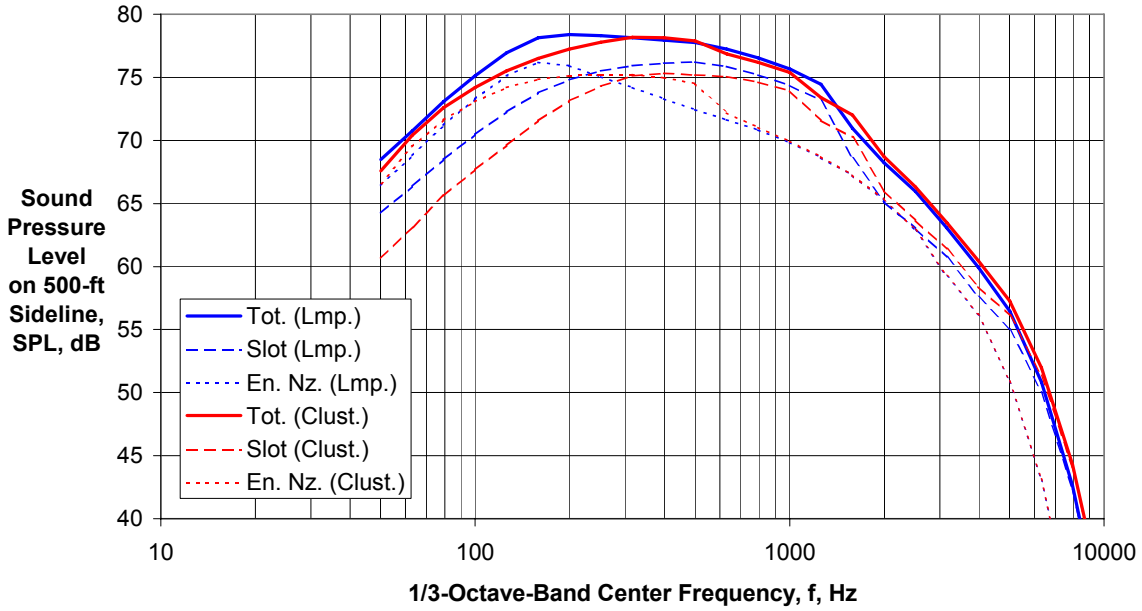

(a) Directivity Angle θ = 30

Figure 21 - Component and Total SPL Spectra for BWB/IBF Airplane at Takeoff on 500-ft Sideline - Unsuppressed Engine Nozzles. ("Lumped Engines" Compared with "Cluster" Approximation.)

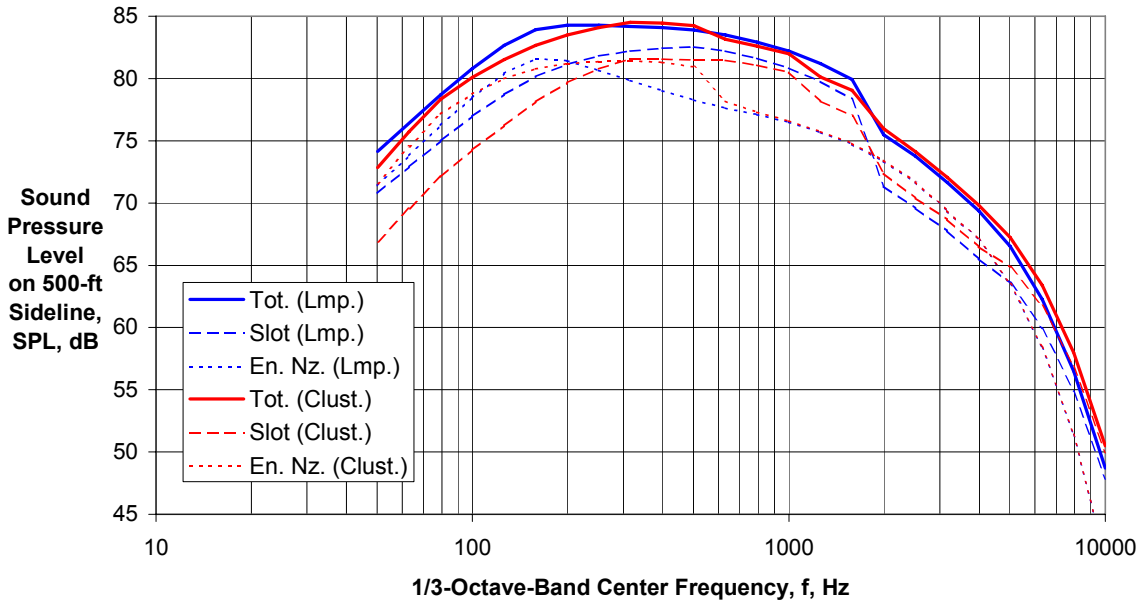

(b) Directivity Angle θ = 60

Figure 21 - Component and Total SPL Spectra for BWB/IBF Airplane at Takeoff on 500-ft Sideline - Unsuppressed Engine Nozzles. ("Lumped Engines" Compared with "Cluster" Approximation.)

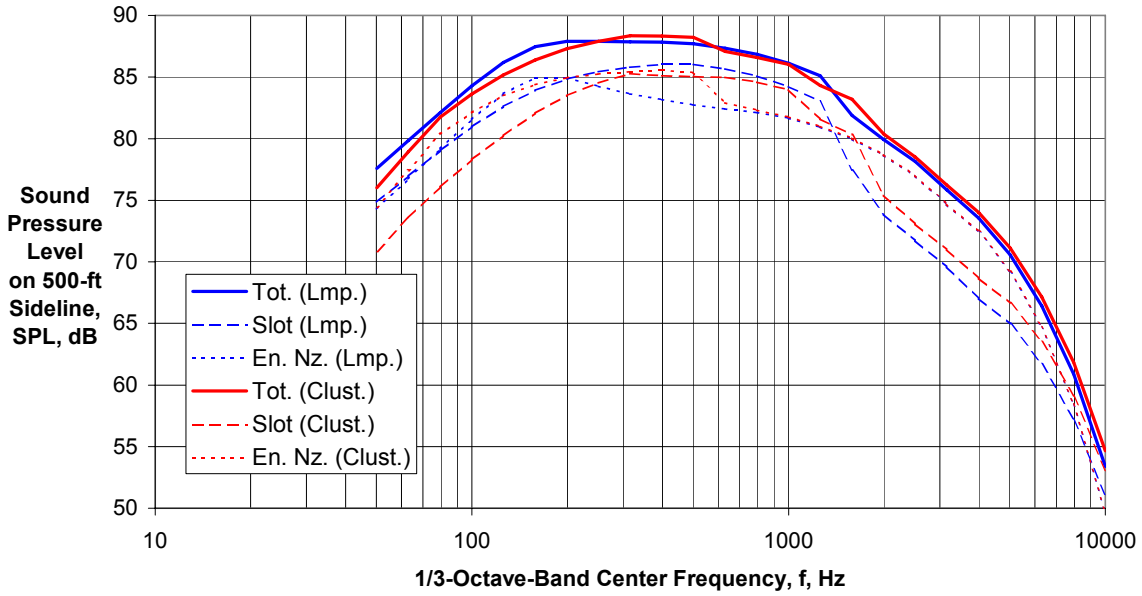

(c) Directivity Angle θ = 90

Figure 21 - Component and Total SPL Spectra for BWB/IBF Airplane at Takeoff on 500-ft Sideline - Unsuppressed Engine Nozzles. ("Lumped Engines" Compared with "Cluster" Approximation.)

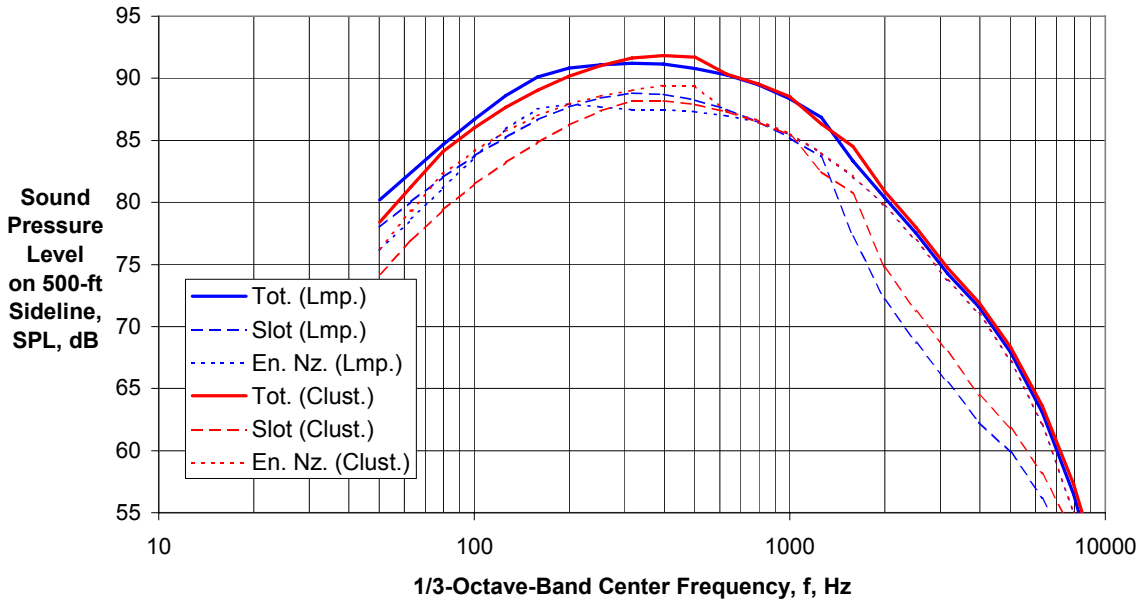

(d) Directivity Angle θ = 120

Figure 21 - Component and Total SPL Spectra for BWB/IBF Airplane at Takeoff on 500-ft Sideline - Unsuppressed Engine Nozzles. ("Lumped Engines" Compared with "Cluster" Approximation.)

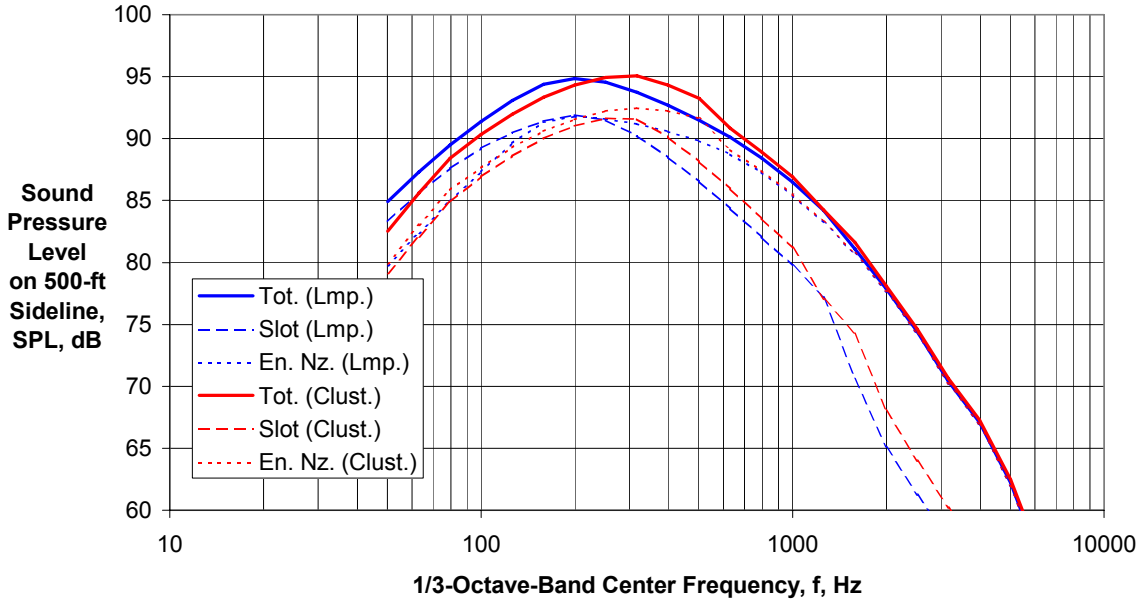

(e) Directivity Angle θ = 140

Figure 21 - Component and Total SPL Spectra for BWB/IBF Airplane at Takeoff on 500-ft Sideline - Unsuppressed Engine Nozzles. ("Lumped Engines" Compared with "Cluster" Approximation.)

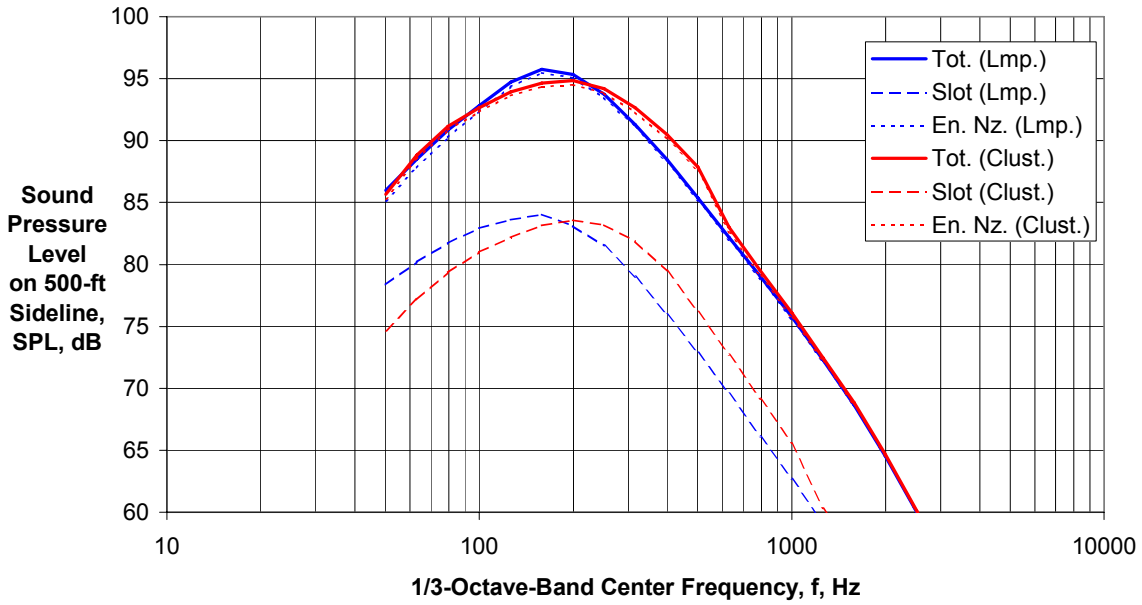

(f) Directivity Angle θ = 160

Figure 21 - Component and Total SPL Spectra for BWB/IBF Airplane at Takeoff on 500-ft Sideline - Unsuppressed Engine Nozzles. ("Lumped Engines" Compared with "Cluster" Approximation.)

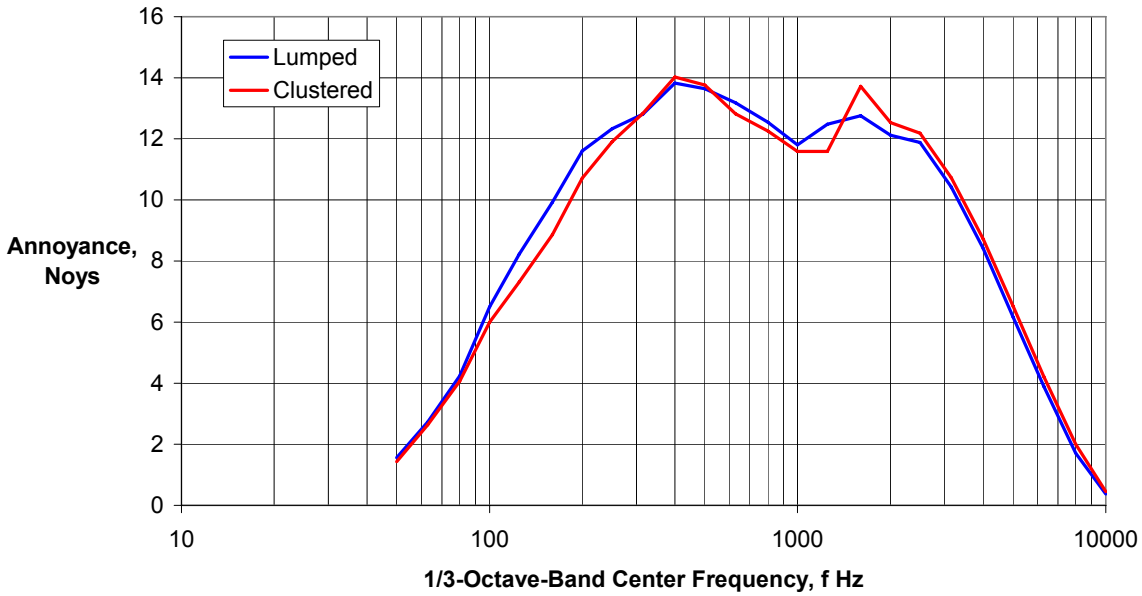

(a) Directivity Angle, θ = 30 deg

Figure 22 - Annoyance Spectrum for BWB/IBF Airplane at Takeoff on 500-ft Sideline - Unsuppressed Engine Nozzles. ("Lumped Engines" Compared with "Cluster" Approximation.)

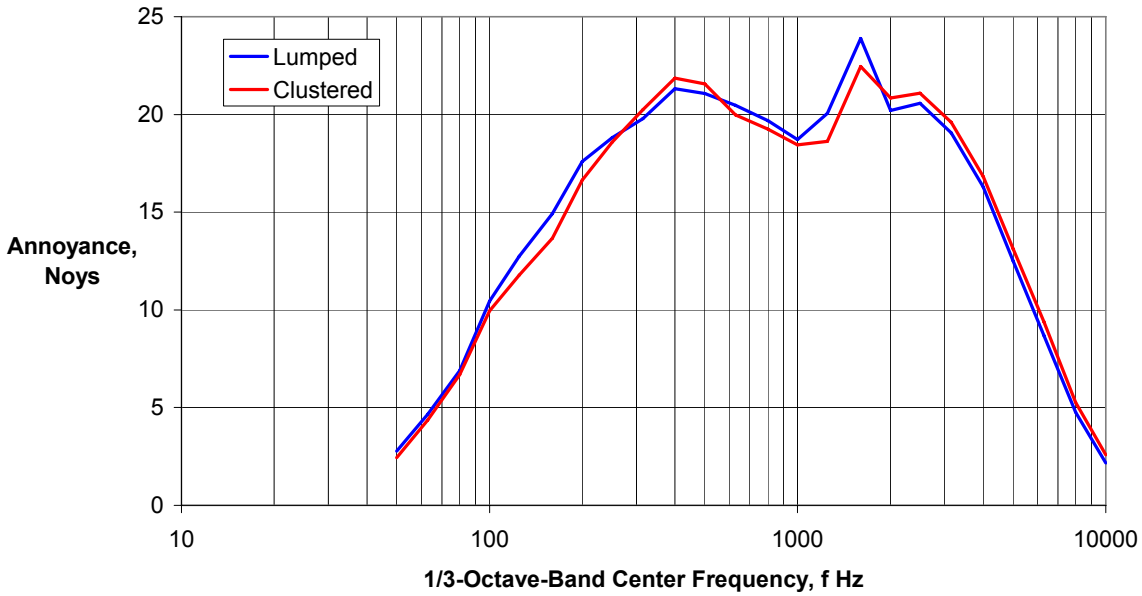

(b) Directivity Angle, θ = 60 deg

Figure 22 - Annoyance Spectrum for BWB/IBF Airplane at Takeoff on 500-ft Sideline - Unsuppressed Engine Nozzles. ("Lumped Engines" Compared with "Cluster" Approximation.)

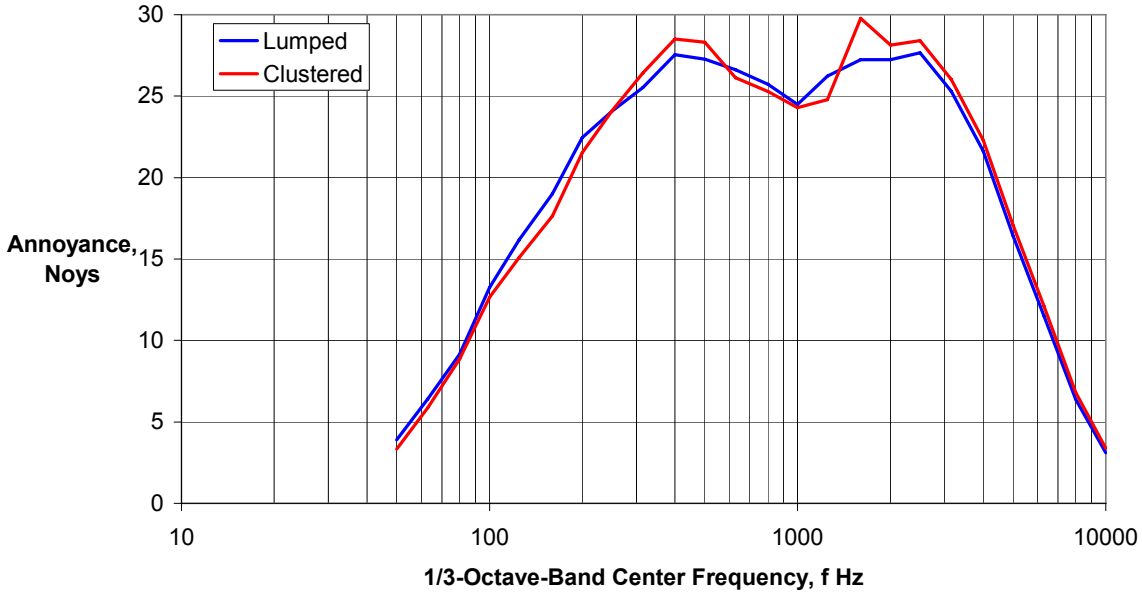

(c) Directivity Angle, θ = 90 deg

Figure 22 - Annoyance Spectrum for BWB/IBF Airplane at Takeoff on 500-ft Sideline - Unsuppressed Engine Nozzles. ("Lumped Engines" Compared with "Cluster" Approximation.)

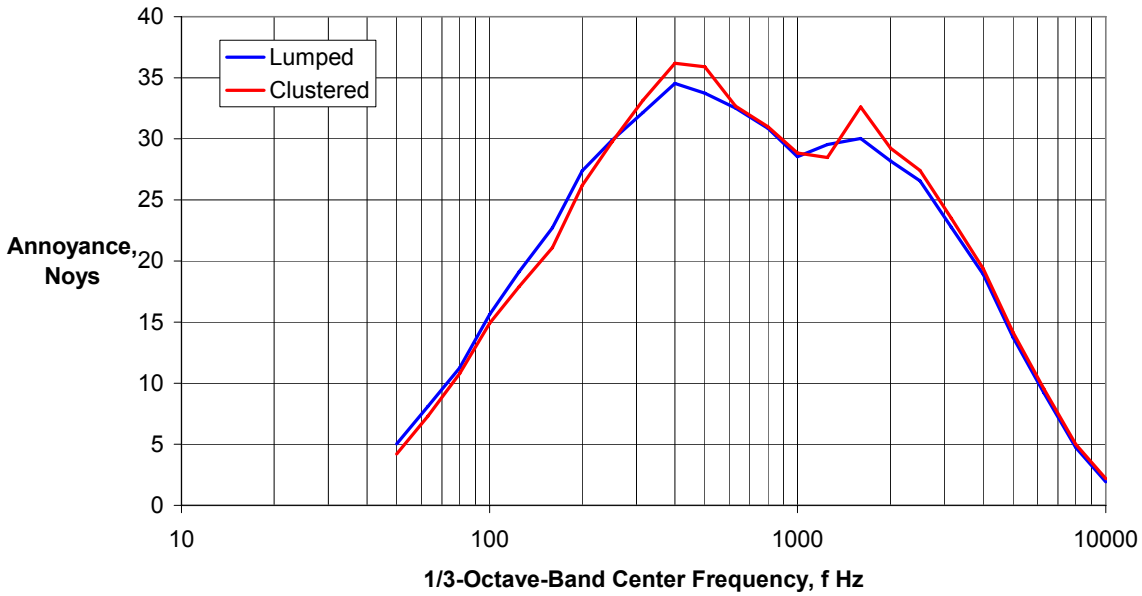

(d) Directivity Angle, θ = 120 deg

Figure 22 - Annoyance Spectrum for BWB/IBF Airplane at Takeoff on 500-ft Sideline - Unsuppressed Engine Nozzles. ("Lumped Engines" Compared with "Cluster" Approximation.)

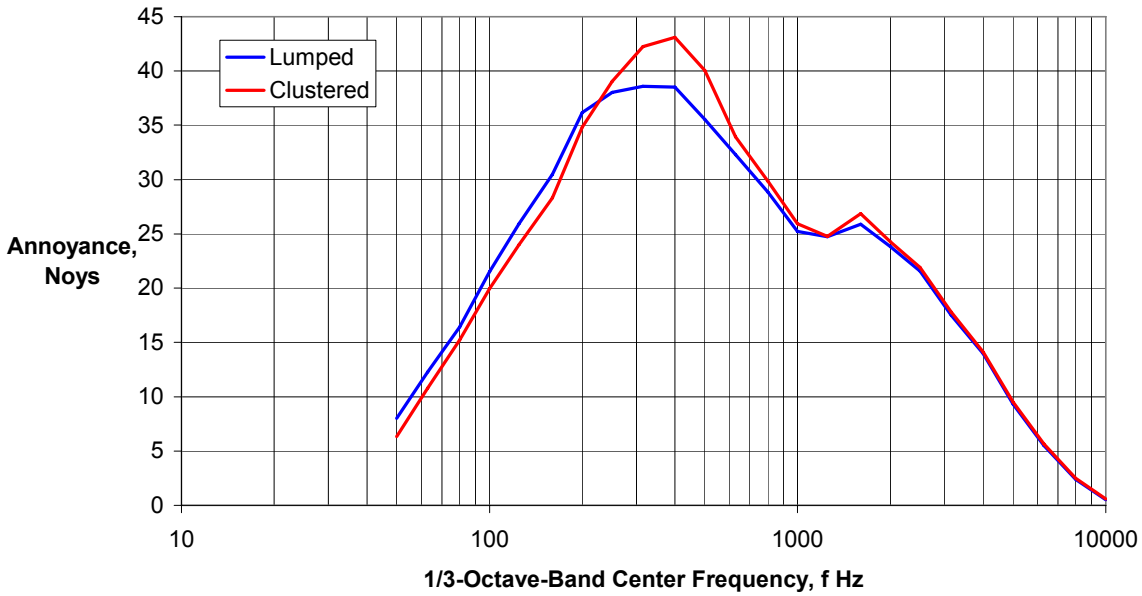

(e) Directivity Angle, θ = 140 deg

Figure 22 - Annoyance Spectrum for BWB/IBF Airplane at Takeoff on 500-ft Sideline - Unsuppressed Engine Nozzles. ("Lumped Engines" Compared with "Cluster" Approximation.)

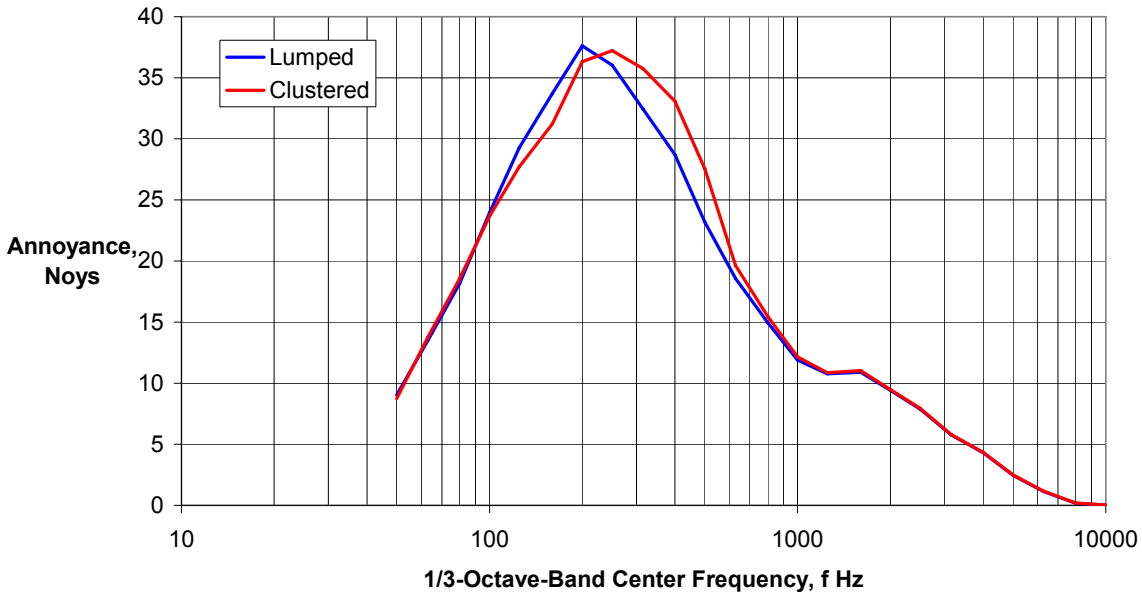

(f) Directivity Angle, θ = 160 deg

Figure 22 - Annoyance Spectrum for BWB/IBF Airplane at Takeoff on 500-ft Sideline - Unsuppressed Engine Nozzles. ("Lumped Engines" Compared with "Cluster" Approximation.)

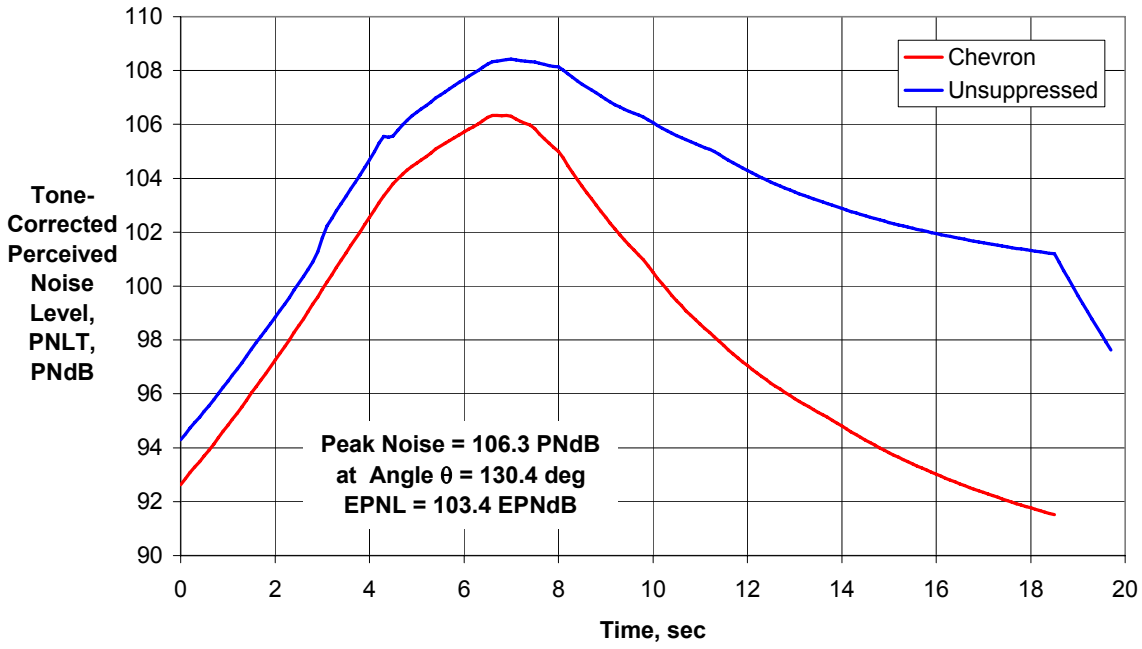

Figure 23 - PNLT Time History for BWB/IBF Airplane with Engine BPR = 5.7 at Takeoff on 500-ft Sideline, for Chevron Nozzles Compared to Unsuppressed.

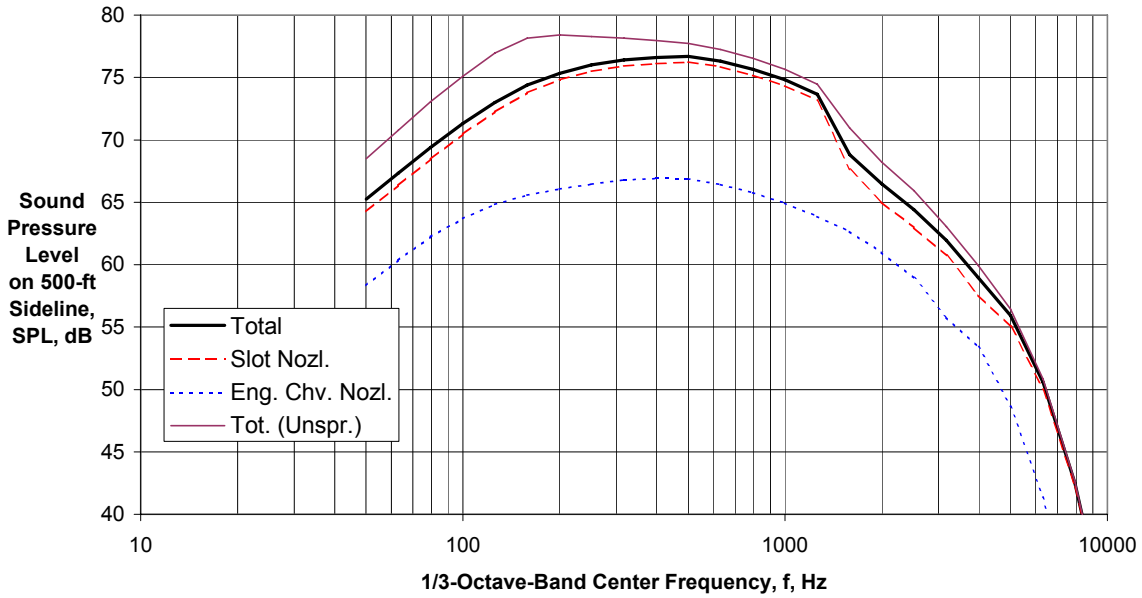

(a) Directivity Angle θ = 30 deg

Figure 24 - Component and Total SPL Spectra for BWB/IBF Airplane with Engine BPR = 5.7 and Chevron Nozzles at Takeoff on 500-ft Sideline.

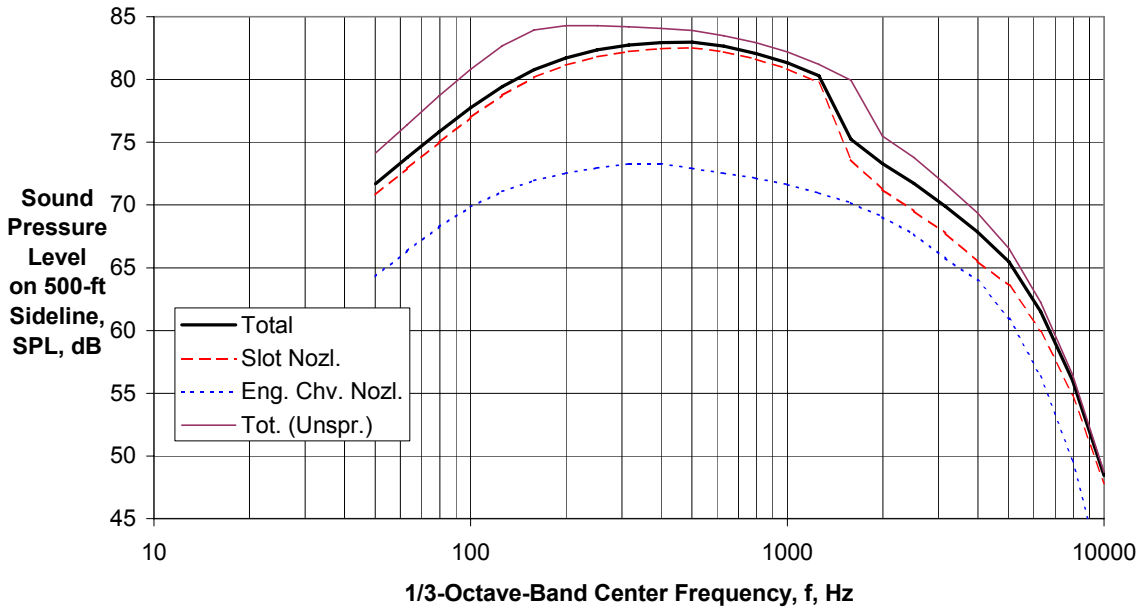

(b) Directivity Angle θ = 60 deg

Figure 24 - Component and Total SPL Spectra for BWB/IBF Airplane with Engine BPR = 5.7 and Chevron Nozzles at Takeoff on 500-ft Sideline.

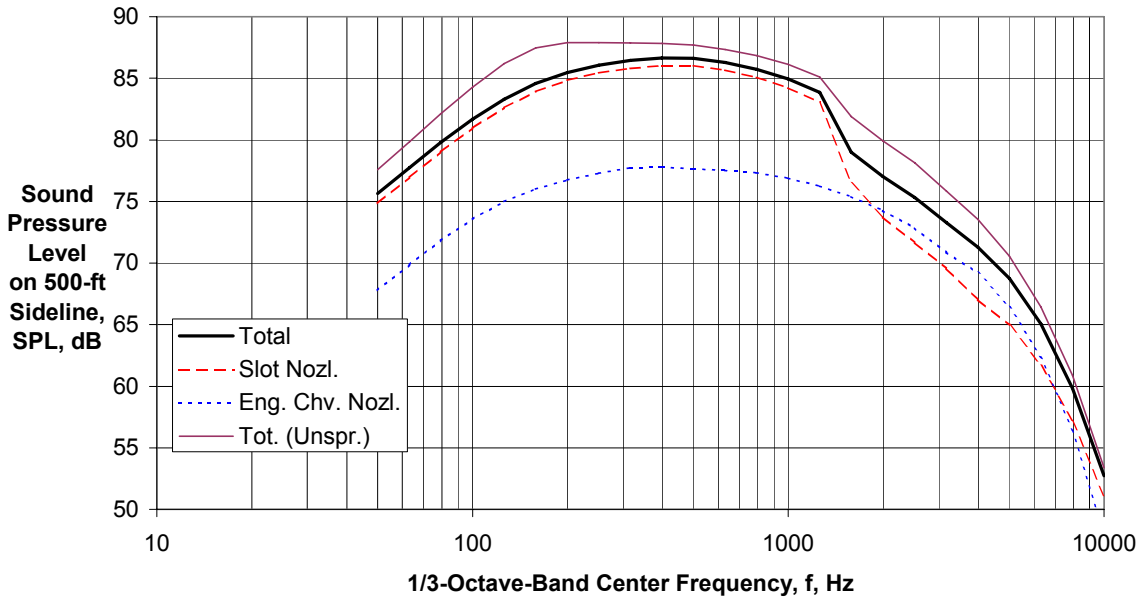

(c) Directivity Angle θ = 90 deg

Figure 24 - Component and Total SPL Spectra for BWB/IBF Airplane with Engine BPR = 5.7 and Chevron Nozzles at Takeoff on 500-ft Sideline.

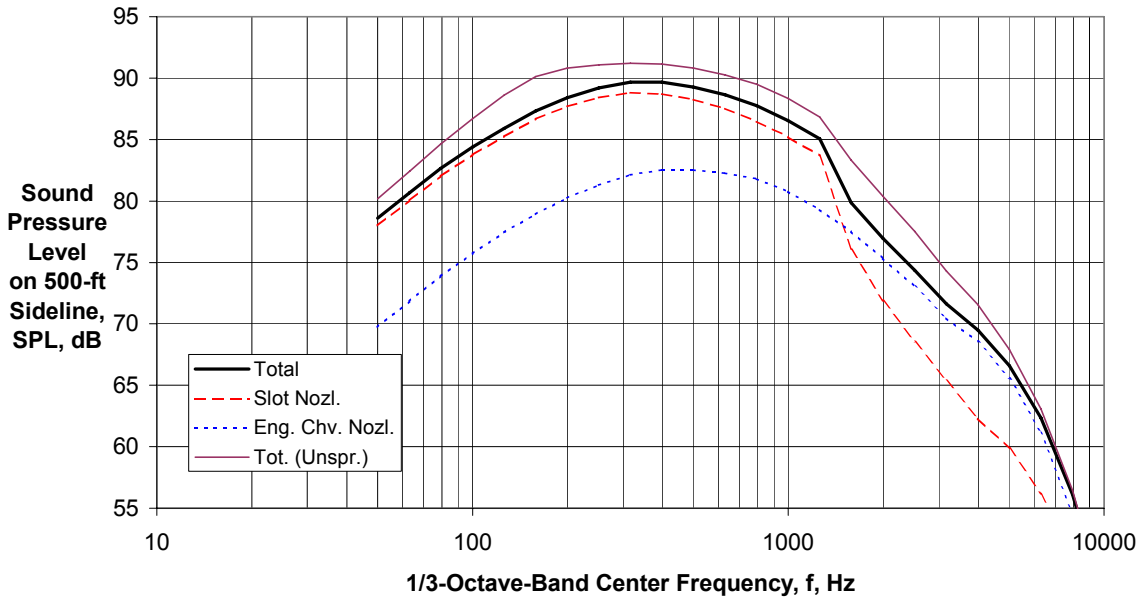

(d) Directivity Angle θ = 120 deg

Figure 24 - Component and Total SPL Spectra for BWB/IBF Airplane with Engine BPR = 5.7 and Chevron Nozzles at Takeoff on 500-ft Sideline.

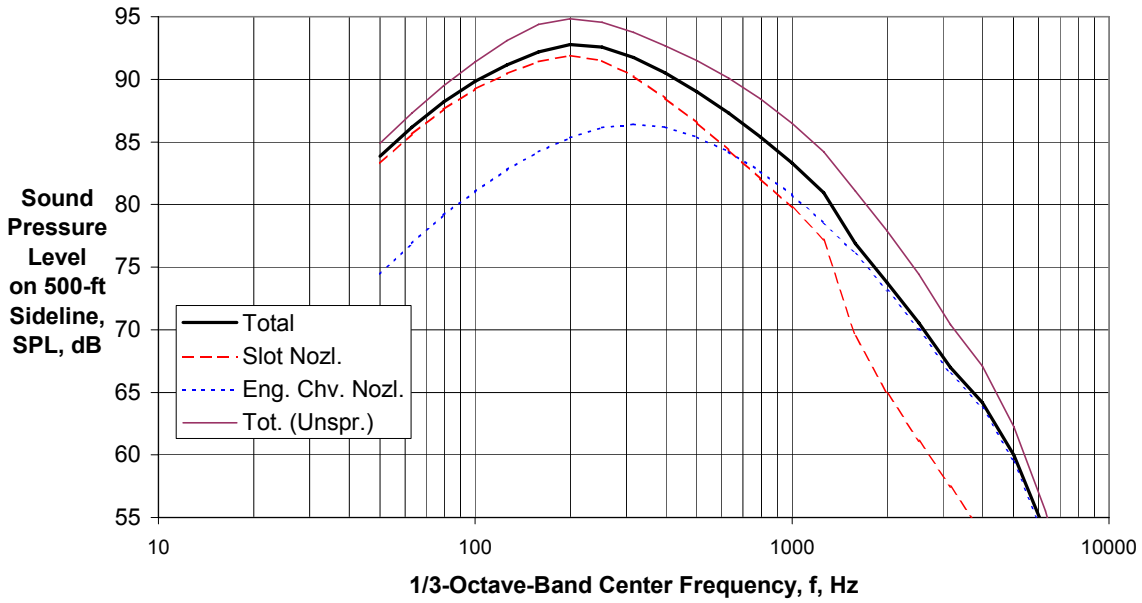

(e) Directivity Angle θ = 140 deg

Figure 24 - Component and Total SPL Spectra for BWB/IBF Airplane with Engine BPR = 5.7 and Chevron Nozzles at Takeoff on 500-ft Sideline.

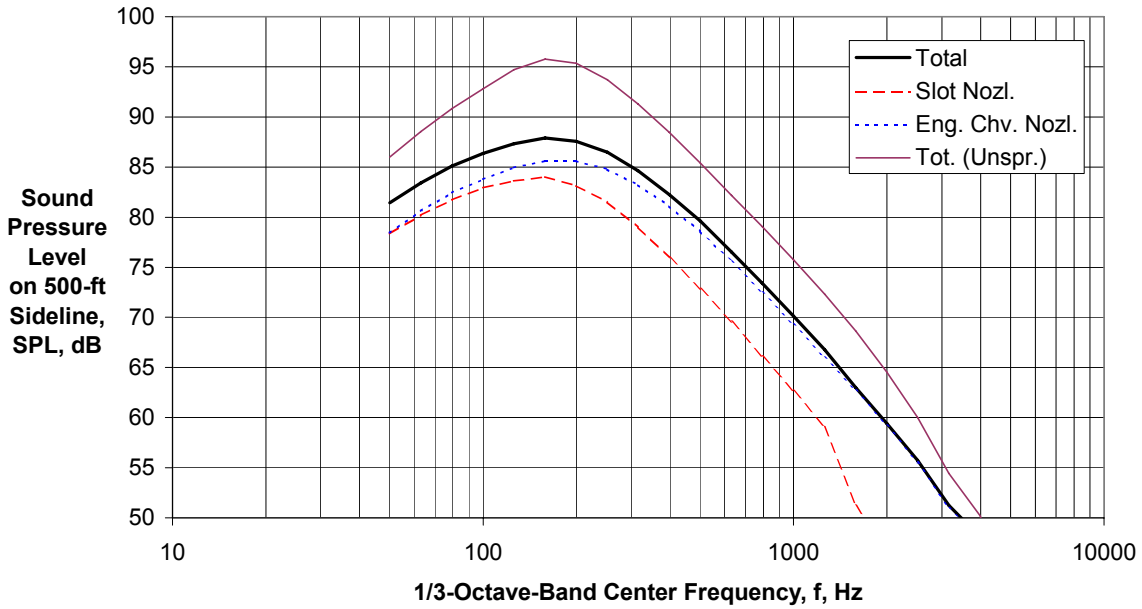

(f) Directivity Angle θ = 160 deg

Figure 24 - Component and Total SPL Spectra for BWB/IBF Airplane with Engine BPR = 5.7 and Chevron Nozzles at Takeoff on 500-ft Sideline.

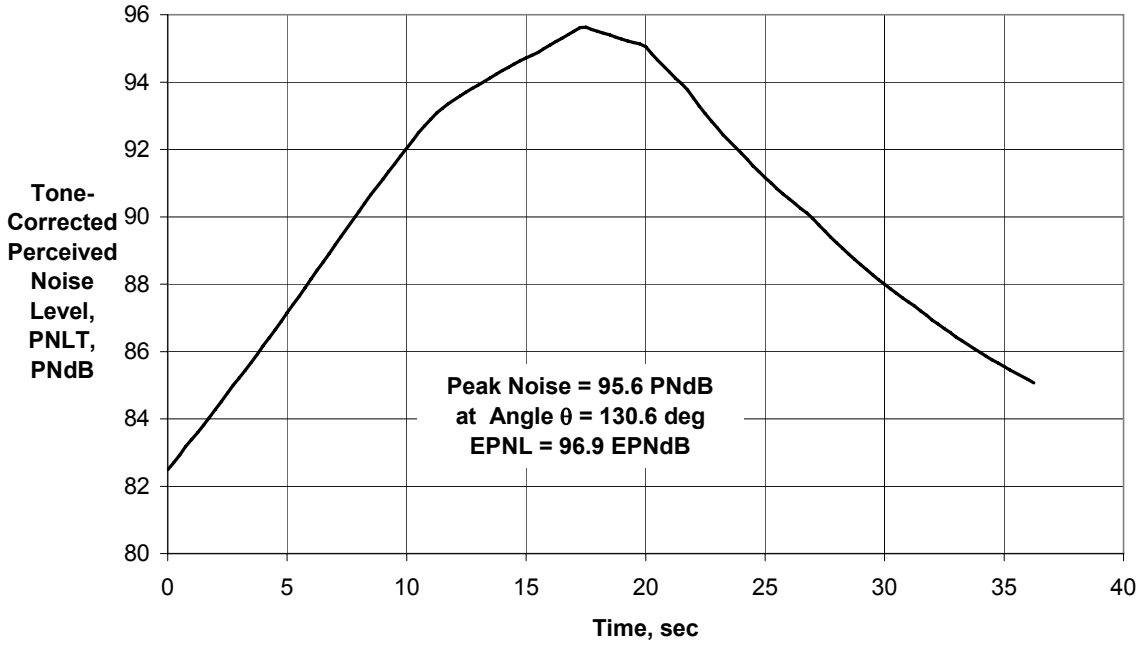

Figure 25 - PNLT Time History for BWB/IBF Airplane with Engine BPR = 5.7 and Chevron Nozzles at Takeoff on FAR-36 450-m (1476-ft) Sideline.

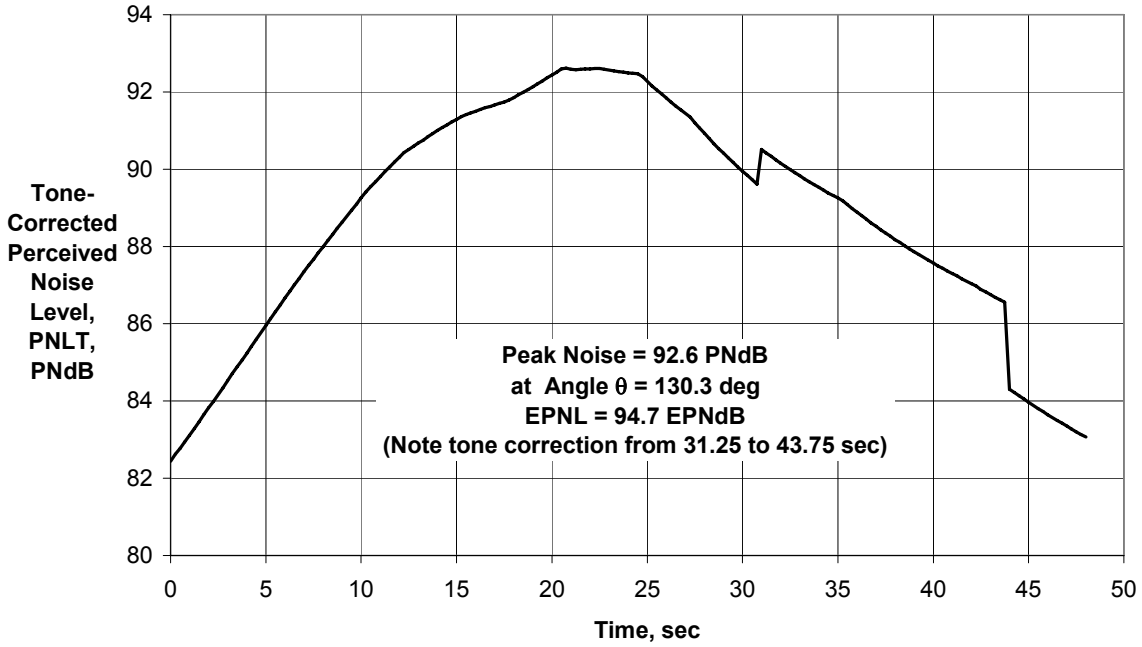

Figure 26 - PNLT Time History for BWB/IBF Airplane with Engine BPR = 5.7 with Chevron Nozzles at FAR-36 Takeoff Flyover 6500 m from Brake Release.

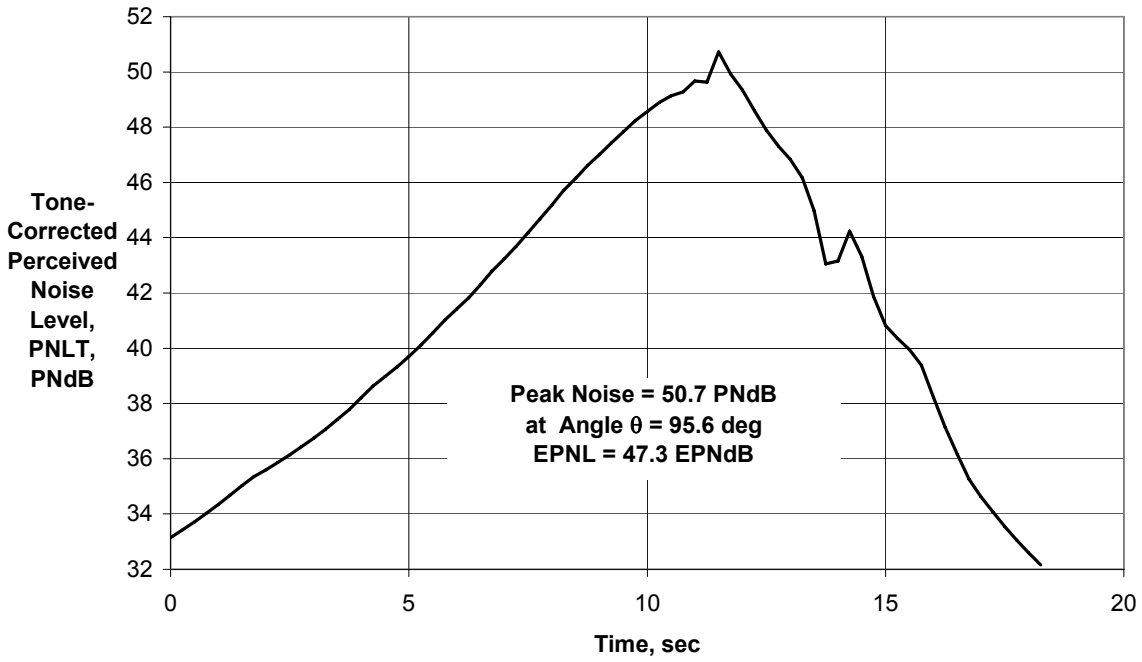

Figure 27 - PNLT Time History for BWB/IBF Airplane with Engine BPR = 5.7 with Chevron Nozzles at FAR-36 Approach 2000 m from Threshold.

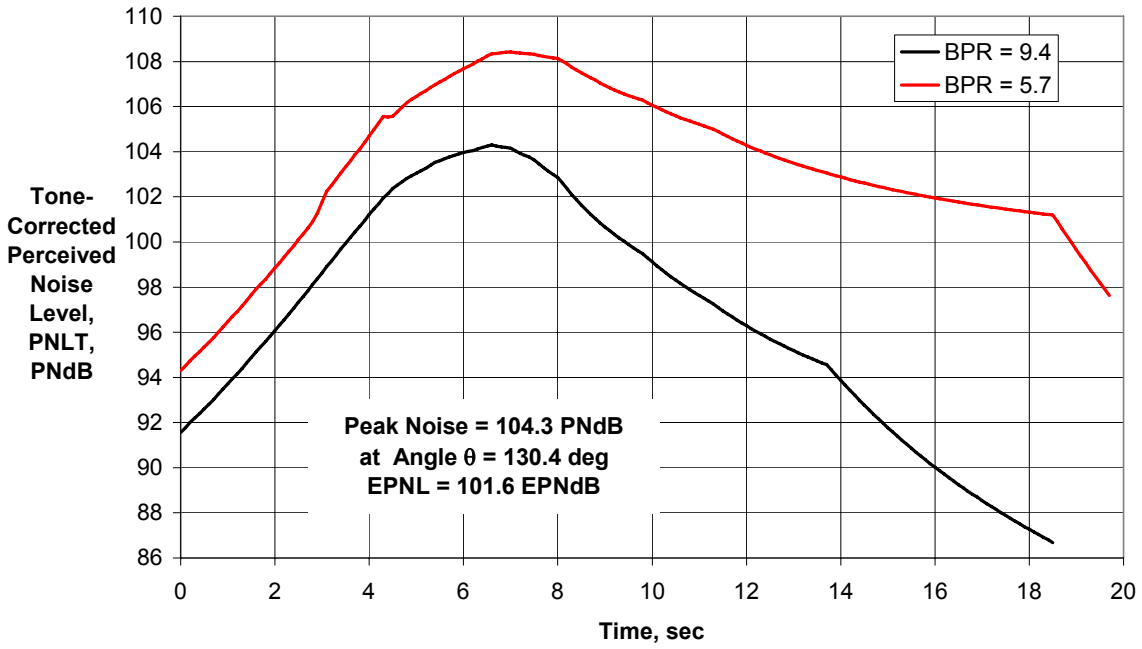

Figure 28 - PNLT Time History for BWB/IBF Airplane with Chevron-Nozzle Engine BPR = 9.4 at Takeoff on 500-ft Sideline (Compared with BPR = 5.7).

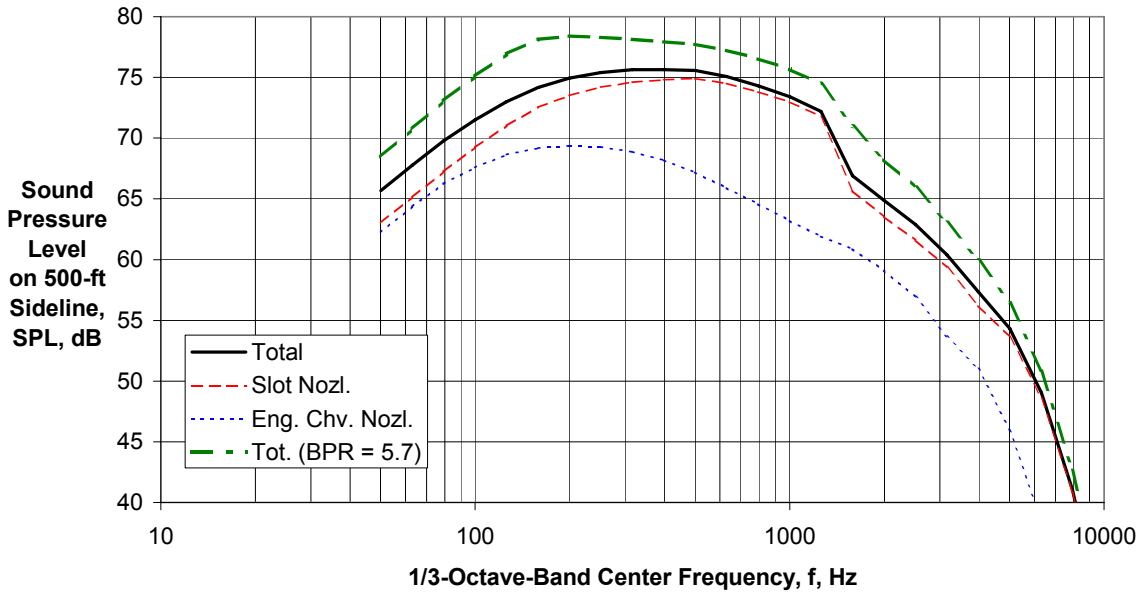

(a) Directivity Angle θ = 30

Figure 29 - Component and Total SPL Spectra for BWB/IBF Airplane with Chevron-Nozzle Engine BPR = 9.4 at Takeoff on 500-ft Sideline (Compared with BPR = 5.7).

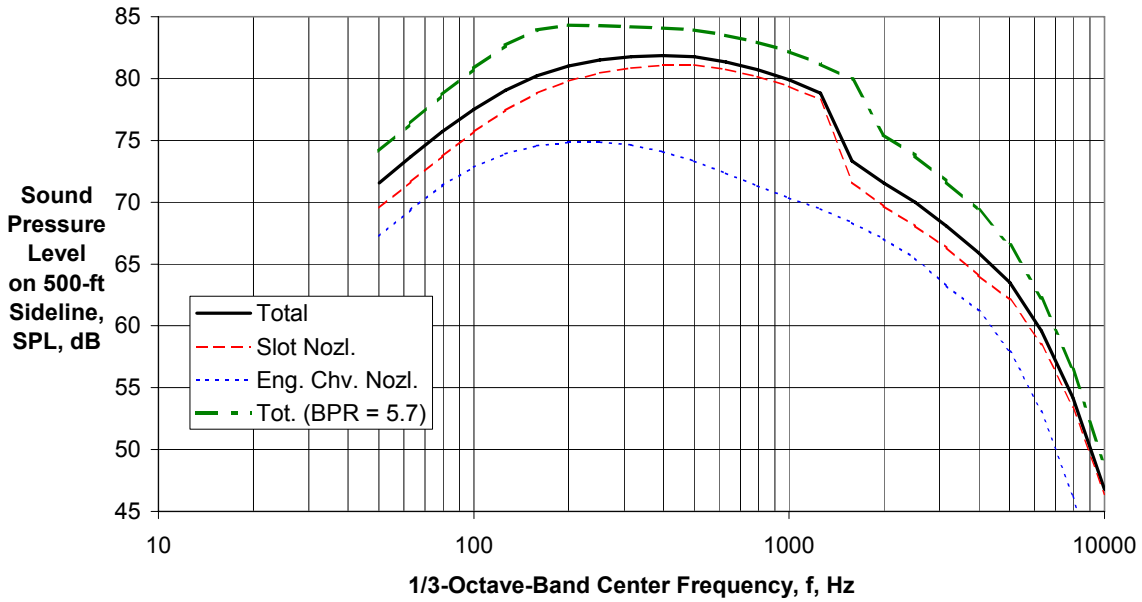

(b) Directivity Angle θ = 60

Figure 29 - Component and Total SPL Spectra for BWB/IBF Airplane with Chevron-Nozzle Engine BPR = 9.4 at Takeoff on 500-ft Sideline (Compared with BPR = 5.7).

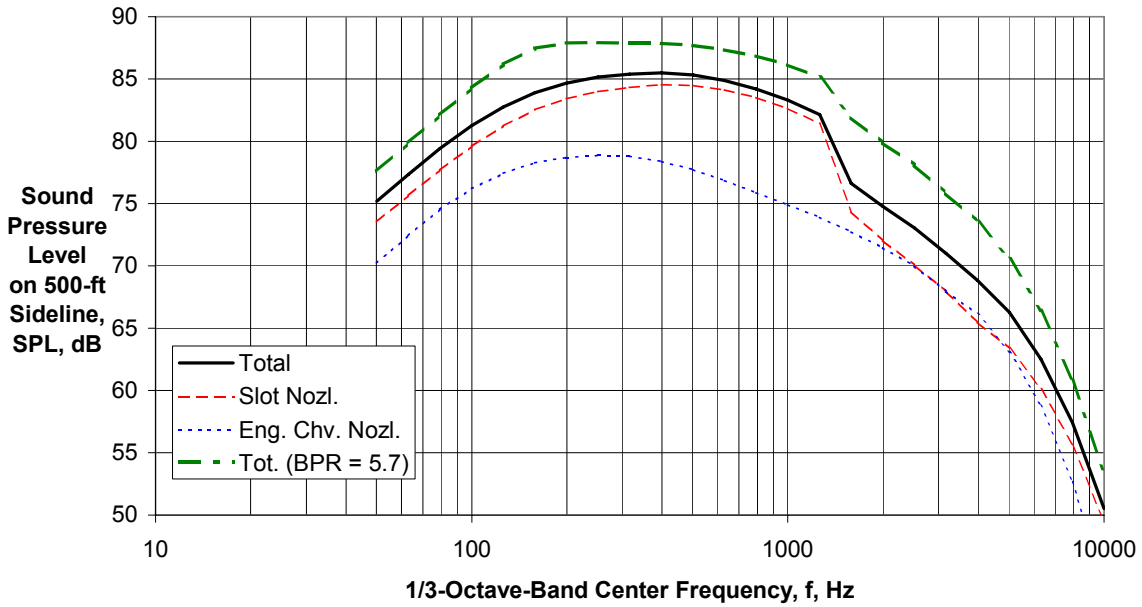

(c) Directivity Angle θ = 90

Figure 29 - Component and Total SPL Spectra for BWB/IBF Airplane with Chevron-Nozzle Engine BPR = 9.4 at Takeoff on 500-ft Sideline (Compared with BPR = 5.7).

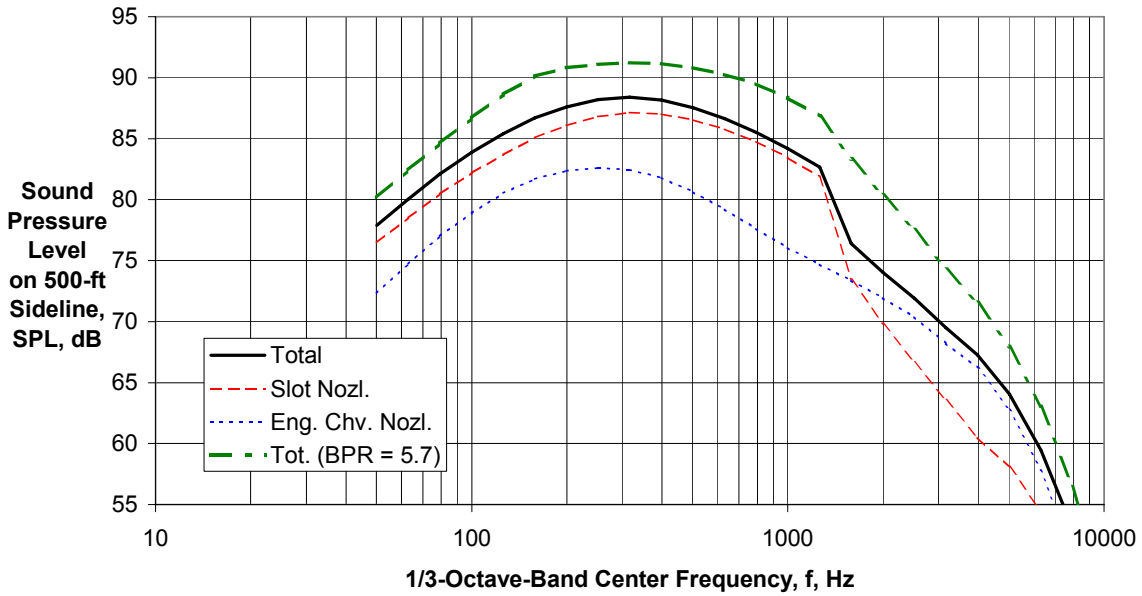

(d) Directivity Angle θ = 120

Figure 29 - Component and Total SPL Spectra for BWB/IBF Airplane with Chevron-Nozzle Engine BPR = 9.4 at Takeoff on 500-ft Sideline (Compared with BPR = 5.7).

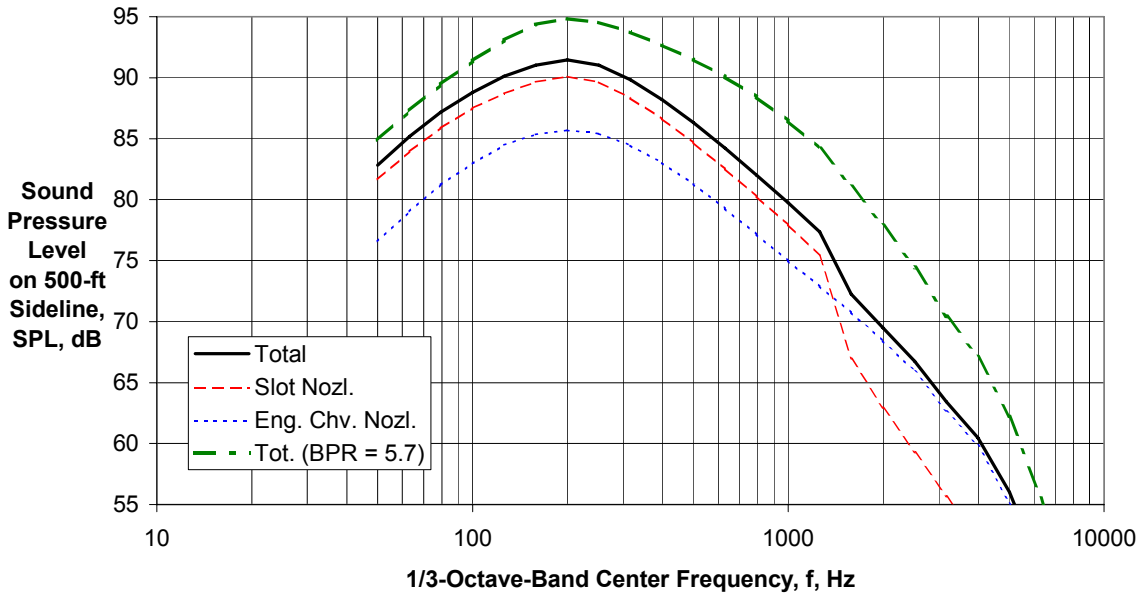

(e) Directivity Angle θ = 140 deg

Figure 29 - Component and Total SPL Spectra for BWB/IBF Airplane with Chevron-Nozzle Engine BPR = 9.4 at Takeoff on 500-ft Sideline (Compared with BPR = 5.7).

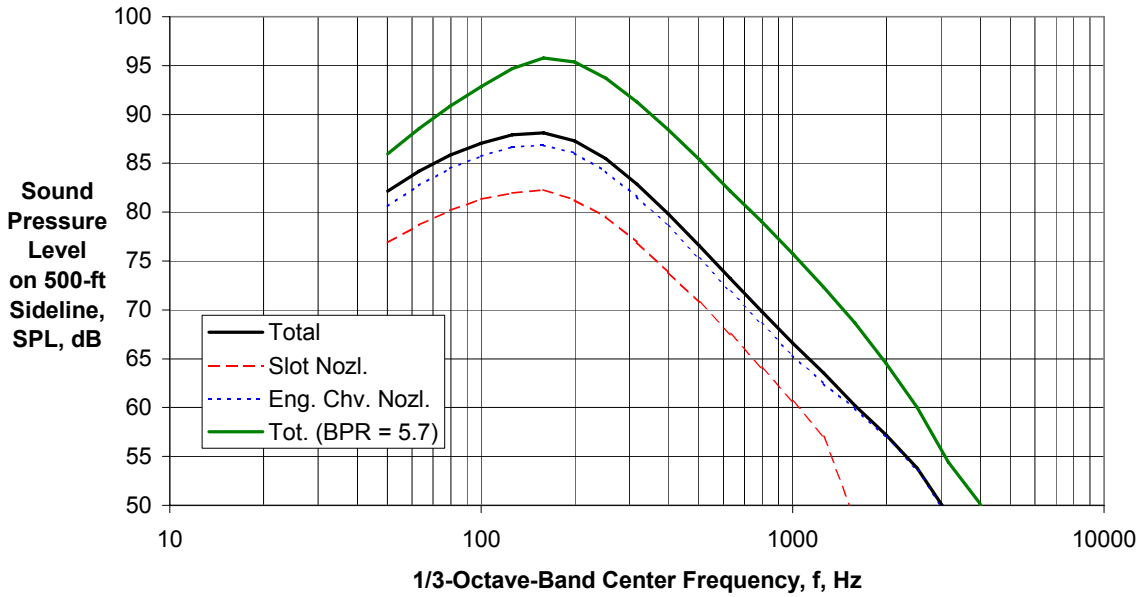

(f) Directivity Angle θ = 160 deg

Figure 29 - Component and Total SPL Spectra for BWB/IBF Airplane with Chevron-Nozzle Engine BPR = 9.4 at Takeoff on 500-ft Sideline (Compared with BPR = 5.7).

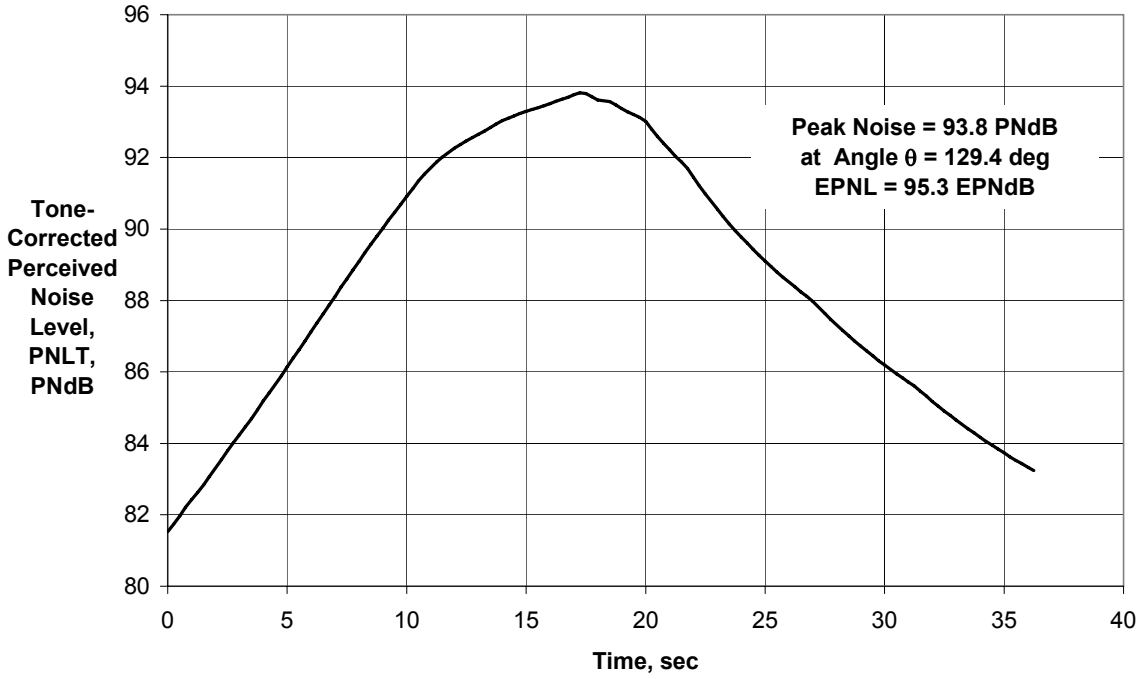

Figure 30 - PNLT Time History for BWB/IBF Airplane with Chevron Nozzle Engine BPR = 9.4 at Takeoff on 450-m (1476-ft) Sideline.

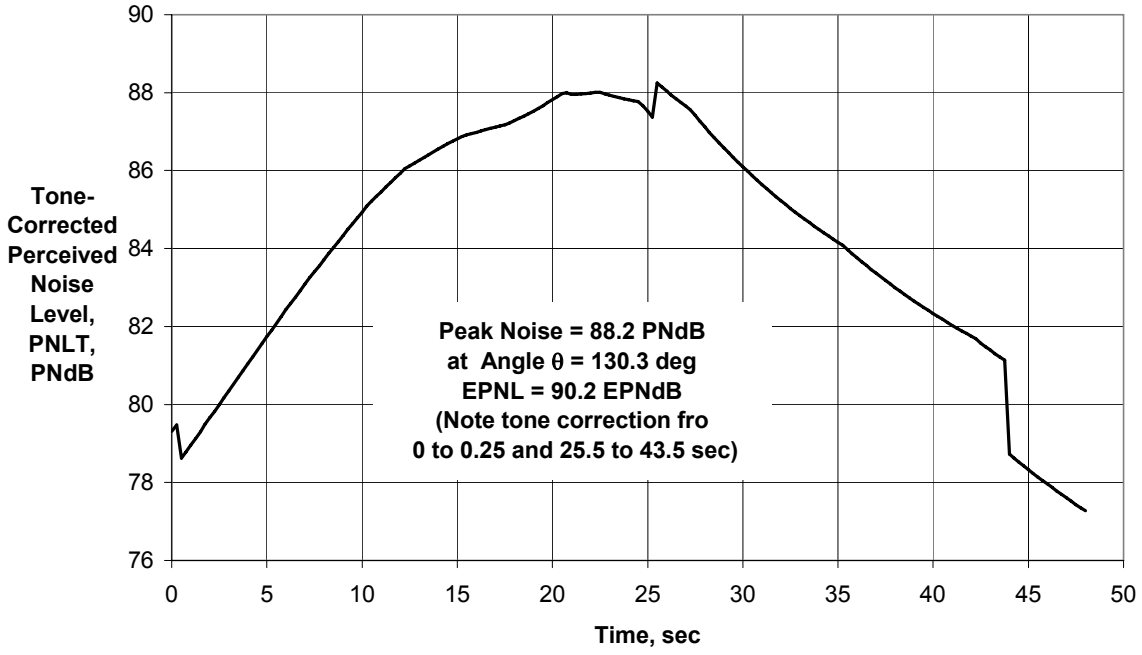

Figure 31 - PNLT Time History for BWB/IBF Airplane with Chevron Nozzle Engine BPR = 9.4 at Takeoff Flyover 6500 m from Brake Release.

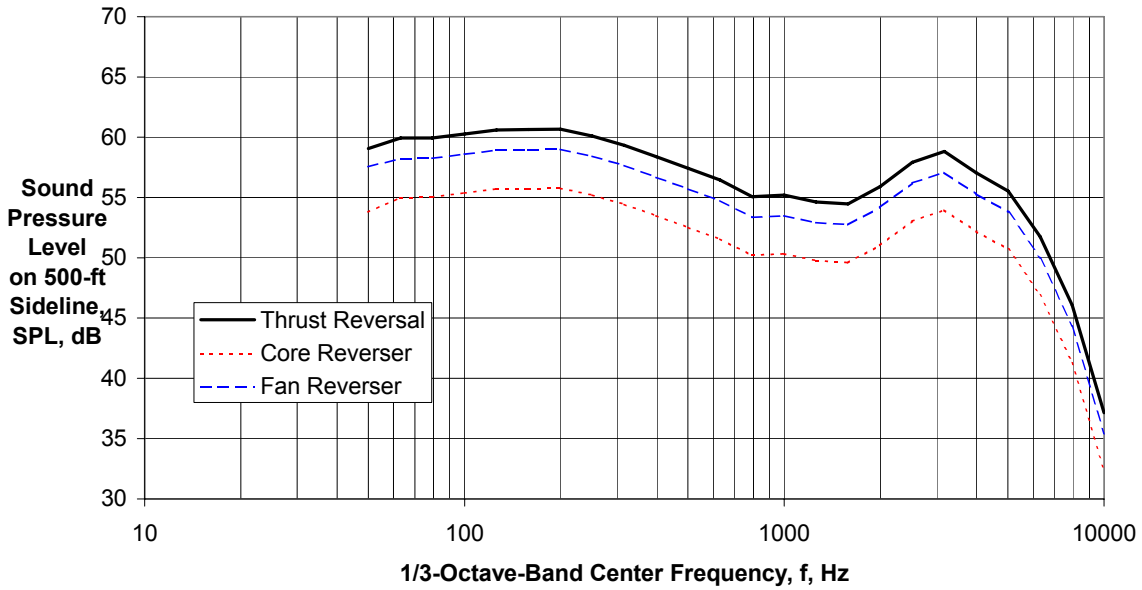

(a) Directivity Angle θ = 30

Figure 32 - Component and Total SPL Spectra for Single Engine Fan and Core Thrust Reversal (BPR = 5.7) of BWB/IBF Airplane on 500-ft Sideline.

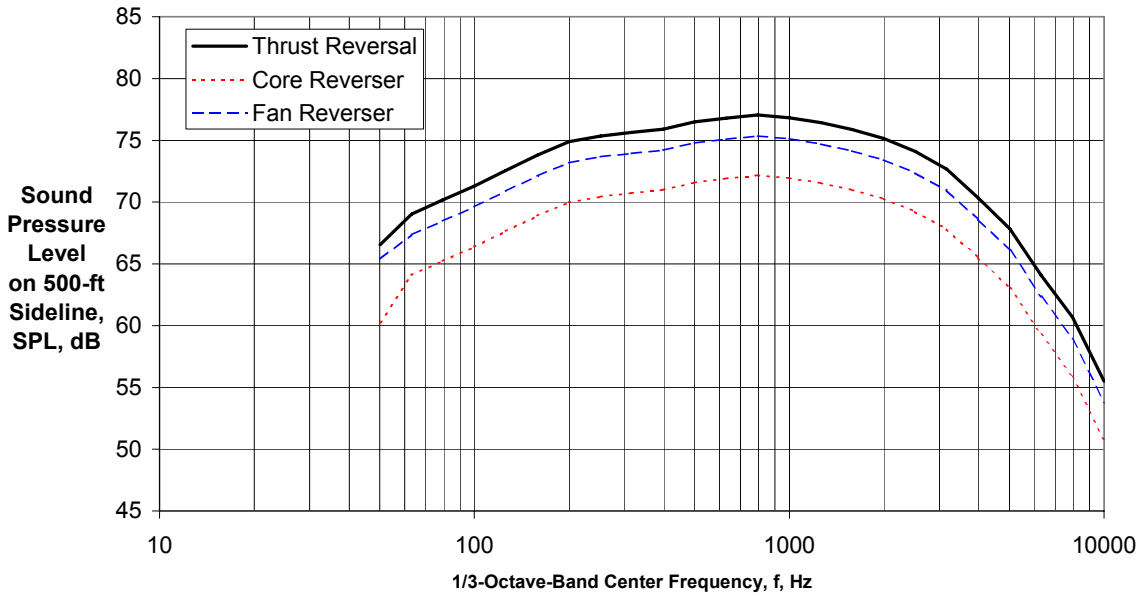

(b) Directivity Angle θ = 60 deg

Figure 32 - Component and Total SPL Spectra for Single Engine Fan and Core Thrust Reversal (BPR = 5.7) of BWB/IBF Airplane on 500-ft Sideline.

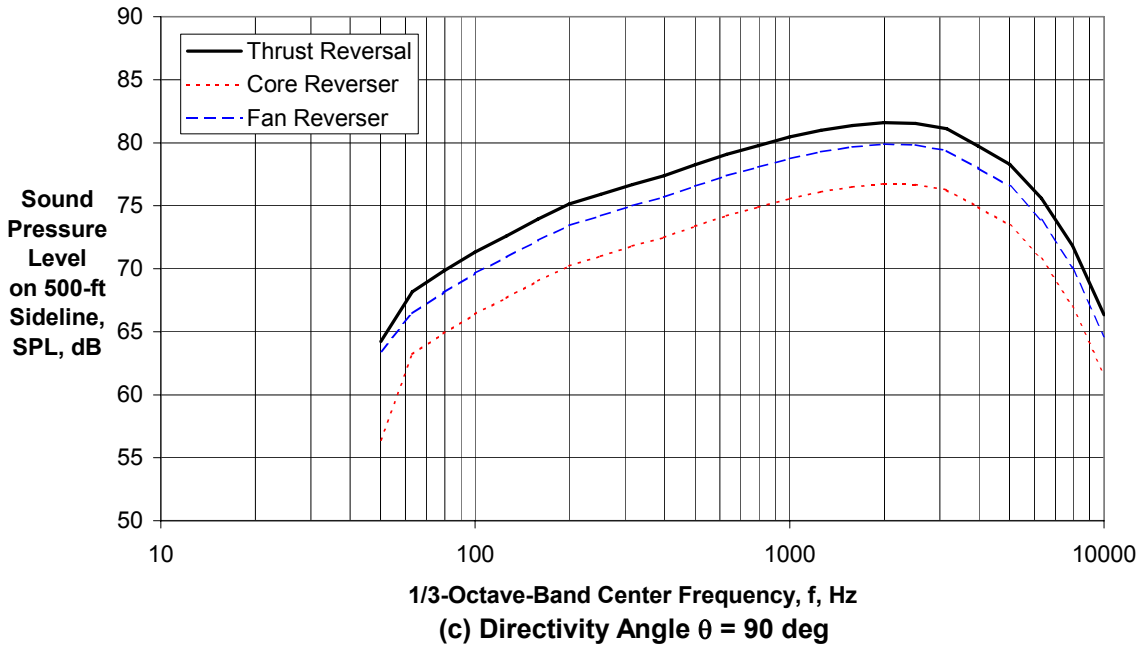

(c) Directivity Angle θ = 90 deg

Figure 32 - Component and Total SPL Spectra for Single Engine Fan and Core Thrust Reversal (BPR = 5.7) of BWB/IBF Airplane on 500-ft Sideline.

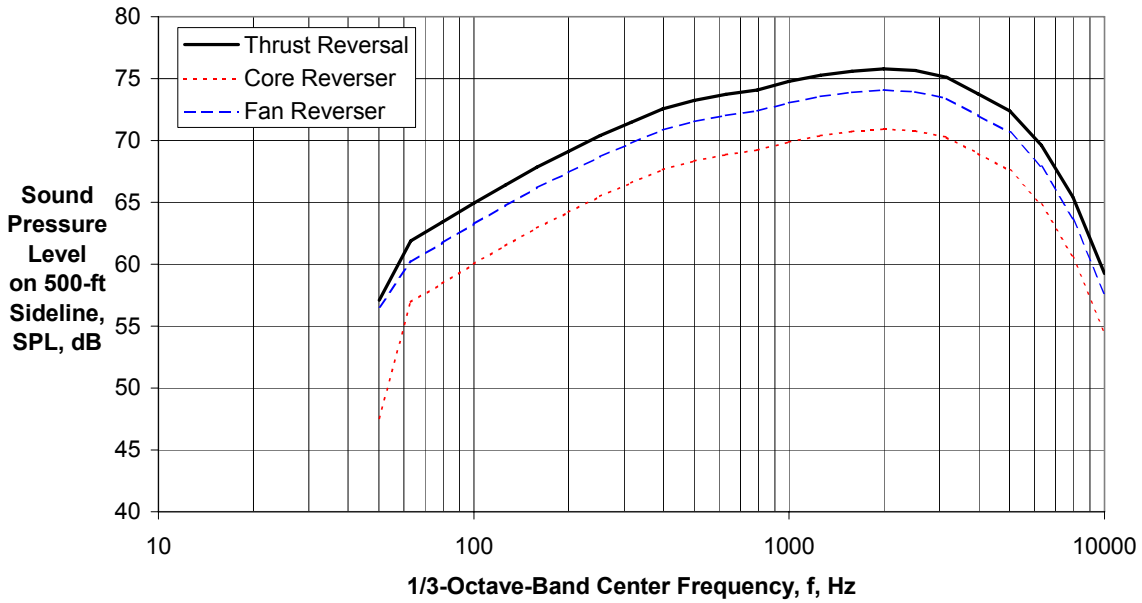

(d) Directivity Angle θ = 120 deg

Figure 32 - Component and Total SPL Spectra for Single Engine Fan and Core Thrust Reversal (BPR = 5.7) of BWB/IBF Airplane on 500-ft Sideline.

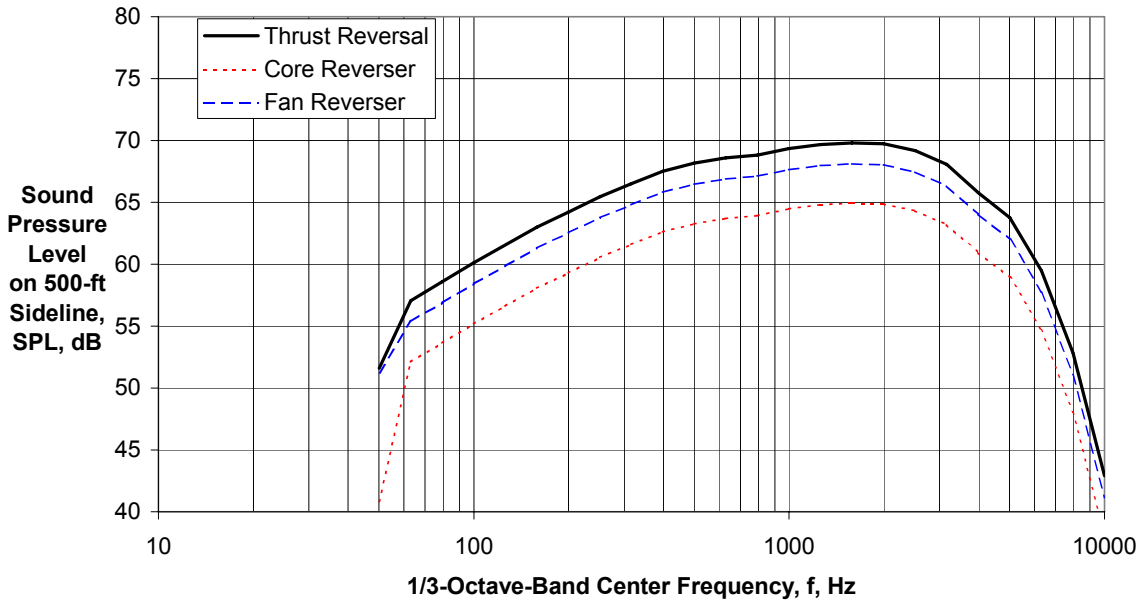

(e) Directivity Angle θ = 150 deg

Figure 32 - Component and Total SPL Spectra for Single Engine Fan and Core Thrust Reversal (BPR = 5.7) of BWB/IBF Airplane on 500-ft Sideline.

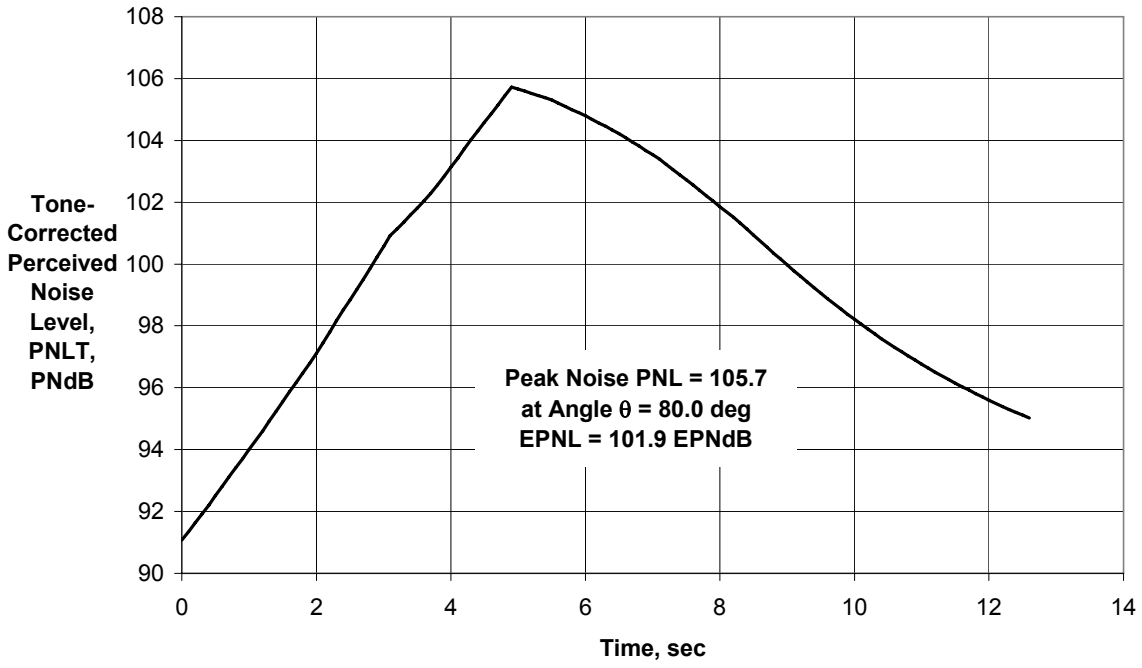

Figure 33 - PNLT Time History for Single Engine Fan and Core Thrust Reversal (BPR = 5.7) of BWB/IBF Airplane on 500-ft Sideline.

REPORT DOCUMENTATION PAGE	Form Approved OMB No. 0704-0188

1. REPORT DATE *(DD-MM-YYYY)*	2. REPORT TYPE	3. DATES COVERED *(From - To)*
01-04-2008	Final Contractor Report	

4. TITLE AND SUBTITLE
Initial Noise Assessment of an Embedded-Wing-Propulsion Concept Vehicle

5a. CONTRACT NUMBER

5b. GRANT NUMBER

5c. PROGRAM ELEMENT NUMBER

6. AUTHOR(S)
Stone, James, R.; Krejsa, Eugene, A.

5d. PROJECT NUMBER
NNC-05VD49P

5e. TASK NUMBER

5f. WORK UNIT NUMBER
WBS 561581.02.08.03.07.01

7. PERFORMING ORGANIZATION NAME(S) AND ADDRESS(ES)
Diversitech, Inc.
29317 Briar Lane
Westlake, Ohio 44145

8. PERFORMING ORGANIZATION REPORT NUMBER
E-16302

9. SPONSORING/MONITORING AGENCY NAME(S) AND ADDRESS(ES)
National Aeronautics and Space Administration
Washington, DC 20546-0001

10. SPONSORING/MONITORS ACRONYM(S)
NASA

11. SPONSORING/MONITORING REPORT NUMBER
NASA/CR-2008-215140

12. DISTRIBUTION/AVAILABILITY STATEMENT
Unclassified-Unlimited
Subject Category: 05
Available electronically at http://gltrs.grc.nasa.gov
This publication is available from the NASA Center for AeroSpace Information, 301-621-0390

13. SUPPLEMENTARY NOTES

14. ABSTRACT
Vehicle acoustic requirements are considered for a Cruise-Efficient Short Take-Off and Landing (CESTOL) vehicle concept using an Embedded-Wing-Propulsion (EWP) system based on a review of the literature. Successful development of such vehicles would enable more efficient use of existing airports in accommodating the anticipated growth in air traffic while at the same time reducing the noise impact on the community around the airport. A noise prediction capability for CESTOL-EWP aircraft is developed, based largely on NASA's FOOTPR code and other published methods, with new relations for high aspect ratio slot nozzles and wing shielding. The predictive model is applied to a preliminary concept developed by Boeing for NASA GRC. Significant noise reduction for such an aircraft relative to the current state-of-the-art is predicted, and technology issues are identified which should be addressed to assure that the potential of this design concept is fully achieved with minimum technical risk.

15. SUBJECT TERMS
Distributed propulsion; STOL

16. SECURITY CLASSIFICATION OF:			17. LIMITATION OF ABSTRACT	18. NUMBER OF PAGES	19a. NAME OF RESPONSIBLE PERSON
a. REPORT	b. ABSTRACT	c. THIS PAGE			STI Help Desk (email:help@sti.nasa.gov)
U	U	U	UU	67	19b. TELEPHONE NUMBER *(include area code)* 301-621-0390